UC Davis
UC Davis Electronic Theses and Dissertations

Title

Mechanisms of Ecosystem Invasion by Salmonella in the Large Intestine

Permalink

https://escholarship.org/uc/item/4m79g92z

Author

Rogers, Andrew Wolff Levy

Publication Date

2024

Peer reviewed|Thesis/dissertation

eScholarship.org Powered by the California Digital Library
University of California

Mechanisms of Ecosystem Invasion by *Salmonella* in the Large Intestine

By

ANDREW WOLFF LEVY ROGERS
DISSERTATION

Submitted in partial satisfaction of the requirements for the degree of

DOCTOR OF PHILOSOPHY

in

Microbiology

in the

OFFICE OF GRADUATE STUDIES

of the

UNIVERSITY OF CALIFORNIA

DAVIS

Approved:

Andreas J. Bäumler, Chair

Bennett H. Penn

Sebastian E. Winter

Committee in Charge

2024

Acknowledgements and Dedication

First and foremost, I thank my mother Erica for absolutely everything. I would not be the person I am today without her unconditional love and continued support. I would also like to thank the rest of my family for putting up with me these 32 years and for always cheering me on. Bud, Will, Hannah, Anna, and all the rest.

My closest friends deserve my unending praise and gratitude. Paul, Angie, Ginger, and Zoe never cease to amaze me with their personal and professional accomplishments. I cannot thank them enough for their support over the years, especially during my time as a PhD student when I needed it most. I also extend my deep thanks to Jessie, Hannah, Griffin, Michelle, Cole, Adam, Kelly, Doyle, Cori and everyone else that formed my support network over the years.

I owe the success of my doctoral studies to my advisor, Dr. Andreas Bäumler. His patience, grace, and mentorship were instrumental in my perseverance, and I cannot thank him enough or ever hope to repay him.

To the other academic mentors that I have had the privilege of learning from, I would like to extend my gratitude and recognize their roles in my development as a scientist. Dr. Fitnat Yildiz was the first to bring me into her lab and provide me with every possible opportunity needed for the commencement of an academic career. I would never have pursued a PhD without her influence. Dr. Jiunn (Nick) Fong was my first scientific instructor and the best supervisor one could hope to have. The techniques that I learned from Dr. Fong have proven invaluable and continue to benefit me as a scientist. I thank the members of my dissertation committee, Drs. Bennett Penn and Sebastian Winter, for their insights, guidance, and support.

To the rest of my peers, mentors, and academic family that have made this dissertation possible, I salute you. Briana, Henry, Brittany, Megan, Greg, Bevin, Lauren, Scott, Connor, Kohei, Anaïs, Hugo, Jee-Yon, Derek, Hannah, Aurore, Sophie, Thaynara, Lalita, Liz, Amber, Leti, Mariela, Eric, Erin, Mariana, Vladimir, Yael, Karryn, and honestly many more. Thank you!

This dissertation is dedicated to loved ones that have passed on.

To Blair, for inspiring me to pursue an intellectual path in life with love, generosity, and an open mind.

To David, for being a father figure and role model even as his time was coming to an end.

To Nick, for being the bright light that brings our community together.

Table of Contents

Abstract

Microbial invaders of the gastrointestinal ecosystem must overcome a myriad of oppositional forces in order to engraft themselves into the gut environment. While commensal gut microbes have evolved dispersal strategies that lack negative consequences for the host, these strategies only rarely allow for successful invasion into a microbiota that has matured past the initial stages of community assembly. In contrast, gastrointestinal pathogens have evolved virulence strategies that facilitate their dispersal into mature gut microbiotas. The mechanisms governing this antagonism and attempted exclusion of microbial newcomers, which we term colonization resistance, are not fully understood. Here, we utilize a model invader of the large intestinal ecosystem, the pathogen *Salmonella enterica* subsp. *enterica* serovar (*S.*) Typhimurium, to gain mechanistic insight into the determinants of gastrointestinal colonization resistance.

In Chapter 1, we review the current understanding of colonization resistance to *S.* Typhimurium in the large intestine. Beginning with the principles microbiota assembly and the properties of the gut ecosystem during both homeostasis and dysbiosis, we provide a framework for understanding gut microbiome as a product of host-derived habitat filters. Evidence of colonization resistance being a phenomenon derived of both host and microbial activities is discussed, as is the fact that newcomer engraftment can occur if either part of this chimera is disturbed. Finally, we highlight the genus *Salmonella*'s contribution to our understanding of the large intestinal microbiota's role in health and disease.

Chapter 2 presents our use of an oral *S.* Typhimurium infection in an antibiotic-naïve mouse model of to study ecosystem invasion by the pathogen in the presence of an intact microbiota. We find that *S.* Typhimurium overcomes colonization resistance on day 3 after infection, as evidenced by its increased population size in both the feces and the cecum. Metabolomics, microbial community profiling by 16S rRNA amplicon sequencing, and literature-informed reverse genetics approaches allowed us to elucidate mechanisms by which *S.* Typhimurium overcomes microbiota-mediated colonization resistance. We establish that *S.* Typhimurium targets the host to abolish epithelial hypoxia, inhibit short-chain fatty acid production by the microbiota, and gain access to simple carbohydrates. The resulting bloom of S. Typhimurium occurs in the presence of a compositionally intact microbiota and is driven by mixed acid fermentation and aerobic respiration via the nitric oxide-resistant cytochrome *bd* oxidase CydAB.

An extended discussion and contextualization of the findings presented in Chapter 2 is provided in Chapter 3. We discuss infection kinetics as a simple yet effective tool for gaining insight into colonization resistance, microbiota composition vs. microbiota function, the roles of Clostridia in colonization resistance, and the importance of host epithelial metabolism as the foundation of the gut ecosystem. Finally, potential future directions for the study of the gut environment using *S.* Typhimurium are discussed.

In conclusion, we provide new insights into the strategies that *S.* Typhimurium uses to successfully overcome microbiota-mediated colonization resistance in the gastrointestinal tract.

Chapter 1: *Salmonella* versus the microbiome

Andrew W.L. Rogers, Renée M. Tsolis and Andreas J. Bäumler

Affiliations:

Department of Medical Microbiology and Immunology, School of Medicine, University of California at Davis, One Shields Avenue, Davis, CA 95616, USA.

Published in:

Microbiology and Molecular Biology Reviews, Volume 85. (Publication date February 2021)

https://journals.asm.org/doi/10.1128/mmbr.00027-19

Reprinted, with permission, from the Annual Review of Immunology, Volume 39 ©2021 by Annual Reviews, http://www.annualreviews.org

Summary

A balanced gut microbiota contributes to health, but the mechanisms maintaining homeostasis remain elusive. Microbiota assembly during infancy is governed by competition between species and by environmental factors, termed habitat filters, that determine the range of successful traits within the microbial community. These habitat filters include the diet, host-derived resources and microbiota-derived metabolites, such as short-chain fatty acids. Once the microbiota has matured, competition and habitat filtering prevent engraftment of new microbes, thereby providing protection against opportunistic infections. Competition with endogenous *Enterobacterales*, habitat filtering by short-chain fatty acids and a host-derived habitat filter, epithelial hypoxia, also contribute to colonization resistance against *Salmonella* serovars. However, at a high challenge dose, these frank pathogens can overcome colonization resistance by using their virulence factors to trigger intestinal inflammation. In turn, inflammation increases the luminal availability of host-derived resources, such as oxygen, nitrate, tetrathionate, and lactate, thereby creating a state of abnormal habitat filtering that enables the pathogen to overcome growth inhibition by short-chain fatty acids. Thus, studying the process of ecosystem invasion by *Salmonella* serovars clarifies that colonization resistance can become weakened by disrupting host-mediated habitat filtering. This insight is relevant for understanding how inflammation triggers dysbiosis linked to non-communicable diseases, conditions in which endogenous *Enterobacterales* expand in the fecal microbiota using some of the same growth-limiting resources required by *Salmonella* serovars for ecosystem invasion. In essence, ecosystem invasion by

Salmonella serovars suggests that homeostasis and dysbiosis simply represent states where competition and habitat filtering are normal or abnormal, respectively.

Introduction

The idea that communicable diseases are due to infection with pathogens emerged with the inception of Louis Pasteur's germ theory in 1865 (1), and Robert Koch's invention of approaches to establish causality in 1882 (2). These game-changing discoveries became a guiding principle of a new discipline, bacteriology, which is the precursor of modern-day microbiology and immunology. Subsequent discoveries of diphtheria toxin in 1888 (3) and Shiga toxin in 1903 (4, 5) gave rise to the concept that pathogens cause disease because they elaborate virulence factors that manipulate host physiology. The century following these seminal discoveries has seen countless studies on how virulence factors enable pathogens to overcome host defenses in individuals with an intact immune system to cause disease. However, this historic focus on host pathogen interaction has left a third player in obscurity, our host-associated microbial communities, the microbiota.

Although research from the 1950s shows that a disruption of the microbiota enhances susceptibility to infection (6), the idea that virulence factors could play a role in overcoming growth inhibition by resident microbial communities was not explored until microbiota analysis became possible by advances in sequencing technologies during the first decade of the 21st century(7-9). Subsequent work shows that virulence factors can target the host to manipulate the environment inhabited by the microbiota (10-13). Through this chain of events, virulence factors can alter the microbiome, which is defined ecologically as the microbiota and its host environment (14, 15) (**Table 1.1 and Fig. 1.1**). The fact that mucosal pathogens can use virulence factors to manipulate the microbiome renders them useful tools for microbiome research (16). As a result, studies on how

virulence factors manipulate the host/microbiota interface are beginning to assemble into a framework for a “new bacteriology”, which studies pathogen physiology and gene regulation in the natural context of the microbiome (17).

Here we will review this new chapter in bacteriology using the paradigm that spearheaded many advances: studies on the pathogenesis of *Salmonella* serovars. We will start by briefly outlining the conceptual framework of microbiome research, followed by discussing how the microbiome protects against infection and how *Salmonella* serovars use their virulence factors to overcome this line of defense. *Salmonella enterica* subspecies *enterica* serovar (*S.*) Typhimurium is commonly studied as a representative of the species, because it is an important human pathogen (18, 19). *S.* Typhimurium was fist described as the causative agent of a typhoid-like disease in mice (20), a mammalian species that is commonly used to model the disease process (21). The luminal *S.* Typhimurium population reaches high numbers in the murine large intestine (22), which also harbors the largest microbial community in the human body. Most of our discussion will therefore revolve around the interaction of *S.* Typhimurium with the microbiota of the large intestine.

The Gut Microbiome

Competition and Habitat Filtering Govern Gut Microbiota Assembly

Principles of community assembly. The infant is thought to be sterile *in utero* (23), suggesting that birth marks the beginning of microbiota assembly. According to ecological theory of plant community assembly, this process is governed by two drivers: competition and habitat filtering. In plant communities, competition involves interactions among species whereas habitat filtering encompasses interactions between species and their abiotic environment (24). These assembly rules also apply to the human gut microbiota (25, 26), except here the host provides a biotic environment that responds dynamically to microbiota-derived signals, which adds additional layers of complexity.

The host could be viewed as an ecological foundation species (27), who filters the habitat of the gut microbiota using biotic factors, which include physical barriers (e.g. peristalsis), the emission of chemicals (e.g. gastric acid and bile acids), the excretion of antimicrobial proteins (e.g. defensins), the secretion of immunoglobulin A (IgA) and epithelial release of resources that shape microbial growth (e.g. mucin) (28, 29). In addition to host-derived habitat filters, the range of successful traits within the microbiota in the gastrointestinal tract is influenced by microbiota-derived habitat filters (e.g. short-chain fatty acids) and by an important abiotic habitat filter: the diet (30). Since the choice of diet is governed by host behavior, diet could also be viewed as an aspect of host-mediated habitat filtering (**Fig. 1.1**).

Competition and habitat filtering select for different functional traits of coexisting species. Competition is common among pairs of similar species and can lead to

competitive exclusion, thereby limiting the number of similar coexisting species (31). In contrast, habitat filtering limits the range of successful strategies among coexisting species (32), which can drive species with particular traits or phenotypes to dominate the microbial community.

Habitat filtering establishes dominant taxa in the colonic microbiota. One important host-derived habitat filter that shapes the abundance of species inhabiting the colon is epithelial hypoxia. The healthy colonic epithelium permanently resides in a state of physiological hypoxia (< 1% oxygen) (33), which limits the amount of oxygen diffusing into the lumen of the colon, thereby maintaining anaerobiosis (34). As a result, obligate anaerobic bacteria dominate the microbial community in the colon (35), a phenotypic convergence in a key ecological trait. Elevating epithelial oxygenation disrupts this biotic habitat filter, thereby increasing oxygen availability in the intestinal lumen, which results in an expansion of facultative anaerobic bacteria in the colonic microbiota (36), a microbial signature of dysbiosis (37).

A second important habitat filter for the colonic microbiota is the diet. Milk oligosaccharides in breast milk represent an important maternal habitat filter, as these dietary carbohydrates do not nurture the infant, are poorly absorbed in the small intestine and reach the colon (38). Milk oligosaccharides drive a predominance of *Bifidobacteriaceae* (phylum *Actinobacteria*), because these obligate anaerobes are among a select few bacteria that contain gene clusters for the consumption of these carbohydrates (39, 40). Weaning removes human milk oligosaccharides from the diet while introducing dietary fiber, an important habitat filter involved in shaping the colonic

microbiota. Dietary fiber is composed of complex carbohydrates that are not degraded and absorbed by host enzymes in the upper gastrointestinal tract, thus making them available as carbon sources for the colonic microbiota (41, 42). Phenotypic traits conferring the ability to utilize dietary fiber are most abundant in members of the classes *Clostridia* (phylum *Firmicutes*) and *Bacteroidia* (phylum *Bacteroidetes*) (43). As a result, weaning is associated with a succession characterized by a disappearance of *Bifidobacteriaceae* and an expansion of *Clostridia* and *Bacteroidia* in the gut microbiota (44).

These observations illustrate that the dominance of certain bacterial taxa in the colonic microbiota is the result of habitat filtering by the host, which involves the host's dietary behavior and host control over the flow of resources from the epithelial lining into the microbial habitat. In other words, dietary fiber and epithelial hypoxia 'filter' the colonic environment in healthy adults so that obligate anaerobic bacteria with a diverse array of glycolytic enzymes predominate, which explains why *Clostridia* and *Bacteroidia* are the most abundant taxa in this habitat patch (35) (**Fig. 1.2**).

Competition and Habitat Filtering Maintain Microbiota Resistance and Resilience

Microbiota resistance. As the microbiota matures, ecological niches carved out through competition and habitat filtering become successively occupied by microorganisms that are acquired stochastically over time from maternal or environmental sources (45). Fecal microbiota transplantation in adult mice increases species diversity compared to the microbiota of both the donor and the recipient, which suggests that the

microbiota assembly process does not reach full saturation (46), a property common to most ecosystems (47, 48). Nonetheless, established members of the microbial community can prevent engraftment of new arrivals either through competition, a process known as niche preemption, or through habitat filtering, an activity referred to as niche modification (45, 49). Niche preemption can involve competition between closely related species for critical resources, such as oxygen (50, 51). An example of niche modification is the production of short-chain fatty acids by *Clostridia* and *Bacteroidia* species (52, 53), which limits the range of successful metabolic strategies among bacterial species inhabiting the large intestine. Niche preemption and niche modification generate priority effects that enable founding members of a mature microbial community to prevent engraftment of additional microbes, thereby generating a stable equilibrium state with invariable species composition (54, 55). The resulting temporal stability of the taxa composition observed for mature gut-associated microbial communities is termed microbiota resistance (45, 56, 57) (**Fig. 1.3A**).

Since historical events that govern the initial exposure to microbes differ between individuals, the outcome of community assembly is different for each person, a phenomenon known as historical contingency (49). Combining historical contingency with microbiota resistance is predicted to generate considerable taxonomic diversity between gut-associated microbial communities from different individuals. Consistent with this idea, the taxa composition exhibits little overlap on the species level when the fecal microbiota composition is compared between healthy volunteers (58).

Microbiota resilience. The principles of microbial community assembly predict that competition and habitat filtering will select for comparable microbial traits in healthy individuals that consume a similar diet, which will result in assembly of microbial communities that are functionally similar even though they differ in their species composition. Consistent with this idea, antibiotics disrupt the fecal microbiota by permanently removing some microorganisms, but after completing therapy, habitat filtering ensures that vacated niches are occupied again by microbes harboring similar traits as their predecessors, thus returning the microbiota to a healthy equilibrium state despite the fact that recovery from antibiotic treatment changes the species composition (54). For example, oral administration of streptomycin diminishes microbial functions, such as short-chain fatty acid production, but concentrations of these metabolites return to normal levels after secession of treatment (59), suggesting that reassembly of the microbiota returns metabolic traits to their ancestral state. Through this mechanism, competition and habitat filtering ensures that the microbiota returns to a healthy state after perturbation, a property called microbiota resilience (56, 60) (**Fig. 1.3A**).

Homeostasis versus dysbiosis. The taxonomic diversity in the microbiota composition between individuals (58) makes it all but impossible to determine what constitutes a balanced microbial community based on cataloguing microbial species names (61). Dysbiosis is commonly described as an imbalance in microbial communities characterized by a decrease in microbial diversity, the presence of potentially harmful microbes or the absence of beneficial ones (62), but this definition becomes untenable when homeostasis cannot be explained by the presence or absence of specific microbial

species (63). Problems with a taxonomic definition for homeostasis and dysbiosis provide a compelling rationale for developing functional definitions for these terms (27). The processes that govern microbial community assembly suggest that homeostasis represents the outcome of normal competition and habitat filtering, which in turn generates microbiota resistance and microbiota resilience. Normal habitat filtering could be defined as an activity characteristic of or appropriate to a healthy or normally functioning host. Conversely, dysregulation of processes involved in microbial community assembly will trigger dysbiosis, which can be defined as a state resulting from abnormal competition or habitat filtering (**Fig. 1.3B**).

Colonization Resistance

A Host-Microbe Chimera Confers Colonization Resistance

Functions of the gut microbiota. Defining homeostasis functionally focuses attention on the role the gut microbiota plays in health. One function of a balanced colonic microbiota is to aid in the digestion of nutrients that cannot be broken down by host enzymes in the small intestine, such as fiber (64). Habitat filters that maintain anaerobiosis ensure that catabolism of fiber has to proceed though pathways that generate fermentation products, such as short-chain fatty acids (65). In turn, microbiota-derived fermentation products are absorbed by the host for nutrition, which provides us with an estimated 6 to 10% of our energy budget (66, 67). The microbiota has thus been likened to an organ containing our “second genome”, which encodes digestive enzymes to harvest otherwise inaccessible nutrients (68, 69) (**Fig. 1.4**).

A second function of a balanced gut microbiota is to educate and prime our host defenses (70-76). Altered production of microbiota-derived metabolites during dysbiosis has been linked to a broad spectrum of non-communicable diseases associated with chronic immune activation, such as colorectal cancer (77), atherosclerosis (78) and allergic airways disease (79). Comparison of germ-free and conventional mice reveals that the microbiota profoundly influences functionality and development of both the mucosal and systemic immune systems (80, 81). It has thus been proposed that the microbiota should be viewed as an organ aiding in immune education (82) (**Fig. 1.4**).

The organ analogy has obvious limitations, as organs are passed down across generations, whereas heritability estimates for the human microbiota are low (83, 84).

Furthermore, the fact that germ-free mice are viable suggests that the digestive function of the microbiota and its role in immune education are not essential for life. However, one could argue that the latter assertion is flawed, because germ-free mice require dietary supplementation with microbial products (e.g. vitamin K) (85) and are exquisitely sensitive to infection. In the absence of a microbiota, environmental exposure would inevitably result in death from opportunistic infections. These considerations underscore that in addition to aiding nutrition and immune education, the microbiota executes a third function that contributes to health, which is to limit the ability of harmful microbes to gain a foothold and expand on body surfaces, a property known as colonization resistance (**Fig. 1.4**). Colonization resistance is a canonical non-specific immune function that is essential for life. This vantage point suggests that our resident microbes should be considered effector cells of our immune system, an idea that requires an expansion of theory to incorporate microbial ecology into the classical framework of immunology (28).

Sterilizing immunity versus microbiota-nourishing immunity. One subdivision of our immune system ensures sterility of host tissues (sterilizing immunity) by detecting invading microorganisms and distinguishing them from self. In turn, self/nonself discrimination induces innate and adaptive immune responses that are aimed at removing the microbial intruders from tissue to restore sterility (86). However, whereas the goal of sterilizing immunity is to remove microbes from host tissues, the goal of our interaction with microbes inhabiting body surfaces is not to detect and remove them, but rather to maintain and balance microbial communities for health (87). It has thus been proposed that host-derived habitat filters that shape microbial communities form a functional unit

with the microbiota, termed microbiota-nourishing immunity, which constitutes an immune system subdivision that is separate from sterilizing immunity (28, 88) (**Fig. 1.1**).

Several fundamental differences between microbiota-nourishing immunity and sterilizing immunity justify such a subdivision. Firstly, at the very core of sterilizing immunity lies the ability to discriminate between self and nonself, which needs to be applied to members of the microbiota. For instance, microbiota entering tissue during traumatic injury necessitates its elimination to restore sterility. However, whereas self/nonself discrimination by sterilizing immunity is essential for hunting down individual microbes in host tissue, this process is not critical for balancing the microbiota on body surfaces using host-derived habitat filters. Although microbiota-derived metabolites can be detected by host cell receptors to regulate host-derived habitat filters (89-91), this process neither distinguishes individual microbes from self nor does it trigger responses aimed at sterilizing body surfaces (92, 93).

Secondly, microbiota-nourishing immunity is a host-microbe chimera, in which the microbial contribution to colonization resistance is mediated through ecological priority effects executed by microbial effector cells (94). In contrast, all components involved in sterilizing immunity are host-derived, which makes the idea that microbial cells could be considered effector cells of our immune system appear strange to card-carrying immunologists (28).

Thirdly, although there is overlap between antimicrobial mechanisms employed by effector cells of sterilizing immunity and by host-derived habitat filters of microbiota-nourishing immunity (e.g. defensins), only the latter employs mechanisms that literally nourish the microbiota (e.g. milk oligosaccharides) (28). Thus, habitat filters of microbiota-

nourishing immunity balance the microbiota using a carrot-and-stick approach that is never utilized by sterilizing immunity.

The emerging picture suggests that microbiota-nourishing immunity constitutes our first line of defense against mucosal pathogens, but our functional understanding of this immune system subdivision lags behind that of sterilizing immunity. Although the concept of microbiota-nourishing immunity is new (28, 88), there is a large body of work on colonization resistance reaching all the way back to the 1950s (6). Taking a fresh look at this literature through the novel lens of microbiota-nourishing immunity provides an opportunity to infuse the conceptual framework of a data-driven discipline, microbiome research, with a wealth of information on bacterial physiology and pathogenesis. Here we will perform this task for *S.* Typhimurium, one the best studied bacterial model organisms that has long been a workhorse of research in bacterial genetics and metabolism (95). *S.* Typhimurium is ideally suited for studying the interplay between the pathogen, the host and its microbiota due to the availability of excellent animal models (21, 96).

Niche Modification by Microbiota-Derived Short-Chain Fatty Acids

Historical overview. A clinical appreciation for the protective functions of the gastrointestinal microbiota began in the 1940s and 50s with the rapid introduction of antibiotics for the treatment of bacterial infections (97). Alongside the profound success of antibiotic therapies came the observation that patients often became susceptible to secondary bacterial infections after antibiotic treatment of a primary infection, implicating an unperturbed microbiota as a key player in the generation of colonization resistance

(98-100). In an effort to study this phenomenon, Marjorie Bohnhoff at the University of Chicago pioneered the use of a mouse model for the study of microbiota-mediated colonization resistance (6). This model, which is still widely used today, involves oral pretreatment of mice with the antibiotic streptomycin. The treatment was found to significantly alter the abundance and composition of the large intestinal microbiota, measured by the contemporary standards of aerobic plate counts and Gram stain (101, 102). An acute susceptibility to intragastric *S.* Enteritidis infection coincides with this streptomycin-dependent alteration of the large intestinal microbiota, with the infectious dose being lowered to <10 colony-forming units, whereas untreated mice resist colonization by *S.* Enteritidis challenges of as high as 10^6 colony-forming units (6). This ten-thousand-fold increase in the challenge dose required for lethal *S.* Enteritidis infection in mice with an intact microbiota compared to mice with streptomycin-ablated microbiota illustrates that colonization resistance provides strong protection against low-dose pathogen challenge. Early work also contributed a prescient description of microbiota resilience, by demonstrating that a drastic reduction in the overall bacterial abundance and morphological diversity triggered by streptomycin treatment rebounded to pre-treatment levels within one week (101, 102).

Initial studies on streptomycin pre-treated mice suggest that an intact microbiota has bacteriostatic or weakly bactericidal activity against *S.* Typhimurium, which is attributable to the metabolic functions of the microbiota (52). The most abundant by-products of the fermentative metabolism of the colonic microbiota are the short-chain fatty acids acetate, propionate, and butyrate. Fecal concentrations of acetate are commonly measured in the 50 mM range while propionate and butyrate levels vary widely from 5 to

30 mM. The observation that short-chain fatty acids are required to inhibit the growth of *S.* Enteritidis *in vivo*, in fecal homogenates *ex vivo*, and in rich media *in vitro* reveals their crucial role in mediating colonization resistance (53). However, the inhibitory mechanism of action of short-chain fatty acids requires an acidic environmental pH as only their protonated forms exhibit significant inhibitory effects on the growth of members of the *Enterobacterales* [*ord. nov.* (103), the order *Salmonella* serovars belong to, by freely diffusing across cellular membranes (104). Initial characterization of the large intestinal environment of mice revealed that short-chain fatty acids are present at high concentrations alongside a mildly acidic pH (53, 101). Disturbance of the microbiota by streptomycin treatment lowers short-chain fatty acid concentrations and increases the luminal pH of the large intestine, thereby generating conditions that are favorable to growth *Salmonella* serovars *in vivo* and *in vitro* (53, 101).

However, the inhibitory activity of short-chain fatty acids alone is not sufficient to explain how a low abundance of *Enterobacterales* is maintained in the microbiota, because this would require short-chain fatty acids to be preset constantly at precisely the right concentration to check population growth, whereas any further increases in the concentration would drive this taxon to extinction (105). Rolf Freter thus proposed that the abundance of *Enterobacterales* in the fecal microbiota is determined by the availability of growth-limiting resources (106). During homeostasis, a low abundance of these growth-limiting resources maintains *Enterobacterales* as minority species in the microbiota (106). A first inkling of the possible nature of these growth-limiting resources comes from the early observation that depletion of short-chain fatty acids increases the redox potential in the cecum to conditions that approximate an aerobic broth culture (101),

which predates the finding that streptomycin increases oxygen availability in the colon by more than 50 years (89). A more detailed discussion of growth-limiting resources that govern the abundance of *Enterobacterales* in the fecal microbiota is provided below in the section on host-derived habitat filters.

Mechanism of growth inhibition by short-chain fatty acids. More recent work on colonization resistance against *Salmonella* serovars and other *Enterobacterales* confirms the importance of short-chain fatty acids and provides mechanistic insights into their mode of growth inhibition (107-109). As weak acids, the degree of dissociation for acetate, propionate, and butyrate decreases as the environmental pH approaches their respective pK_a values (the negative base-10 logarithm of the acid dissociation constant) of 4.76, 4.87, and 4.82. In order to maintain a proton motive force and cellular homeostasis, *Enterobacterales* maintain their intracellular pH in the range of 7.2 to 7.8 (110-113). This cytosolic pH range is essential for driving ATP production by oxidative phosphorylation, which relies on protons translocating through ATP synthase and down their concentration gradient. When protonated short-chain fatty acids (HAc) diffuse into a bacterial cell, intracellular proton release ($H^+ + Ac^-$) disrupts pH homeostasis in the cytosol (101, 110, 114, 115). If enough protonated short-chain fatty acids are present in the environment, then this process will proceed until the intracellular pH matches the environmental pH, thereby disturbing cellular pH homeostasis (108). Therefore, the inhibitory capacity of short-chain fatty acids is determined both by their concentration and the luminal pH, which is described by the Henderson-Hasselbalch equation ($pH = pK_a +$

$\log_{10}\{[Ac^-]/[HAc]\}$). Through this mechanism, short-chain fatty acids act as a habitat filter that maintains a low abundance of *Enterobacterales* during homeostasis.

Short-chain fatty acid-producers. Acetate is produced by a broad range of bacterial species and cannot be attributed to a specific taxon within the gut microbiota. In contrast, *Bacteroidaceae* (class *Bacteroidia*) are the main producers of propionate (107), whereas the bulk of butyrate production in the colon is attributed to *Ruminococcaceae* (class *Clostridia*) and *Lachnospiraceae* (class *Clostridia*) (116, 117). Variation in the abundance of *Bacteroidaceae* between different inbred mouse lines reveals that propionate production by members of this family contributes to colonization resistance against *S.* Typhimurium (107). Colonization resistance in mice harboring a gut microbiota with low *Bacteroidaceae* abundance can be strengthened by administering *Bacteroides thetaiotaomicron*, but not a *B. thetaiotaomicron* mutant deficient for propionate-production (107). Similarly, a streptomycin-mediated depletion of *Ruminococcaceae* and *Lachnospiraceae* weakens colonization resistance against *S.* Typhimurium, which can be restored by administering butyrate or butyrate-producing *Clostridia* isolates (89, 118).

Beyond short-chain fatty acids. Recent work suggests that suppression of *S.* Typhimurium growth by microbiota-mediated habitat filtering is not limited to the production of short-chain fatty acids, but also includes a depletion of critical resources, such as amino acids. A microbiota-mediated depletion of amino acids filters the environment to exclude bacteria that lack amino acid biosynthesis pathways (119), a selective pressure that helps maintain prototrophy in *S.* Typhimurium. This selective

pressure no longer acts on *Salmonella* serovars that are exclusively associated with extraintestinal disease, such as the human-adapted *S.* Typhi or *S.* Paratyphi A (120), which might explain why these pathogens are auxotrophic for tryptophan or cysteine and arginine, respectively (121, 122). Depletion of the gut microbiota with antibiotics increases concentrations of amino acids in the colonic lumen (123). In turn, *S.* Typhimurium can take advantage of the increased availability of amino acids after antibiotic treatment by utilizing aspartate as an exogenous electron acceptor for fumarate respiration (124).

Host-Derived Habitat Filters Uphold Colonization Resistance

A microbial signature of dysbiosis. *Salmonella* serovars belong to the order *Enterobacterales* [*ord. nov.* (103), phylum *Proteobacteria*], a taxon comprising less than 0.1% of the human fecal microbiota in healthy volunteers (35). However, disruption of the microbiota during antibiotic therapy weakens colonization resistance, which gives rise to a dysbiotic expansion of endogenous *Enterobacterales* in the fecal microbiota (125). Hence, the main experimental approach for studying colonization resistance against *Enterobacterales* has been to disrupt the microbiota using antibiotics, causing the majority of studies to become fixated on microbial factors contributing to this non-specific immune function. As a result, conventional wisdom, summarized in a number of recent review articles (126-130) stipulates that colonization resistance is mediated solely by the gut microbiota through a “battle of the bugs”, a process that does not involve the host.

However, the advent of microbiome research is beginning to shift this paradigm by revealing that in addition to the microbiota, the host makes important contributions to

colonization resistance against *Enterobacterales* (**Fig. 1.4**)(34, 131). During homeostasis, anaerobiosis in the large intestine maintains a dominance of obligate anaerobic bacteria (**Fig. 1.5A**). However, profiling of the human fecal microbiota reveals that an expansion of facultative anaerobic *Enterobacterales* is one of the most consistent and robust ecological patterns associated with dysbiosis (37), which is commonly observed in the absence of antibiotic therapy. For example, this microbial signature of dysbiosis is associated with chronic alcohol consumption (132), radiotherapy (133), malnutrition (134), inflammaging (135) and observed in individuals with inflammatory bowel disease (IBD) (136), colorectal cancer (77), necrotizing enterocolitis (137), HIV enteropathy (138), graft versus host disease (139), and infectious diarrhea (140). There is now mounting evidence that in many of these diseases, a dysbiotic expansion of *Enterobacterales* in the fecal microbiota is driven by an underlying dysregulation of host-mediated habitat-filtering.

Host phagocytes transform the gut environment during inflammation. Studies on *Salmonella* pathogenesis spearheaded this research by showing that, paradoxically, severe acute intestinal inflammation drives a pathogen expansion in the gut microbiota (7, 8), in part because phagocytes migrating into the intestinal lumen release antimicrobial compounds, such as reactive oxygen species (ROS) and reactive nitrogen species (RNS) (10, 141). Although direct exposure to these antimicrobial compounds can kill the pathogen (142, 143), phagocyte-derived ROS and RNS diffuse into the gut lumen, where they react to form non-toxic by-products, such as tetrathionate and nitrate, which serve as electron acceptors for anaerobic respiration, thereby promoting *S.* Typhimurium growth (10, 141, 144, 145) (**Fig. 1.5B**). Subsequent work

shows that intestinal inflammation also weakens colonization resistance against other members of the *Enterobacterales* through similar mechanisms. For instance, intestinal inflammation triggered by virulence factors of the enteric pathogen *Yersinia enterocolitica* causes the pathogen to expand in the gut microbiota through tetrathionate respiration (12). Similarly, nitrate respiration drives a dysbiotic expansion of commensal *E. coli* (order *Enterobacterales*) in mouse models of *Toxoplasma gondii*-induced colitis (146), chemically-induced colitis (147, 148) or genetically induced colitis (147, 148). Host-derived nitrate also weakens colonization resistance against *Klebsiella oxytoca* in a mouse model of cancer cachexia (149). In conclusion, migration of phagocytes into the intestinal lumen during intestinal inflammation lowers colonization resistance against *Enterobacterales* by inducing a state of abnormal habitat filtering, which creates increased luminal concentrations of electron acceptors that drive an expansion of facultative anaerobic bacteria through anaerobic respiration (131).

Epithelial metabolism shapes the gut microbiota. Research on *Salmonella* pathogenesis was also at the forefront of discovering that the metabolism of the colonic epithelium functions as a control switch, mediating a shift between homeostatic and dysbiotic microbial communities (34). Virulence factors of *S.* Typhimurium trigger a shift in epithelial energy metabolism from mitochondrial oxidative phosphorylation to aerobic glycolysis, thereby reducing epithelial oxygen consumption in the colonic epithelium (118). The resulting loss of epithelial hypoxia increases the amount of oxygen diffusing into the intestinal lumen, thereby disrupting anaerobiosis and driving a pathogen expansion through aerobic respiration (50, 59, 118) (**Fig. 1.5B**). Loss of epithelial hypoxia

in the colon is also induced by virulence factors of *Citrobacter rodentium*, a murine pathogen that expands in the colonic microbiota by exploiting the resulting increase in luminal oxygen bioavailability to fuel its growth (9, 11, 150, 151). Reduced mitochondrial bioenergetics in the colonic epithelium are not only linked to aerobic growth of enteric pathogens, but also contribute to a weakening of colonization resistance against commensal *Enterobacterales* in mouse models of non-communicable diseases, such as ulcerative colitis (152, 153) or colorectal cancer (154). Collectively, these data suggest that physiological hypoxia of the colonic surface limits growth of *Enterobacterales* during homeostasis (34, 36). However, conditions that reduce mitochondrial bioenergetics in the colonic epithelium increase the luminal availability of host-derived oxygen, thereby creating a state of abnormal habitat filtering that lowers colonization resistance against *Enterobacterales* (155).

Notably, a loss of epithelial hypoxia weakens colonization resistance against *S.* Typhimurium even in the presence of normal concentrations of microbiota-derived short-chain fatty acids (89). These results appear to be at odds with *in vitro* findings that the presence of short-chain fatty acids inhibits growth of *Enterobacterales* in murine fecal homogenates, and that oxygen alone is not sufficient to overcome this growth inhibition (108). A factor lacking in the *in vitro* experiments is a shift in epithelial energy metabolism, which is required to lower colonization resistance against an avirulent *S.* Typhimurium strain (i.e. a strain lacking both type III secretion systems [T3SSs]) in mice harboring normal levels of microbiota-derived short-chain fatty acids (89). These observations suggest that when cells derive energy through aerobic glycolysis (the conversion of

glucose into lactate even in the presence of oxygen (156)), the epithelium releases factors in addition to oxygen that weaken colonization resistance against *S.* Typhimurium.

Metabolite profiling reveals that lactate is the most abundant metabolite in the gut lumen during *S.* Typhimurium-induced colitis, while only small amounts of this compound are detected in mock-infected mice (59). A similar increase in the luminal lactate concentration is also observed after antibiotic treatment, but this increase is blunted when mice are treated with a PPAR-γ (peroxisome proliferator-activated receptor gamma) agonist that polarizes host cell metabolism towards oxidative phosphorylation, which is consistent with the idea that an increase in the luminal lactate concentration is mostly derived from a conversion of glucose into lactate by host cells (59). During its expansion in the gut microbiota, *S.* Typhimurium converts lactate into pyruvate using a NAD-independent lactate dehydrogenase (encoded by *lldD*), which transfers electrons from lactate to oxygen using cytochrome *bd* oxidase (encoded by *cydA*), thus linking lactate utilization in the gut to the presence of host-derived oxygen (59). Notably, *S.* Enteritidis can overcome growth inhibition by short-chain fatty acids *in vitro* when lactate is added to murine fecal homogenates (53), pointing to catabolism of host-derived lactate as a possible mechanism to overcome niche modification by microbiota-derived short-chain fatty acids. Finally, the terminal steps in acetate production through the phosphotransacetylase-acetate kinase (Pta-AckA) pathway are required for *S.* Typhimurium to overcome colonization resistance in chickens (157). Thus, it is tempting to speculate that epithelial release of lactate and oxygen cooperatively enables *S.* Typhimurium to ramp up intracellular acetate production to limit diffusion of microbiota-

derived acetic acid into the cytosol, thereby preventing disruption of pH homeostasis. However, additional work is needed to test this hypothesis.

Considering all of these studies suggests that an increased abundance of *Enterobacterales* is a microbial signature of dysbiosis that often involves abnormal habitat filtering by the host. During homeostasis, epithelial hypoxia limits the availability of respiratory electron acceptors (i.e. oxygen and nitrate), thereby filtering the habitat to ensure *Enterobacterales* remain minority species within the colonic microbiota. However, intestinal inflammation and/or a loss of epithelial hypoxia weaken colonization resistance by inducing a state of abnormal habitat filtering. In turn, abnormal habitat filtering leads to an elevated release of host-derived critical resources that enable commensal and pathogenic *Enterobacterales* to overcome niche modification by microbiota-derived short-chain fatty acids. The abundance of these limiting resources determines the abundance of *Enterobacterales* in the gut microbiota. In other words, limited availability of critical resources, such as respiratory electron acceptors and lactate, keeps a tight rein on *Enterobacterales*, which is responsible for the low abundance of this taxon during homeostasis. However, conditions that enlarge the availability of limiting resources drive dysbiosis characterized by an *Enterobacterales* expansion.

Niche Preemption by Endogenous *Enterobacterales*

Competition with closely related species. In addition to habitat filtering by the microbiota and the host, colonization resistance against *Salmonella* serovars also involves competition with closely related bacterial species that are resident in the gut

microbiota. Commensal species within the *Enterobacterales* that are closely related genetically to *Salmonella* serovars (103) are a normal constituent in the fecal microbiota of humans (35) and other mammals (158). There are currently no approaches to specifically deplete *Enterobacterales* from the gut microbiota to ascertain their contribution to colonization resistance. However, not all laboratory mice harbor endogenous *Enterobacterales* (51), which is due to variability in animal husbandry practices between vendors. Many vendors of laboratory mice engraft germ-free animals with altered Schaedler flora (159) to establish a baseline microbiota in their foundation breeding colonies, prior to transferring animals into barrier production, where microbiota assembly proceeds while animals are screened to prevent specific pathogens from entering the colony (specific pathogen-free mice) (160). The screening procedures for specific pathogens differ between vendors, resulting in mice from some suppliers to remain *Enterobacterales*-free, while specific pathogen-free procedures from others do not exclude commensal or opportunistic *Enterobacterales* from engrafting during microbiota assembly. Notably, comparison of genetically similar mice from different vendors reveals that the presence of endogenous *Enterobacterales*, which are minority species in the gut microbiota, results in a 100-fold increase in colonization resistance against *S.* Typhimurium, illustrating that competition with closely related species plays an important role in protecting against infection (51). Commensal *Enterobacterales*, such as *E. coli*, also enhance colonization resistance against *Salmonella* serovars in gnotobiotic mice (161), gnotobiotic piglets (162), day-of-hatch chicks (50) or in a mouse model of high-fat diet (163).

Keystone species limit the availability of critical resources. Recent work is beginning to elucidate the mechanisms through which endogenous *Enterobacterales* contribute to colonization resistance against *Salmonella* serovars. Germ-free mice engrafted with defined microbial communities fail to confer colonization resistance against *S.* Typhimurium when pathways involved in microbial respiration are underrepresented compared to microbiota of conventional mice (164). However, colonization resistance can be strengthened by supplementing the defined microbial community with facultative anaerobic species, including *E. coli*, *Streptococcus danieliae* and *Staphylococcus xylosus*, a correlation that points to the presence of respiratory pathways in the microbial community as a factor important for protection against *S.* Typhimurium infection (164). Interestingly, a commensal avian *E. coli* isolate competes more successfully with *S.* Enteritidis for oxygen when the commensal establishes gut colonization in neonatal chicks prior to pathogen challenge, compared to when both species are introduced simultaneously (50). This finding suggests that endogenous *Enterobacterales* have a competitive advantage over similar species that attempt to enter the ecosystem since priority effects provide them with access to growth-limiting resources. Although the precise mechanisms by which niche preemption enables endogenous *Enterobacterales* to gain priority access to oxygen remain obscure, an intact aerobic metabolism (i.e. a functional cytochrome *bd* oxidase) is required for endogenous *E. coli* to confer colonization resistance against *Salmonella* serovars in mice (51). Thus, one of the mechanisms contributing to colonization resistance against *Salmonella* serovars is competition with endogenous *Enterobacterales* for host-derived respiratory electron acceptors.

In addition to respiratory electron acceptors, *Enterobacterales* compete for nutritional resources. For example, the concentrations of many monosaccharides become elevated in colon contents during antibiotic treatment (123), which supports growth of *S.* Typhimurium in the gut (165, 166). Some monosaccharides become oxidized (167), because an antibiotic-mediated depletion of short-chain fatty acids induces nitric oxide production by recruiting inflammatory monocytes to the colonic mucosa (168) and by increasing inducible nitric oxide synthase (iNOS) production in the colonic epithelium (89). Oxidation of monosaccharides by RNS in the gut lumen generates acidic sugars, such as glucarate and galactarate, which drive a post-antibiotic expansion of *S.* Typhimurium (167). There is evidence to suggest that pathogen engraftment in the microbiota can be blocked through nutrient competition with endogenous *Enterobacterales. Klebsiella michiganensis* is a commensal member of the *Enterobacterales* that confers colonization resistance against *E. coli* in a mouse model (169). However, *K. michiganensis*-mediated colonization resistance against *E. coli* is lost when mice receive galacitol, a poorly absorbed sugar alcohol that reaches the colon, where it promotes growth of *E. coli* over *K. michiganensis*, because the latter cannot utilize this carbon source (169). These data suggest that antibiotic treatment generates an environment in which growth of *Enterobacterales* is fueled by monosaccharide catabolism. Niche preemption mediated by endogenous *Enterobacterales* likely involves competition for these critical resources with pathogens that attempt to enter the ecosystem.

In essence, although members of the *Enterobacterales* are minority species within the gut microbiota that are often present at levels below the limit of detection by

conventional microbiota profiling (51), they play a key role in conferring protection against facultative anaerobic pathogens, such as *Salmonella* serovars. Thus, endogenous *Enterobacterales* have a disproportionally large effect on colonization resistance relative to their abundance within the microbial community, which renders them keystone species. Studies on the underlying mechanism reveal that endogenous *Enterobacterales* contribute to colonization resistance through niche preemption, a process that involves competition with *Salmonella* serovars for critical resources, such as respiratory electron acceptors and monosaccharides.

Niche Opportunities Created by Virulence Factors

Ecosystem Engineering by Virulence Factors Licenses Pathogen Engraftment

Pathogens overcome colonization resistance - opportunists do not. A mature gut microbiota is resistant to change (45, 56, 57), because the microbiome prevents engraftment of newly arriving commensal or opportunistic microbes through competition and habitat filtering (49). The phenomenon of microbiota resistance is testament to the fact that once the microbiota reaches a stable equilibrium state, priority effects pose an all but impenetrable barrier to engraftment of new commensal or opportunistic bacterial species belonging to the *Enterobacterales*. For example, priority effects prevent replacement of resident endogenous *Enterobacterales* present in the human fecal microbiota (35), with recently emerged opportunistic pathogens, such as carbapenem-resistant *Enterobacteriaceae* (CRE), thereby limiting community spread of CRE. Due to priority effects, the only way for opportunistic CRE to engraft in the gut microbiota is during microbiota assembly or after microbiota disruption (e.g. after antibiotic therapy). Disruption of the microbiota with antibiotics can clear a niche (54) and provide an advantage for opportunistic CRE over antibiotic-sensitive competitors. As a result, an antibiotic-mediated disruption of the gut microbiota predisposes patients in the intensive care unit to developing carriage and nosocomial infection with CRE, which commonly includes strains of *Klebsiella pneumoniae* and *E. coli* (170-174). Due to weakened colonization resistance in individuals on broad-spectrum antibiotics, nosocomial CRE infections are readily transmitted between patients by hospital workers. In turn, a weakening of colonization resistance drives an expansion of CRE in the gut microbiota,

which is a source of opportunistic bloodstream infections in immunocompromised patients (175, 176). Due to lack of treatment options, 40% of CRE infections lead to death (177, 178), which makes these opportunistic pathogens one of the most urgent threats to public health worldwide (179).

A key difference between infection with opportunistic pathogens, such as CRE, and pathogens, such as *Salmonella* serovars, is that only the latter can overcome host defenses in individuals with an intact immune system. In other words, whereas CRE infection requires that colonization resistance is weakened by antibiotics, *Salmonella* serovars can engraft in individuals even when their microbiota-nourishing immunity is intact. In immunocompetent individuals, both CRE and *Salmonella* serovars initially enter an ecosystem that does not support their growth because the host and the microbiota limit critical resources through competition and habitat filtering. As a result, CRE numbers decline, resulting in an extinction of the opportunistic pathogen. Colonization resistance can also lead to an extinction of *Salmonella* serovars, particularly when the challenge dose is low (51) (**Fig 1.6)**. However, if the challenge dose is high enough to ensure the pathogen can deploy its virulence factors prior to becoming extinct, the initial decline in *S.* Typhimurium numbers is halted and followed by a marked expansion, resulting in pathogen engraftment in the gut ecosystem (118). *S.* Typhimurium virulence factors are long known to trigger disease in an immunocompetent host (180-182), a characteristic that distinguishes pathogens from opportunists, but the importance of virulence factors in overcoming colonization resistance has come to light only recently (7, 8). Importantly, virulence factors of *S.* Typhimurium weaken colonization resistance not by targeting the

microbiota, but by manipulating the physiology of host cells, thereby inducing a state of abnormal habitat filtering that opens new niche opportunities (183).

Virulence factors carve out a new nutrient-niche for the pathogen. The main virulence factors of *S.* Typhimurium are two T3SSs that enable the pathogen to invade the epithelial lining (T3SS-1)(180) and survive in host tissue (T3SS-2)(181). Each T3SS injects several dozen proteins, called effectors, into the cytosol of epithelial cells (for T3SS-1) or macrophages (for T3SS-2)(184) to induce bacterial entry (185) or ensure the spread of bacteria in tissue (186), respectively. For a detailed discussion type III secreted effector proteins and their activity on host cell physiology, the reader is referred to a recent review article devoted to this subject (187).

The presence of bacteria in tissue induces sterilizing immunity by activating pathogen recognition receptors (188-193), thereby triggering innate immune responses that orchestrate severe acute intestinal inflammation (182, 194, 195). Detection of fecal leukocytes in salmonellosis patients illustrates that *Salmonella*-induced intestinal inflammation is accompanied by migration of phagocytes into the intestinal lumen (196), where these host cells contribute to the production of tetrathionate and nitrate as discussed above (10, 141)(**Fig 1.6)**. In addition, migration of neutrophils into the intestinal lumen leads to a depletion of *Clostridia* (197, 198), the main butyrate producers in the gut microbiota (116, 117), thereby reducing butyrate concentrations in colon contents (118). Since butyrate is an agonist of PPAR-γ, a nuclear receptor that activates mitochondrial bioenergetics in the colonic epithelium, depletion of this short-chain fatty acid shifts the epithelial energy metabolism towards aerobic glycolysis, thereby increasing epithelial

oxygenation and diffusion of oxygen into the intestinal lumen (89, 118). *Salmonella*-induced colitis also makes host-derived lactate the most abundant metabolite in the gut lumen (59).

Collectively, these virulence factor-induced changes in the gut environment trigger a state of abnormal habitat filtering, which is characterized by markedly elevated luminal concentrations of critical resources to support pathogen growth, including tetrathionate (10), nitrate (144, 145), oxygen (118) and lactate (59) (**Fig 1.6)**. These observations establish the concept that *S.* Typhimurium uses its virulence factors for ecosystem engineering, a process culminating in the generation of a new nutrient-niche that supports pathogen engraftment into the gut ecosystem (94, 183). The consequent expansion of *S.* Typhimurium in the gut microbiota is required for pathogen transmission by the fecal-oral route (118, 199), which represents the principal driving force of natural selection for this strategy of ecosystem invasion.

New niche opportunities create competition. A drawback of ecosystem engineering is that the new nutrient-niche generated by *S.* Typhimurium virulence factors can also be occupied by endogenous *Enterobacterales*. Since *S.* Typhimurium and endogenous *Enterobacterales* encounter the newly engineered nutrient-niche simultaneously, presumably neither one gains an advantage through priority effects, which levels the playing field. During the fierce competition that ensues for niche occupancy, contestants deploy antimicrobial weaponry to gain the upper hand in battling for critical resources. *S.* Typhimurium-induced intestinal inflammation increases concentrations of bile acids in the colon (200), a signal to induce expression of a type VI

secretion system (T6SS), which is used by the pathogen to kill commensal competitors, such as *K. oxytoca* (201) (**Fig. 1.6)**. One of the resources *S.* Typhimurium and endogenous *Enterobacterales* compete for is iron, because the availability of this trace element is reduced in the inflamed gut. Reduced iron availability during inflammation requires bacteria to release small molecular weight ferric iron chelators, termed siderophores, to acquire this essential metal (202). The siderophore produced by most *Enterobacterales*, enterobactin, is neutralized by the host protein lipocalin-2 (203, 204), which is released into the gut lumen during intestinal inflammation (205, 206). *Salmonella* serovars adapt to this environment by producing a glycosylated derivative of enterobactin, termed salmochelin (207), which is not neutralized by lipocalin-2 (208), thus providing the pathogen with a growth advantage over competitors that rely solely on enterobactin for iron acquisition (209). However, the probiotic *E. coli* strain Nissle 1917 releases salmochelin-derivatives conjugated to antimicrobial peptides, termed microcins M and H47 (210), which are internalized by salmochelin uptake systems of *Salmonella* serovars, thereby providing the commensal with a competitive advantage over the pathogen (211). The need to synthesize outer membrane siderophore receptors in the inflamed gut also provides an opportunity to battle related *Enterobacterales* by releasing colicins, which are bacteriocins with limited host range that commonly use siderophore receptors to enter their target cell (212). However, the T6SS is only induced when inflammation increases the concentration of bile acids (201) and neither microcins nor colicins provide a competitive advantage in the absence of intestinal inflammation, because iron limitation generated by this host response induces expression of receptors for microcins and

colicins in *Enterobacterales* (211, 212). Thus, *Enterobacterales* restrict the use of their antimicrobial weaponry to a state of abnormal habitat filtering.

All things considered, colonization resistance of mature microbial communities constitutes a formidable barrier that blocks an engraftment of commensal or opportunistic *Enterobacterales*. As a result, windows of opportunity for engrafting these species are limited to microbiota assembly in childhood or to episodes of weakened colonization resistance, which can be induced, for example, by antibiotics (**Fig. 1.3A**). In contrast, pathogenic *Enterobacterales*, such as *Salmonella* serovars, can overcome colonization resistance in immunocompetent individuals by using their virulence factors for ecosystem engineering (**Fig 1.6)**. The pathogen remodels the gut ecosystem by using its virulence factors to trigger intestinal inflammation. The consequent changes in the metabolite landscape create a state of abnormal habitat filtering that provides niche opportunities, which is a crucial determinant of the pathogen's success in ecosystem invasion. Importantly, this strategy for ecosystem invasion is limited to pathogens, because ecosystem engineering by virulence factors generates collateral damage, thereby producing signs of disease, the defining characteristic of pathogens. However, a drawback of this strategy for ecosystem invasion is that virulence factors engineer a nutrient-niche that also accommodates related *Enterobacterales* species. As a result, the nutrient-niche engineered by virulence factors of the pathogen provides a playground in which *S.* Typhimurium and endogenous *Enterobacterales* use their antimicrobial weaponry to fight for supremacy (94).

Reconstructing *Salmonella's* Nutrient-Niche from the Ruins

Genome-guided assembly of a metabolic network for gut colonization. Information on how intestinal inflammation alters the luminal habitat is key to understanding why this condition gives rise to imbalances in the gut microbiota that are linked to various non-communicable diseases, such as IBD (152), colorectal cancer (77) or cardiovascular disease (78). Intestinal inflammation induced by *Salmonella* serovars can be used to model this state of abnormal habitat filtering, but our knowledge of the consequent changes in the luminal environment is still incomplete. The metabolic pathways the pathogen uses to fuel its growth in the inflamed gut can provide a window into the nutrient-niche *S.* Typhimurium occupies, which in turn offers clues about how inflammation alters the habitat of the gut microbiota (96). Notably, an experiment of nature makes it possible to identify these metabolic pathways through whole genome comparison of *Salmonella* serovars (213-215).

Whereas the vast majority of *Salmonella* serovars are associated with gastroenteritis in humans, an infection that remains localized to the intestine and mesenteric lymph nodes, a few specialists have evolved to cause exclusively extraintestinal disease (e.g. *S.* Typhi) (216, 217). These specialists transmit from an extraintestinal reservoir (e.g. the gall bladder in case of *S.* Typhi) and no longer cause gastroenteritis in their respective hosts, thereby removing the driving force of natural selection for maintaining metabolic pathways required for growth in the inflamed gut (120). Consequently, genes that provide an adaptation to the nutrient-niche gastrointestinal *Salmonella* serovars (e.g. *S.* Typhimurium) occupy in the inflamed intestine are dispensable in extraintestinal *Salmonella* serovars and are beginning to

randomly degrade by point mutation. This ongoing experiment of nature explains the large numbers of degraded genes (pseudogenes) detected in the genomes of extraintestinal *Salmonella* serovars compared to gastrointestinal pathogens (218-222), a prominent genetic fingerprint that resembles an unsaturated mutagenesis of the pathways required for pathogen growth in the lumen of the inflamed gut (213, 223, 224). However, the emergence of extraintestinal *Salmonella* serovars is a relatively recent event linked to the Neolithic transition towards an agricultural and pastoralist economy (225, 226), suggesting that there was limited time for genome decay to leave its mark on their genomes. Since the process of genome degradation is quite incomplete, analysis of a single *Salmonella* serovar does not unveil a decaying metabolic network. Instead, whole genome comparison of multiple extraintestinal and gastrointestinal *Salmonella* serovars is required to bring a network of genes to light that is degrading in genomes of extraintestinal pathogens but intact in genomes of gastrointestinal pathogens (**Fig. 1.7**) (213-215).

The metabolic network identified by such an *in silico* analysis contains more than 400 genes (213), only a fraction of which has yet been tested experimentally for their contribution to growth in an inflamed intestine (**Fig. 1.7**). The emerging experimental validation of these *in silico* predictions shows that genes for the import of host-derived lactate (*lldP*) and its cytochrome *bd* oxidase-dependent conversion into pyruvate (*lldD*), are required for luminal growth of *S.* Typhimurium during colitis (59). Pyruvate generated through this reaction can be converted by pyruvate formate lyase (encoded by *pflDC*) into acetyl-CoA and formate, two metabolites important for growth in the gut. The conversion of acetyl-CoA into acetate (*ackA pta*) is required for intestinal colonization of *S.* Enteritidis

(157). Formate is degraded to carbon dioxide (CO_2) and hydrogen (H_2) by a nitrate respiration-dependent formate dehydrogenase (encoded by *fdnGHI*), which is required for growth of *E. coli* in the inflamed intestine (153). Hydrogen generated through this reaction supports growth of *S.* Typhimurium in the gut by serving as an electron donor (*hybOABCDEFG*) (227) for fumarate respiration (*frdABCD*), which is powered by exogenous aspartate or malate (*dcuABC*, *aspA* and *fumB*) (124). Chemotaxis towards nitrate (encoded by *tsr*) (228), nitrate respiration (mediated by a periplasmic nitrate reductase encoded by *napFDAGHBC*) (145) and tetrathionate respiration (mediated by a tetrathionate reductase encoded by *ttrABC*) (10) are required for growth of *S.* Typhimurium in the niche it occupies in the inflamed intestine, in part because anaerobic respiration powers bacterial microcompartments that function in the catabolism of microbiota-derived fermentation products, including 1,2-propanediol (*pduABCDEGHJKLMNOPQSTUVWX*) (229) and ethanolamine (*eutSPQTDMNEJGHABCLKR*) (230). Nitrate respiration is also required for *S.* Typhimurium to catabolize microbiota-derived fermentation products, including succinate (231) (*sdhCDAB*) and butyrate (*ydiFO ydiQRST fadHIJK*) (232, 233). Finally, catabolism of some monosaccharides plays a role during *S.* Typhimurium gut colonization, as shown for fucose (*fucAO fucPIKUR*), glucarate (*gudDT*) and galactarate (*garDL STM2959*) (165, 167). Thus, the computer-generated concept that gene decay in extraintestinal *Salmonella* serovars defines a large metabolic network required for growth of gastrointestinal *Salmonella* serovars in the gut lumen (213-215) has been validated by numerous experimental studies (59, 124, 145, 153, 157, 167, 229, 231, 233). However, the majority of genes in this web still remain to be analyzed.

Predicting the metabolic landscape in *Salmonella's* nutrient-niche. Glancing at the hypothetical metabolic pathways identified by comparative genome analysis (213) provides a preview of the resources that might be available in the nutrient-niche engineered by *S.* Typhimurium virulence factors. The metabolic network suggests that *S.* Typhimurium has access to numerous monosaccharides (including glucose, gluconate, galactose, galactonate, trehalose, rhamnose, ribose, xylose, arabinose, idonate, 2,3-diketo-gulonate, hexunonate, and galacitol) and amino acids (including serine, histidine, arginine, glutamate, aspartate and proline) (**Fig. 1.7**), indicating its nutrient-niche differs from the habitat of the non-inflamed gut, where the microbiota depletes these critical resources (119, 165). It is also apparent from this model that the inflammatory host response might generate several respiratory electron acceptors in addition to nitrate (144), tetrathionate (10) and oxygen (118), which includes sulfite, thiosulfate, nitric oxide, nitrite, *S*-oxides (R_2-SO) and *N*-oxides (R_3-N^+-O^-), such as trimethylamine *N*-oxide (TMAO) (**Fig. 1.7**). Whereas nitric oxide is directly derived from inflammatory monocytes (141), *S*-oxides and *N*-oxides can be generated in the gut lumen when ROS and RNS diffuse away from host cells and react with organic sulfides and tertiary amines present in the intestinal lumen (234, 235). Furthermore, ROS and RNS released by luminal phagocytes react to form nitrate and tetrathionate, which are converted to nitrite and thiosulfate through nitrate respiration and tetrathionate respiration, respectively (10, 141, 147). Finally, sulfite is the product of thiosulfate respiration (236). Thus, the projected generation of an array of different respiratory electron acceptors in the gut lumen (**Fig.**

1.7) is expected to require recruitment of phagocytes into the intestinal lumen, which is a by-product of intestinal inflammation triggered by *S.* Typhimurium virulence factors (131).

In a nutshell, *in silico* analysis predicts that T3SS-1 and T3SS-2-mediated intestinal inflammation engineers a nutrient-niche that is characterized by an increased availability of diverse repertoires of monosaccharides, amino acids and respiratory electron acceptors (213). These sweeping changes in the luminal metabolite landscape are projected to create a state of abnormal habitat filtering to support pathogen engraftment and drive its expansion in the gut microbiota, which is required for transmission (118, 199). The latter provides the ultimate driving force of natural selection that maintains the metabolic network depicted in **Fig. 1.7** in gastrointestinal *Salmonella* serovars (213).

Concluding Remarks

What *Salmonella* serovars teach us about dysbiosis

To summarize the above, the host and its microbiota cooperate to execute a non-specific host defense mechanism, termed colonization resistance, which prevents ecosystem invasion by opportunistic pathogens. Microbiota-derived short-chain fatty acids filter the environment to exclude bacteria lacking mechanisms to maintain pH homeostasis with the available resources. The resources used for maintenance of pH homeostasis in *Clostridia* and *Bacteroidia* remain to be described, but the dominance of these obligate anaerobic bacteria in the gut microbiota is testament to their ability to avert disruption of pH homeostasis by short-chain fatty acids. Facultative anaerobic *Enterobacterales*, on the other hand, require respiratory electron acceptors (such as oxygen and nitrate) and additional unidentified host-derived resources to overcome growth inhibition by short-chain fatty acids. Hence, the availability of these critical resources determines the abundance of *Enterobacterales* within the gut microbiota. During homeostasis, epithelial hypoxia severely limits the availability of respiratory electron acceptors, thereby relegating *Enterobacterales* to an existence as minority species within the gut microbiota (**Fig. 1.2**). Despite their low abundance, these minority species have a disproportionally large effect on colonization resistance against *Salmonella* serovars by limiting the pathogen's access to critical resources through priority effects, which identifies endogenous *Enterobacterales* as keystone species within the gut microbiota.

During homeostasis, engraftment of opportunistic pathogens, such as CRE, is efficiently blocked through niche modification by microbiota-derived short-chain fatty acids, habitat filtering by epithelial hypoxia and niche preemption by endogenous *Enterobacterales*. However, frank pathogens, such as gastrointestinal *Salmonella* serovars, can use their virulence factors to overcome these defenses in an immunocompetent individual by disturbing host-mediated habitat filtering. Ecosystem invasion forces gastrointestinal *Salmonella* serovars to overcome growth inhibition by microbiota-derived short-chain fatty acids, an ecological problem demanding an increased availability of critical resources, such as respiratory electron acceptors, that are kept in short supply by host-mediated habitat filtering and are poorly accessible to the pathogen due to competition with endogenous *Enterobacterales.* Success in gut ecosystem invasion requires the pathogen to endure until its virulence factors generate inflammatory host responses that boost the luminal availability of these critical resources, an outcome that becomes more likely when the challenge dose is high. Framing the outcome of infection as an ecological problem highlights the importance of virulence factors in remodeling the gut ecosystem by triggering inflammation, a host response that ultimately creates a state of abnormal habitat filtering, thereby providing new niche opportunities for the pathogen. These considerations identify gastrointestinal *Salmonella* serovars as ecosystem engineers, a pathogenic strategy inevitably linked to disease (i.e. gastroenteritis).

S. Typhimurium virulence factors engineer a nutrient-niche that also accommodates related *Enterobacterales* species (**Fig. 1.6**). Thus, the state of abnormal habitat filtering created by *S.* Typhimurium virulence factors might share features with

non-communicable diseases associated with an expansion of *Enterobacterales* in the fecal microbiota (37, 237). Notably, *S.* Typhimurium virulence factors induce this state of abnormal habitat filtering by targeting only the host (7, 10, 118, 144). Extrapolating this insight to non-communicable diseases suggests that a dysbiotic *Enterobacterales* expansion in the fecal microbiota is secondary to an underlying defect in host-mediated habitat filtering (34, 36, 131). Recent studies using mouse models of IBD and colorectal cancer provide compelling experimental support for this concept (147, 148, 150, 152-154, 238). Thus, lessons learned from studying *S.* Typhimurium ecosystem invasion paved the way for developing a mechanistic understanding of factors driving a microbial signature of dysbiosis in the fecal microbiota, which is observed in a spectrum of non-communicable diseases.

Where do we go from here?

New strategies to rebalance the microbiota. The finding that dysbiosis is linked to many human diseases has generated hopes that microbiome research will identify novel treatment strategies. Whereas targeting the microbes themselves with fecal microbiota transplants (239), probiotics (240), antibiotics (241), or precision editing of the microbiota (148, 238) shows promise in treating some conditions, great challenges remain to adapt these therapies to the broad spectrum of diseases associated with dysbiosis. By trailblazing the concept that an expansion of *Enterobacterales* in the fecal microbiota is a signature of dysbiosis that is triggered by an underlying defect in host-mediated habitat filtering (34, 36, 131), research on *S.* Typhimurium pathogenesis has

created great prospects for identifying alternative treatment targets for remediating dysbiosis. Provided that dysbiosis results from abnormal habitat filtering by the host, it stands to reason that the microbiota can be rebalanced by normalizing host-mediated habitat filtering. A proof of concept for this therapeutic strategy comes from studies on IBD. Environmental risk factors for IBD include a history of antibiotic usage and a Western-style high-fat diet (242-244). These environmental risk factors cooperate to reduce mitochondrial bioenergetics in the colonic epithelium, thereby increasing epithelial oxygenation in the murine colon (152). In turn, oxygen emanating from the epithelial surface drives an expansion of endogenous *Enterobacterales* in the fecal microbiota, which exacerbates pre-IBD (152). Treatment with an agonist of PPAR-γ, a nuclear receptor in the colonic epithelium that activates mitochondrial bioenergetics, restores epithelial hypoxia, thereby blunting an *Enterobacterales* expansion in mice with pre-IBD (152) and in ulcerative colitis patients (245). Thus, host-derived habitat filters represent promising treatment targets for rebalancing the microbiota in a broad range of non-communicable diseases linked to gut dysbiosis.

Expanding the microbiome toolbox. Studies on *S.* Typhimurium ecosystem invasion have provided first insights into how normal habitat filtering can be disrupted, but our understanding of host-derived habitat filters in the colon is still incomplete. Furthermore, identifying host-derived habitat filters that govern microbiota assembly at body surfaces other than the colon represents an immense task that remains to be achieved before we can hope to understand dysbiosis at these habitats. Following the example of *Salmonella* serovars, virulence factors of pathogens colonizing other

surfaces, such as the respiratory tract or the reproductive tract, provide countless opportunities for identifying host-derived habitat filters at these sites. In turn, this information is expected to reveal what conditions contribute to normal habitat filtering at these body surfaces and how virulence factors induce a state of abnormal habitat filtering that enables pathogens to invade the respective ecosystem. Researchers in bacterial pathogenesis are well-positioned to produce such mechanistic insights into how normal habitat filtering maintains homeostasis at various body surfaces. Input from the bacterial pathogenesis field will be needed to identify habitat filters, because this information cannot be gleaned simply from cataloging bacterial species names. In turn, identification of habitat filters will aid in the interpretation of microbiota profiling data, by linking microbial signatures of dysbiosis to the disruption of habitat filtering by virulence factors. As more information becomes available, it might become possible to read microbiota profiling data in ways similar to a blood test result. In the not so distant future, a microbial signature of dysbiosis at a given body surface might indicate an underlying defect in a specific host-derived habitat filter, which in turn might suggest a treatment aimed at normalizing that function. These prospects make the study of ecosystem invasion by mucosal pathogens one of the most exciting emerging areas in microbiome research.

Acknowledgements

A.W.L.R. was supported by Public Health Service grant AI060555. Work in R.M.T.'s laboratory was supported by Public Health Service grants AI143253, AI149632, AI112949, AI089078, and AI109799. Work in A.J.B.'s laboratory was supported by award 650976 from the Crohn's and Colitis Foundation of America and by Public Health Service grants AI044170, AI096528, AI112949, AI146432, and AI153069.

References

1. Bordenave G. 2003. Louis Pasteur (1822-1895). Microbes Infect 5:553-60.

2. Koch R. 1882. Die Aetiologie der Tuberkulose. Berliner klinische Wochenschrift 15:221–230.

3. Roux E YA. 1888. Contribution à l'étude de la diphtérie Ann Inst Pasteur 2:421–99.

4. Neisser M, Shiga K. 1903. Ueber freie Receptoren von Typhus- und Dysenteriebazillen und über das Dysenterietoxin. Dtsch Med Wochenschr 29:61–62.

5. Conradi H. 1903. Über lösliche, durch aseptische Autolyse erhaltene Giftstoffe von Ruhr- und Typhus-Bazillen. . Dtsch Med Wochenschr 29:26–28.

6. Bohnhoff M, Drake BL, Miller CP. 1954. Effect of streptomycin on susceptibility of intestinal tract to experimental Salmonella infection. Proc Soc Exp Biol Med 86:132-7.

7. Stecher B, Robbiani R, Walker AW, Westendorf AM, Barthel M, Kremer M, Chaffron S, Macpherson AJ, Buer J, Parkhill J, Dougan G, von Mering C, Hardt WD. 2007. Salmonella enterica serovar typhimurium exploits inflammation to compete with the intestinal microbiota. PLoS Biol 5:2177-89.

8. Barman M, Unold D, Shifley K, Amir E, Hung K, Bos N, Salzman N. 2008. Enteric salmonellosis disrupts the microbial ecology of the murine gastrointestinal tract. Infect Immun 76:907-15.

9. Kamada N, Kim YG, Sham HP, Vallance BA, Puente JL, Martens EC, Nunez G. 2012. Regulated virulence controls the ability of a pathogen to compete with the gut microbiota. Science 336:1325-9.

10. Winter SE, Thiennimitr P, Winter MG, Butler BP, Huseby DL, Crawford RW, Russell JM, Bevins CL, Adams LG, Tsolis RM, Roth JR, Baumler AJ. 2010. Gut inflammation provides a respiratory electron acceptor for Salmonella. Nature 467:426-9.

11. Lopez CA, Miller BM, Rivera-Chávez F, Velazquez EM, Byndloss MX, Chávez-Arroyo A, Lokken KL, Tsolis RM, Winter SE, Bäumler AJ. 2016. Virulence factors enhance Citrobacter rodentium expansion through aerobic respiration. Science 353:1249-53.

12. Kamdar K, Khakpour S, Chen J, Leone V, Brulc J, Mangatu T, Antonopoulos DA, Chang EB, Kahn SA, Kirschner BS, Young G, DePaolo RW. 2016. Genetic and Metabolic Signals during Acute Enteric Bacterial Infection Alter the Microbiota and Drive Progression to Chronic Inflammatory Disease. Cell Host Microbe 19:21-31.

13. Rivera-Chavez F, Mekalanos JJ. 2019. Cholera toxin promotes pathogen acquisition of host-derived nutrients. Nature 572:244-248.

14. Tipton L, Darcy JL, Hynson NA. 2019. A Developing Symbiosis: Enabling Cross-Talk Between Ecologists and Microbiome Scientists. Front Microbiol 10:292.

15. Berg G, Rybakova D, Fischer D, Cernava T, Verges MC, Charles T, Chen X, Cocolin L, Eversole K, Corral GH, Kazou M, Kinkel L, Lange L, Lima N, Loy A, Macklin JA, Maguin E, Mauchline T, McClure R, Mitter B, Ryan M, Sarand I, Smidt H, Schelkle B, Roume H, Kiran GS, Selvin J, Souza RSC, van Overbeek L, Singh BK, Wagner M, Walsh A, Sessitsch A, Schloter M. 2020. Microbiome definition re-visited: old concepts and new challenges. Microbiome 8:103.

16. Spiga L, Winter SE. 2019. Using Enteric Pathogens to Probe the Gut Microbiota. Trends Microbiol 27:243-253.

17. Pedron T, Nigro G, Sansonetti PJ. 2016. From homeostasis to pathology: decrypting microbe-host symbiotic signals in the intestinal crypt. Philos Trans R Soc Lond B Biol Sci 371.

18. Majowicz SE, Musto J, Scallan E, Angulo FJ, Kirk M, O'Brien SJ, Jones TF, Fazil A, Hoekstra RM. 2010. The global burden of nontyphoidal Salmonella gastroenteritis. Clin Infect Dis 50:882-9.

19. Ao TT, Feasey NA, Gordon MA, Keddy KH, Angulo FJ, Crump JA. 2015. Global burden of invasive nontyphoidal Salmonella disease, 2010(1). Emerg Infect Dis 21.

20. Loeffler F. 1892. Ueber Epidemieen unter den im hygienishcen Institute zu Greifswald gehaltenen Mäusen und über die Bekämpfung der Feldmausplage. Zbl Bakt Parasitenkunde 11:129-141.

21. Tsolis RM, Xavier MN, Santos RL, Baumler AJ. 2011. How to become a top model: impact of animal experimentation on human Salmonella disease research. Infect Immun 79:1806-14.

22. Carter PB, Collins FM. 1974. The route of enteric infection in normal mice. J Exp Med 139:1189-1203.

23. de Goffau MC, Lager S, Sovio U, Gaccioli F, Cook E, Peacock SJ, Parkhill J, Charnock-Jones DS, Smith GCS. 2019. Human placenta has no microbiome but can contain potential pathogens. Nature doi:10.1038/s41586-019-1451-5.

24. Cornwell WK, Schwilk LD, Ackerly DD. 2006. A trait-based test for habitat filtering: convex hull volume. Ecology 87:1465-71.

25. Walter J, Ley R. 2011. The human gut microbiome: ecology and recent evolutionary changes. Annu Rev Microbiol 65:411-29.

26. Davenport ER, Sanders JG, Song SJ, Amato KR, Clark AG, Knight R. 2017. The human microbiome in evolution. BMC Biol 15:127.

27. Tiffany CR, Baumler AJ. 2019. Dysbiosis: from fiction to function. Am J Physiol Gastrointest Liver Physiol 317:G602-G608.

28. Litvak Y, Baumler AJ. 2019. Microbiota-Nourishing Immunity: A Guide to Understanding Our Microbial Self. Immunity 51:214-224.

29. van Best N, Rolle-Kampczyk U, Schaap FG, Basic M, Olde Damink SWM, Bleich A, Savelkoul PHM, von Bergen M, Penders J, Hornef MW. 2020. Bile acids drive the newborn's gut microbiota maturation. Nat Commun 11:3692.

30. David LA, Maurice CF, Carmody RN, Gootenberg DB, Button JE, Wolfe BE, Ling AV, Devlin AS, Varma Y, Fischbach MA, Biddinger SB, Dutton RJ, Turnbaugh PJ. 2014. Diet rapidly and reproducibly alters the human gut microbiome. Nature 505:559-63.

31. Macarthur R, Levins R. 1967. Limiting Similarity Convergence and Divergence of Coexisting Species. American Naturalist 101:377-+.

32. Keddy PA. 1992. Assembly and Response Rules - 2 Goals for Predictive Community Ecology. Journal of Vegetation Science 3:157-164.

33. Zheng L, Kelly CJ, Colgan SP. 2015. Physiologic hypoxia and oxygen homeostasis in the healthy intestine. A Review in the Theme: Cellular Responses to Hypoxia. Am J Physiol Cell Physiol 309:C350-60.

34. Litvak Y, Byndloss MX, Baumler AJ. 2018. Colonocyte metabolism shapes the gut microbiota. Science 362.

35. Human Microbiome Project C. 2012. Structure, function and diversity of the healthy human microbiome. Nature 486:207-14.

36. Litvak Y, Byndloss MX, Tsolis RM, Baumler AJ. 2017. Dysbiotic Proteobacteria expansion: a microbial signature of epithelial dysfunction. Curr Opin Microbiol 39:1-6.

37. Shin NR, Whon TW, Bae JW. 2015. Proteobacteria: microbial signature of dysbiosis in gut microbiota. Trends Biotechnol 33:496-503.

38. Garrido D, Dallas DC, Mills DA. 2013. Consumption of human milk glycoconjugates by infant-associated bifidobacteria: mechanisms and implications. Microbiology 159:649-64.

39. Sela DA, Chapman J, Adeuya A, Kim JH, Chen F, Whitehead TR, Lapidus A, Rokhsar DS, Lebrilla CB, German JB, Price NP, Richardson PM, Mills DA. 2008. The genome sequence of Bifidobacterium longum subsp. infantis reveals adaptations for milk utilization within the infant microbiome. Proc Natl Acad Sci U S A 105:18964-9.

40. Sela DA, Mills DA. 2010. Nursing our microbiota: molecular linkages between bifidobacteria and milk oligosaccharides. Trends Microbiol 18:298-307.

41. Shepherd ES, DeLoache WC, Pruss KM, Whitaker WR, Sonnenburg JL. 2018. An exclusive metabolic niche enables strain engraftment in the gut microbiota. Nature 557:434-438.

42. Sonnenburg JL, Xu J, Leip DD, Chen CH, Westover BP, Weatherford J, Buhler JD, Gordon JI. 2005. Glycan foraging in vivo by an intestine-adapted bacterial symbiont. Science 307:1955-9.

43. El Kaoutari A, Armougom F, Gordon JI, Raoult D, Henrissat B. 2013. The abundance and variety of carbohydrate-active enzymes in the human gut microbiota. Nat Rev Microbiol 11:497-504.

44. Mackie RI, Sghir A, Gaskins HR. 1999. Developmental microbial ecology of the neonatal gastrointestinal tract. Am J Clin Nutr 69:1035S-1045S.

45. Sprockett D, Fukami T, Relman DA. 2018. Role of priority effects in the early-life assembly of the gut microbiota. Nat Rev Gastroenterol Hepatol 15:197-205.

46. Martinez I, Maldonado-Gomez MX, Gomes-Neto JC, Kittana H, Ding H, Schmaltz R, Joglekar P, Cardona RJ, Marsteller NL, Kembel SW, Benson AK, Peterson DA, Ramer-Tait AE, Walter J. 2018. Experimental evaluation of the importance of colonization history in early-life gut microbiota assembly. Elife 7.

47. Cornell HV, Lawton JH. 1992. Species Interactions, Local and Regional Processes, and Limits to the Richness of Ecological Communities - a Theoretical Perspective. Journal of Animal Ecology 61:1-12.

48. Pinto-Sanchez NR, Crawford AJ, Wiens JJ. 2014. Using historical biogeography to test for community saturation. Ecology Letters 17:1077-1085.

49. Fukami T. 2015. Historical Contingency in Community Assembly: Integrating Niches, Species Pools, and Priority Effects. Annu Rev Ecol Evol Syst 46:1-23.

50. Litvak Y, Mon KKZ, Nguyen H, Chanthavixay G, Liou M, Velazquez EM, Kutter L, Alcantara MA, Byndloss MX, Tiffany CR, Walker GT, Faber F, Zhu Y, Bronner DN, Byndloss AJ, Tsolis RM, Zhou H, Baumler AJ. 2019. Commensal Enterobacteriaceae Protect against Salmonella Colonization through Oxygen Competition. Cell Host Microbe 25:128-139 e5.

51. Velazquez EM, Nguyen H, Heasley KT, Saechao CH, Gil LM, Rogers AWL, Miller BM, Rolston MR, Lopez CA, Litvak Y, Liou MJ, Faber F, Bronner DN, Tiffany CR, Byndloss MX, Byndloss AJ, Baumler AJ. 2019. Endogenous Enterobacteriaceae underlie variation in susceptibility to Salmonella infection. Nat Microbiol doi:10.1038/s41564-019-0407-8.

52. Meynell GG, Subbaiah TV. 1963. Antibacterial mechanisms of the mouse gut. I. Kinetics of infection by Salmonella typhi-murium in normal and streptomycin-treated mice studied with abortive transductants. Br J Exp Pathol 44:197-208.

53. Bohnhoff M, Miller CP, Martin WR. 1964. Resistance of the Mouse's Intestinal Tract to Experimental Salmonella Infection. Ii. Factors Responsible for Its Loss Following Streptomycin Treatment. J Exp Med 120:817-28.

54. David LA, Materna AC, Friedman J, Campos-Baptista MI, Blackburn MC, Perrotta A, Erdman SE, Alm EJ. 2014. Host lifestyle affects human microbiota on daily timescales. Genome Biol 15:R89.

55. Faith JJ, Guruge JL, Charbonneau M, Subramanian S, Seedorf H, Goodman AL, Clemente JC, Knight R, Heath AC, Leibel RL, Rosenbaum M, Gordon JI. 2013. The long-term stability of the human gut microbiota. Science 341:1237439.

56. Sommer F, Anderson JM, Bharti R, Raes J, Rosenstiel P. 2017. The resilience of the intestinal microbiota influences health and disease. Nat Rev Microbiol 15:630-638.

57. Litvak Y, Baumler AJ. 2019. The founder hypothesis: A basis for microbiota resistance, diversity in taxa carriage, and colonization resistance against pathogens. PLoS Pathog 15:e1007563.

58. Tap J, Mondot S, Levenez F, Pelletier E, Caron C, Furet JP, Ugarte E, Munoz-Tamayo R, Paslier DL, Nalin R, Dore J, Leclerc M. 2009. Towards the human intestinal microbiota phylogenetic core. Environ Microbiol 11:2574-84.

59. Gillis CC, Hughes ER, Spiga L, Winter MG, Zhu W, Furtado de Carvalho T, Chanin RB, Behrendt CL, Hooper LV, Santos RL, Winter SE. 2018. Dysbiosis-Associated Change in Host Metabolism Generates Lactate to Support Salmonella Growth. Cell Host Microbe 23:54-64 e6.

60. Relman DA. 2012. The human microbiome: ecosystem resilience and health. Nutr Rev 70 Suppl 1:S2-9.

61. Proctor L. 2019. Priorities for the next 10 years of human microbiome research. Nature 569:623-625.

62. Petersen C, Round JL. 2014. Defining dysbiosis and its influence on host immunity and disease. Cell Microbiol 16:1024-33.

63. Olesen SW, Alm EJ. 2016. Dysbiosis is not an answer. Nat Microbiol 1:16228.

64. Backhed F, Ley RE, Sonnenburg JL, Peterson DA, Gordon JI. 2005. Host-bacterial mutualism in the human intestine. Science 307:1915-20.

65. Byndloss MX, Baumler AJ. 2018. The germ-organ theory of non-communicable diseases. Nat Rev Microbiol 16:103-110.

66. Gill SR, Pop M, Deboy RT, Eckburg PB, Turnbaugh PJ, Samuel BS, Gordon JI, Relman DA, Fraser-Liggett CM, Nelson KE. 2006. Metagenomic analysis of the human distal gut microbiome. Science 312:1355-9.

67. van Duynhoven J, Vaughan EE, Jacobs DM, Kemperman RA, van Velzen EJ, Gross G, Roger LC, Possemiers S, Smilde AK, Dore J, Westerhuis JA, Van de Wiele T. 2011. Metabolic fate of polyphenols in the human superorganism. Proc Natl Acad Sci U S A 108 Suppl 1:4531-8.

68. Stainier DY. 2005. No organ left behind: tales of gut development and evolution. Science 307:1902-4.

69. O'Hara AM, Shanahan F. 2006. The gut flora as a forgotten organ. EMBO Rep 7:688-93.

70. McFall-Ngai M. 2007. Adaptive immunity: care for the community. Nature 445:153.

71. Lee YK, Mazmanian SK. 2010. Has the microbiota played a critical role in the evolution of the adaptive immune system? Science 330:1768-73.

72. Olszak T, An D, Zeissig S, Vera MP, Richter J, Franke A, Glickman JN, Siebert R, Baron RM, Kasper DL, Blumberg RS. 2012. Microbial exposure during early life has persistent effects on natural killer T cell function. Science 336:489-93.

73. Hooper LV, Littman DR, Macpherson AJ. 2012. Interactions between the microbiota and the immune system. Science 336:1268-73.

74. Gallo RL, Hultsch T, Farnaes L. 2016. Recognizing that the microbiome is part of the human immune system will advance treatment of both cancer and infections. J Am Acad Dermatol 74:772-4.

75. Marchesi JR, Adams DH, Fava F, Hermes GD, Hirschfield GM, Hold G, Quraishi MN, Kinross J, Smidt H, Tuohy KM, Thomas LV, Zoetendal EG, Hart A. 2016. The gut microbiota and host health: a new clinical frontier. Gut 65:330-9.

76. Khlystova ZS. 1976. Lymph-Node and Spleen Morphology in Gnotobiotic Rats. Bulletin of Experimental Biology and Medicine 81:770-772.

77. Arthur JC, Perez-Chanona E, Muhlbauer M, Tomkovich S, Uronis JM, Fan TJ, Campbell BJ, Abujamel T, Dogan B, Rogers AB, Rhodes JM, Stintzi A, Simpson KW, Hansen JJ, Keku TO, Fodor AA, Jobin C. 2012. Intestinal inflammation targets cancer-inducing activity of the microbiota. Science 338:120-3.

78. Wang Z, Klipfell E, Bennett BJ, Koeth R, Levison BS, Dugar B, Feldstein AE, Britt EB, Fu X, Chung YM, Wu Y, Schauer P, Smith JD, Allayee H, Tang WH, DiDonato JA, Lusis AJ, Hazen SL. 2011. Gut flora metabolism of phosphatidylcholine promotes cardiovascular disease. Nature 472:57-63.

79. Trompette A, Gollwitzer ES, Yadava K, Sichelstiel AK, Sprenger N, Ngom-Bru C, Blanchard C, Junt T, Nicod LP, Harris NL, Marsland BJ. 2014. Gut microbiota metabolism of dietary fiber influences allergic airway disease and hematopoiesis. Nat Med 20:159-66.

80. Arrieta MC, Finlay BB. 2012. The commensal microbiota drives immune homeostasis. Front Immunol 3:33.

81. Al-Asmakh M, Zadjali F. 2015. Use of Germ-Free Animal Models in Microbiota-Related Research. J Microbiol Biotechnol 25:1583-8.

82. Bocci V. 1992. The neglected organ: bacterial flora has a crucial immunostimulatory role. Perspect Biol Med 35:251-60.

83. Dethlefsen L, McFall-Ngai M, Relman DA. 2007. An ecological and evolutionary perspective on human-microbe mutualism and disease. Nature 449:811-8.

84. Rothschild D, Weissbrod O, Barkan E, Kurilshikov A, Korem T, Zeevi D, Costea PI, Godneva A, Kalka IN, Bar N, Shilo S, Lador D, Vila AV, Zmora N, Pevsner-Fischer M, Israeli D, Kosower N, Malka G, Wolf BC, Avnit-Sagi T, Lotan-Pompan M, Weinberger A, Halpern Z, Carmi S, Fu J, Wijmenga C, Zhernakova A, Elinav

E, Segal E. 2018. Environment dominates over host genetics in shaping human gut microbiota. Nature 555:210-215.

85. Komai M, Shirakawa H, Kimura S. 1988. Newly developed model for vitamin K deficiency in germfree mice. Int J Vitam Nutr Res 58:55-9.

86. Janeway CA, Jr., Medzhitov R. 2002. Innate immune recognition. Annu Rev Immunol 20:197-216.

87. Kisseleva EP. 2014. Innate immunity underlies symbiotic relationships. Biochemistry (Mosc) 79:1273-85.

88. Byndloss MX, Litvak Y, Baumler AJ. 2019. Microbiota-nourishing Immunity and Its Relevance for Ulcerative Colitis. Inflamm Bowel Dis doi:10.1093/ibd/izz004.

89. Byndloss MX, Olsan EE, Rivera-Chávez F, Tiffany CR, Cevallos SA, Lokken KL, Torres TP, Byndloss AJ, Faber F, Gao Y, Litvak Y, Lopez CA, Xu G, Napoli E, Giulivi C, Tsolis RM, Revzin A, Lebrilla CB, Bäumler AJ. 2017. Microbiota-activated PPAR-g signaling inhibits dysbiotic Enterobacteriaceae expansion. Science 357:570-575.

90. Nadjsombati MS, McGinty JW, Lyons-Cohen MR, Jaffe JB, DiPeso L, Schneider C, Miller CN, Pollack JL, Nagana Gowda GA, Fontana MF, Erle DJ, Anderson MS, Locksley RM, Raftery D, von Moltke J. 2018. Detection of Succinate by Intestinal Tuft Cells Triggers a Type 2 Innate Immune Circuit. Immunity 49:33-41 e7.

91. Morita N, Umemoto E, Fujita S, Hayashi A, Kikuta J, Kimura I, Haneda T, Imai T, Inoue A, Mimuro H, Maeda Y, Kayama H, Okumura R, Aoki J, Okada N, Kida T, Ishii M, Nabeshima R, Takeda K. 2019. GPR31-dependent dendrite protrusion of intestinal CX3CR1(+) cells by bacterial metabolites. Nature 566:110-114.

92. Levy M, Blacher E, Elinav E. 2017. Microbiome, metabolites and host immunity. Curr Opin Microbiol 35:8-15.

93. Levy M, Thaiss CA, Elinav E. 2016. Metabolites: messengers between the microbiota and the immune system. Genes Dev 30:1589-97.

94. Tsolis RM, Baumler AJ. 2020. Gastrointestinal host-pathogen interaction in the age of microbiome research. Curr Opin Microbiol 53:78-89.

95. Liao MK. 2011. The Lure of Bacterial Genetics: A Tribute to John Roth. Journal of Microbiology & Biology Education 12:85-+.

96. Rivera-Chavez F, Baumler AJ. 2015. The Pyromaniac Inside You: Salmonella Metabolism in the Host Gut. Annu Rev Microbiol 69:31-48.

97. Nicolaou KC, Rigol S. 2018. A brief history of antibiotics and select advances in their synthesis. J Antibiot (Tokyo) 71:153-184.

98. Keefer CS. 1951. Alterations in normal bacterial flora of man and secondary infections during antibiotic therapy. Am J Med 11:665-6.

99. Smith MH, Lossli CG. 1952. Hospital cross-infections and their control. J Pediatr 41:844-52.

100. Smith DT. 1952. The disturbance of the normal bacterial ecology by the administration of antibiotics with the development of new clinical syndromes. Ann Intern Med 37:1135-43.

101. Meynell GG. 1963. Antibacterial mechanisms of the mouse gut. II. The role of Eh and volatile fatty acids in the normal gut. British journal of experimental pathology 44:209-19.

102. Miller CP, Bohnhoff M. 1963. Changes in the Mouse's Enteric Microflora Associated with Enhanced Susceptibility to Salmonella Infection Following Streptomycin Treatment. J Infect Dis 113:59-66.

103. Adeolu M, Alnajar S, Naushad S, R SG. 2016. Genome-based phylogeny and taxonomy of the 'Enterobacteriales': proposal for Enterobacterales ord. nov. divided into the families Enterobacteriaceae, Erwiniaceae fam. nov., Pectobacteriaceae fam. nov., Yersiniaceae fam. nov., Hafniaceae fam. nov., Morganellaceae fam. nov., and Budviciaceae fam. nov. Int J Syst Evol Microbiol 66:5575-5599.

104. Russell JB, Diez-Gonzalez F. 1998. The effects of fermentation acids on bacterial growth. Adv Microb Physiol 39:205-34.

105. Freter R, Brickner H, Botney M, Cleven D, Aranki A. 1983. Mechanisms that control bacterial populations in continuous-flow culture models of mouse large intestinal flora. Infect Immun 39:676-85.

106. Freter R, Brickner H, Fekete J, Vickerman MM, Carey KE. 1983. Survival and implantation of Escherichia coli in the intestinal tract. Infect Immun 39:686-703.

107. Jacobson A, Lam L, Rajendram M, Tamburini F, Honeycutt J, Pham T, Van Treuren W, Pruss K, Stabler SR, Lugo K, Bouley DM, Vilches-Moure JG, Smith M, Sonnenburg JL, Bhatt AS, Huang KC, Monack D. 2018. A Gut Commensal-Produced Metabolite Mediates Colonization Resistance to Salmonella Infection. Cell Host Microbe 24:296-307 e7.

108. Sorbara MT, Dubin K, Littmann ER, Moody TU, Fontana E, Seok R, Leiner IM, Taur Y, Peled JU, van den Brink MRM, Litvak Y, Baumler AJ, Chaubard JL,

Pickard AJ, Cross JR, Pamer EG. 2019. Inhibiting antibiotic-resistant Enterobacteriaceae by microbiota-mediated intracellular acidification. J Exp Med 216:84-98.

109. Osbelt L, Thiemann S, Smit N, Lesker TR, Schroter M, Galvez EJC, Schmidt-Hohagen K, Pils MC, Muhlen S, Dersch P, Hiller K, Schluter D, Neumann-Schaal M, Strowig T. 2020. Variations in microbiota composition of laboratory mice influence Citrobacter rodentium infection via variable short-chain fatty acid production. PLoS Pathog 16:e1008448.

110. Salmond CV, Kroll RG, Booth IR. 1984. The effect of food preservatives on pH homeostasis in Escherichia coli. J Gen Microbiol 130:2845-50.

111. Slonczewski JL, Rosen BP, Alger JR, Macnab RM. 1981. pH homeostasis in Escherichia coli: measurement by 31P nuclear magnetic resonance of methylphosphonate and phosphate. Proc Natl Acad Sci U S A 78:6271-5.

112. Zilberstein D, Agmon V, Schuldiner S, Padan E. 1984. Escherichia coli intracellular pH, membrane potential, and cell growth. J Bacteriol 158:246-52.

113. Chakraborty S, Liu L, Fitzsimmons L, Porwollik S, Kim JS, Desai P, McClelland M, Vazquez-Torres A. 2020. Glycolytic reprograming in Salmonella counters NOX2-mediated dissipation of DeltapH. Nat Commun 11:1783.

114. Bohnhoff M, Miller CP, Martin WR. 1964. Resistance of the Mouse's Intestinal Tract to Experimental Salmonella Infection. I. Factors Which Interfere with the Initiation of Infection by Oral Inoculation. J Exp Med 120:805-16.

115. Roe AJ, McLaggan D, Davidson I, O'Byrne C, Booth IR. 1998. Perturbation of anion balance during inhibition of growth of Escherichia coli by weak acids. J Bacteriol 180:767-72.

116. Louis P, Flint HJ. 2009. Diversity, metabolism and microbial ecology of butyrate-producing bacteria from the human large intestine. FEMS Microbiol Lett 294:1-8.

117. Vital M, Howe AC, Tiedje JM. 2014. Revealing the bacterial butyrate synthesis pathways by analyzing (meta)genomic data. MBio 5:e00889.

118. Rivera-Chavez F, Zhang LF, Faber F, Lopez CA, Byndloss MX, Olsan EE, Xu G, Velazquez EM, Lebrilla CB, Winter SE, Baumler AJ. 2016. Depletion of Butyrate-Producing Clostridia from the Gut Microbiota Drives an Aerobic Luminal Expansion of Salmonella. Cell Host Microbe 19:443-54.

119. Caballero-Flores G, Pickard JM, Fukuda S, Inohara N, Nunez G. 2020. An Enteric Pathogen Subverts Colonization Resistance by Evading Competition for Amino Acids in the Gut. Cell Host Microbe doi:10.1016/j.chom.2020.06.018.

120. Hiyoshi H, Tiffany CR, Bronner DN, Baumler AJ. 2018. Typhoidal Salmonella serovars: ecological opportunity and the evolution of a new pathovar. FEMS Microbiol Rev 42:527-541.

121. Stokes JL, Bayne HG. 1958. Growth-factor-dependent strains of Salmonellae. J Bacteriol 76:417-21.

122. Virgilio R, Cordano AM. 1981. Naturally occurring prototrophic strains of Salmonella typhi. Can J Microbiol 27:1272-5.

123. Theriot CM, Koenigsknecht MJ, Carlson PE, Jr., Hatton GE, Nelson AM, Li B, Huffnagle GB, J ZL, Young VB. 2014. Antibiotic-induced shifts in the mouse gut microbiome and metabolome increase susceptibility to Clostridium difficile infection. Nat Commun 5:3114.

124. Nguyen BD, Cuenca VM, Hartl J, Gul E, Bauer R, Meile S, Ruthi J, Margot C, Heeb L, Besser F, Escriva PP, Fetz C, Furter M, Laganenka L, Keller P, Fuchs L, Christen M, Porwollik S, McClelland M, Vorholt JA, Sauer U, Sunagawa S, Christen B, Hardt WD. 2020. Import of Aspartate and Malate by DcuABC Drives H2/Fumarate Respiration to Promote Initial Salmonella Gut-Lumen Colonization in Mice. Cell Host Microbe 27:922-936 e6.

125. Vollaard EJ, Clasener HA, Janssen AJ. 1992. Co-trimoxazole impairs colonization resistance in healthy volunteers. J Antimicrob Chemother 30:685-91.

126. Sorbara MT, Pamer EG. 2019. Interbacterial mechanisms of colonization resistance and the strategies pathogens use to overcome them. Mucosal Immunol 12:1-9.

127. Ducarmon QR, Zwittink RD, Hornung BVH, van Schaik W, Young VB, Kuijper EJ. 2019. Gut Microbiota and Colonization Resistance against Bacterial Enteric Infection. Microbiol Mol Biol Rev 83.

128. Pickard JM, Nunez G. 2019. Pathogen Colonization Resistance in the Gut and Its Manipulation for Improved Health. Am J Pathol 189:1300-1310.

129. Libertucci J, Young VB. 2019. The role of the microbiota in infectious diseases. Nat Microbiol 4:35-45.

130. Iacob S, Iacob DG, Luminos LM. 2018. Intestinal Microbiota as a Host Defense Mechanism to Infectious Threats. Front Microbiol 9:3328.

131. Winter SE, Lopez CA, Baumler AJ. 2013. The dynamics of gut-associated microbial communities during inflammation. EMBO Rep 14:319-27.

132. Dubinkina VB, Tyakht AV, Odintsova VY, Yarygin KS, Kovarsky BA, Pavlenko AV, Ischenko DS, Popenko AS, Alexeev DG, Taraskina AY, Nasyrova RF, Krupitsky EM, Shalikiani NV, Bakulin IG, Shcherbakov PL, Skorodumova LO, Larin AK, Kostryukova ES, Abdulkhakov RA, Abdulkhakov SR, Malanin SY, Ismagilova RK, Grigoryeva TV, Ilina EN, Govorun VM. 2017. Links of gut microbiota composition with alcohol dependence syndrome and alcoholic liver disease. Microbiome 5:141.

133. Wang Z, Wang Q, Wang X, Zhu L, Chen J, Zhang B, Chen Y, Yuan Z. 2019. Gut microbial dysbiosis is associated with development and progression of radiation enteritis during pelvic radiotherapy. J Cell Mol Med 23:3747-3756.

134. Pham TA, Clare S, Goulding D, Arasteh JM, Stares MD, Browne HP, Keane JA, Page AJ, Kumasaka N, Kane L, Mottram L, Harcourt K, Hale C, Arends MJ, Gaffney DJ, Sanger Mouse Genetics P, Dougan G, Lawley TD. 2014. Epithelial IL-22RA1-mediated fucosylation promotes intestinal colonization resistance to an opportunistic pathogen. Cell Host Microbe 16:504-16.

135. Mueller S, Saunier K, Hanisch C, Norin E, Alm L, Midtvedt T, Cresci A, Silvi S, Orpianesi C, Verdenelli MC, Clavel T, Koebnick C, Zunft HJ, Dore J, Blaut M. 2006. Differences in fecal microbiota in different European study populations in relation to age, gender, and country: a cross-sectional study. Appl Environ Microbiol 72:1027-33.

136. Frank DN, St Amand AL, Feldman RA, Boedeker EC, Harpaz N, Pace NR. 2007. Molecular-phylogenetic characterization of microbial community imbalances in human inflammatory bowel diseases. Proceedings of the National Academy of Sciences of the United States of America 104:13780-5.

137. Normann E, Fahlen A, Engstrand L, Lilja HE. 2013. Intestinal microbial profiles in extremely preterm infants with and without necrotizing enterocolitis. Acta paediatrica 102:129-36.

138. Vujkovic-Cvijin I, Dunham RM, Iwai S, Maher MC, Albright RG, Broadhurst MJ, Hernandez RD, Lederman MM, Huang Y, Somsouk M, Deeks SG, Hunt PW, Lynch SV, McCune JM. 2013. Dysbiosis of the gut microbiota is associated with HIV disease progression and tryptophan catabolism. Sci Transl Med 5:193ra91.

139. Fredricks DN. 2019. The gut microbiota and graft-versus-host disease. J Clin Invest 129:1808-1817.

140. Braun T, Di Segni A, BenShoshan M, Asaf R, Squires JE, Farage Barhom S, Glick Saar E, Cesarkas K, Smollan G, Weiss B, Amit S, Keller N, Haberman Y. 2017. Fecal microbial characterization of hospitalized patients with suspected infectious diarrhea shows significant dysbiosis. Sci Rep 7:1088.

141. McLaughlin PA, Bettke JA, Tam JW, Leeds J, Bliska JB, Butler BP, van der Velden AWM. 2019. Inflammatory monocytes provide a niche for Salmonella expansion in the lumen of the inflamed intestine. PLoS Pathog 15:e1007847.

142. Loetscher Y, Wieser A, Lengefeld J, Kaiser P, Schubert S, Heikenwalder M, Hardt WD, Stecher B. 2012. Salmonella transiently reside in luminal neutrophils in the inflamed gut. PLoS One 7:e34812.

143. Vazquez-Torres A, Jones-Carson J, Mastroeni P, Ischiropoulos H, Fang FC. 2000. Antimicrobial actions of the NADPH phagocyte oxidase and inducible nitric oxide synthase in experimental salmonellosis. I. Effects on microbial killing by activated peritoneal macrophages in vitro. J Exp Med 192:227-36.

144. Lopez CA, Winter SE, Rivera-Chavez F, Xavier MN, Poon V, Nuccio SP, Tsolis RM, Baumler AJ. 2012. Phage-mediated acquisition of a type III secreted effector protein boosts growth of salmonella by nitrate respiration. MBio 3.

145. Lopez CA, Rivera-Chavez F, Byndloss MX, Baumler AJ. 2015. The Periplasmic Nitrate Reductase NapABC Supports Luminal Growth of Salmonella enterica Serovar Typhimurium during Colitis. Infect Immun 83:3470-8.

146. Wang S, El-Fahmawi A, Christian DA, Fang Q, Radaelli E, Chen L, Sullivan MC, Misic AM, Ellringer JA, Zhu XQ, Winter SE, Hunter CA, Beiting DP. 2019. Infection-Induced Intestinal Dysbiosis Is Mediated by Macrophage Activation and Nitrate Production. mBio 10.

147. Winter SE, Winter MG, Xavier MN, Thiennimitr P, Poon V, Keestra AM, Laughlin RC, Gomez G, Wu J, Lawhon SD, Popova IE, Parikh SJ, Adams LG, Tsolis RM, Stewart VJ, Baumler AJ. 2013. Host-derived nitrate boosts growth of E. coli in the inflamed gut. Science 339:708-11.

148. Zhu W, Winter MG, Byndloss MX, Spiga L, Duerkop BA, Hughes ER, Buttner L, de Lima Romao E, Behrendt CL, Lopez CA, Sifuentes-Dominguez L, Huff-Hardy K, Wilson RP, Gillis CC, Tukel C, Koh AY, Burstein E, Hooper LV, Baumler AJ, Winter SE. 2018. Precision editing of the gut microbiota ameliorates colitis. Nature 553:208-211.

149. Potgens SA, Brossel H, Sboarina M, Catry E, Cani PD, Neyrinck AM, Delzenne NM, Bindels LB. 2018. Klebsiella oxytoca expands in cancer cachexia and acts as a gut pathobiont contributing to intestinal dysfunction. Sci Rep 8:12321.

150. Lupp C, Robertson ML, Wickham ME, Sekirov I, Champion OL, Gaynor EC, Finlay BB. 2007. Host-mediated inflammation disrupts the intestinal microbiota and promotes the overgrowth of Enterobacteriaceae. Cell Host Microbe 2:204.

151. Carson D, Barry R, Hopkins EGD, Roumeliotis TI, Garcia-Weber D, Mullineaux-Sanders C, Elinav E, Arrieumerlou C, Choudhary JS, Frankel G. 2019. Citrobacter rodentium induces rapid and unique metabolic and inflammatory responses in mice suffering from severe disease. Cell Microbiol doi:10.1111/cmi.13126:e13126.

152. Lee JY, Cevallos SA, Byndloss MX, Tiffany CR, Olsan EE, Butler BP, Young BM, Rogers AWL, Nguyen H, Kim K, Choi SW, Bae E, Lee JH, Min UG, Lee DC, Baumler AJ. 2020. High-Fat Diet and Antibiotics Cooperatively Impair Mitochondrial Bioenergetics to Trigger Dysbiosis that Exacerbates Pre-inflammatory Bowel Disease. Cell Host Microbe doi:10.1016/j.chom.2020.06.001.

153. Hughes ER, Winter MG, Duerkop BA, Spiga L, Furtado de Carvalho T, Zhu W, Gillis CC, Buttner L, Smoot MP, Behrendt CL, Cherry S, Santos RL, Hooper LV, Winter SE. 2017. Microbial Respiration and Formate Oxidation as Metabolic Signatures of Inflammation-Associated Dysbiosis. Cell Host Microbe 21:208-219.

154. Cevallos SA, Lee JY, Tiffany CR, Byndloss AJ, Johnston L, Byndloss MX, Baumler AJ. 2019. Increased Epithelial Oxygenation Links Colitis to an Expansion of Tumorigenic Bacteria. MBio 10.

155. Rivera-Chavez F, Lopez CA, Baumler AJ. 2017. Oxygen as a driver of gut dysbiosis. Free Radic Biol Med 105:93-101.

156. Warburg O, Wind F, Negelein E. 1927. The Metabolism of Tumors in the Body. J Gen Physiol 8:519-30.

157. Barrow PA, Berchieri A, Freitas Neto OC, Lovell M. 2015. The contribution of aerobic and anaerobic respiration to intestinal colonization and virulence for Salmonella typhimurium in the chicken. Avian Pathol 44:401-7.

158. Ley RE, Hamady M, Lozupone C, Turnbaugh PJ, Ramey RR, Bircher JS, Schlegel ML, Tucker TA, Schrenzel MD, Knight R, Gordon JI. 2008. Evolution of mammals and their gut microbes. Science 320:1647-51.

159. Orcutt RP, Gianni FJ, Judge RJ. 1987. Development of an Altered Schaedler Flora for Nci Gnotobiotic Rodents. Microecology and Therapy, Vol 17 17:59-59.

160. Brand MW, Wannemuehler MJ, Phillips GJ, Proctor A, Overstreet AM, Jergens AE, Orcutt RP, Fox JG. 2015. The Altered Schaedler Flora: Continued Applications of a Defined Murine Microbial Community. Ilar Journal 56:169-178.

161. Lima-Filho JV, Vieira LQ, Arantes RM, Nicoli JR. 2004. Effect of the Escherichia coli EMO strain on experimental infection by Salmonella enterica serovar Typhimurium in gnotobiotic mice. Braz J Med Biol Res 37:1005-13.

162. Splichalova A, Trebichavsky I, Rada V, Vlkova E, Sonnenborn U, Splichal I. 2011. Interference of Bifidobacterium choerinum or Escherichia coli Nissle 1917 with Salmonella Typhimurium in gnotobiotic piglets correlates with cytokine patterns in blood and intestine. Clin Exp Immunol 163:242-9.

163. Wotzka SY, Kreuzer M, Maier L, Arnoldini M, Nguyen BD, Brachmann AO, Berthold DL, Zund M, Hausmann A, Bakkeren E, Hoces D, Gul E, Beutler M, Dolowschiak T, Zimmermann M, Fuhrer T, Moor K, Sauer U, Typas A, Piel J, Diard M, Macpherson AJ, Stecher B, Sunagawa S, Slack E, Hardt WD. 2019. Escherichia coli limits Salmonella Typhimurium infections after diet shifts and fat-mediated microbiota perturbation in mice. Nat Microbiol 4:2164-2174.

164. Brugiroux S, Beutler M, Pfann C, Garzetti D, Ruscheweyh HJ, Ring D, Diehl M, Herp S, Lotscher Y, Hussain S, Bunk B, Pukall R, Huson DH, Munch PC, McHardy AC, McCoy KD, Macpherson AJ, Loy A, Clavel T, Berry D, Stecher B. 2016. Genome-guided design of a defined mouse microbiota that confers colonization resistance against Salmonella enterica serovar Typhimurium. Nat Microbiol 2:16215.

165. Ng KM, Ferreyra JA, Higginbottom SK, Lynch JB, Kashyap PC, Gopinath S, Naidu N, Choudhury B, Weimer BC, Monack DM, Sonnenburg JL. 2013. Microbiota-liberated host sugars facilitate post-antibiotic expansion of enteric pathogens. Nature 502:96-9.

166. Stecher B, Barthel M, Schlumberger MC, Haberli L, Rabsch W, Kremer M, Hardt WD. 2008. Motility allows S. Typhimurium to benefit from the mucosal defence. Cell Microbiol 10:1166-80.

167. Faber F, Tran L, Byndloss MX, Lopez CA, Velazquez EM, Kerrinnes T, Nuccio SP, Wangdi T, Fiehn O, Tsolis RM, Baumler AJ. 2016. Host-mediated sugar oxidation promotes post-antibiotic pathogen expansion. Nature 534:697-9.

168. Spees AM, Wangdi T, Lopez CA, Kingsbury DD, Xavier MN, Winter SE, Tsolis RM, Baumler AJ. 2013. Streptomycin-induced inflammation enhances Escherichia coli gut colonization through nitrate respiration. MBio 4.

169. Oliveira RA, Ng KM, Correia MB, Cabral V, Shi H, Sonnenburg JL, Huang KC, Xavier KB. 2020. Klebsiella michiganensis transmission enhances resistance to Enterobacteriaceae gut invasion by nutrition competition. Nat Microbiol 5:630-641.

170. Daikos GL, Vryonis E, Psichogiou M, Tzouvelekis LS, Liatis S, Petrikkos P, Kosmidis C, Tassios PT, Bamias G, Skoutelis A. 2010. Risk factors for bloodstream infection with Klebsiella pneumoniae producing VIM-1 metallo-beta-lactamase. J Antimicrob Chemother 65:784-8.

171. Shanthi M, Sekar U. 2010. Extended spectrum beta lactamase producing Escherichia coli and Klebsiella pneumoniae: risk factors for infection and impact of resistance on outcomes. J Assoc Physicians India 58 Suppl:41-4.

172. Razazi K, Derde LP, Verachten M, Legrand P, Lesprit P, Brun-Buisson C. 2012. Clinical impact and risk factors for colonization with extended-spectrum beta-lactamase-producing bacteria in the intensive care unit. Intensive Care Med 38:1769-78.

173. Lowe CF, Kus JV, Salt N, Callery S, Louie L, Khan MA, Vearncombe M, Simor AE. 2013. Nosocomial transmission of New Delhi metallo-beta-lactamase-1-producing Klebsiella pneumoniae in Toronto, Canada. Infect Control Hosp Epidemiol 34:49-55.

174. Zhao SY, Zhang J, Zhang YL, Wang YC, Xiao SZ, Gu FF, Guo XK, Ni YX, Han LZ. 2016. Epidemiology and risk factors for faecal extended-spectrum beta-lactamase-producing Enterobacteriaceae (ESBL-E) carriage derived from residents of seven nursing homes in western Shanghai, China. Epidemiol Infect 144:695-702.

175. Gorrie CL, Mirceta M, Wick RR, Edwards DJ, Thomson NR, Strugnell RA, Pratt NF, Garlick JS, Watson KM, Pilcher DV, McGloughlin SA, Spelman DW, Jenney AWJ, Holt KE. 2017. Gastrointestinal Carriage Is a Major Reservoir of Klebsiella pneumoniae Infection in Intensive Care Patients. Clin Infect Dis 65:208-215.

176. Tamburini FB, Andermann TM, Tkachenko E, Senchyna F, Banaei N, Bhatt AS. 2018. Precision identification of diverse bloodstream pathogens in the gut microbiome. Nat Med 24:1809-1814.

177. Doi Y, Paterson DL. 2015. Carbapenemase-producing Enterobacteriaceae. Semin Respir Crit Care Med 36:74-84.

178. Tangden T, Giske CG. 2015. Global dissemination of extensively drug-resistant carbapenemase-producing Enterobacteriaceae: clinical perspectives on detection, treatment and infection control. J Intern Med 277:501-12.

179. Prevention CfDCa. 2014. Antibiotic resistance threats in the United States, 2013. http://www.cdc.gov/drugresistance/threat-report-2013/index.html.

180. Galán JE, Curtiss III R. 1989. Cloning and molecular characterization of genes whose products allow *Salmonella typhimurium* to penetrate tissue culture cells. Proc Natl Acad Sci USA 86:6383-6387.

181. Hensel M, Shea JE, Gleeson C, Jones MD, Dalton E, Holden DW. 1995. Simultaneous identification of bacterial virulence genes by negative selection. Science 269:400-3.

182. Tsolis RM, Adams LG, Ficht TA, Baumler AJ. 1999. Contribution of Salmonella typhimurium virulence factors to diarrheal disease in calves. Infect Immun 67:4879-85.

183. Costello EK, Stagaman K, Dethlefsen L, Bohannan BJ, Relman DA. 2012. The application of ecological theory toward an understanding of the human microbiome. Science 336:1255-62.

184. Srikanth CV, Mercado-Lubo R, Hallstrom K, McCormick BA. 2011. Salmonella effector proteins and host-cell responses. Cell Mol Life Sci 68:3687-97.

185. Raffatellu M, Wilson RP, Chessa D, Andrews-Polymenis H, Tran QT, Lawhon S, Khare S, Adams LG, Baumler AJ. 2005. SipA, SopA, SopB, SopD, and SopE2 contribute to Salmonella enterica serotype typhimurium invasion of epithelial cells. Infect Immun 73:146-54.

186. Grant AJ, Morgan FJ, McKinley TJ, Foster GL, Maskell DJ, Mastroeni P. 2012. Attenuated Salmonella Typhimurium lacking the pathogenicity island-2 type 3 secretion system grow to high bacterial numbers inside phagocytes in mice. PLoS Pathog 8:e1003070.

187. LaRock DL, Chaudhary A, Miller SI. 2015. Salmonellae interactions with host processes. Nat Rev Microbiol 13:191-205.

188. Tukel C, Raffatellu M, Humphries AD, Wilson RP, Andrews-Polymenis HL, Gull T, Figueiredo JF, Wong MH, Michelsen KS, Akcelik M, Adams LG, Baumler AJ. 2005. CsgA is a pathogen-associated molecular pattern of Salmonella enterica serotype Typhimurium that is recognized by Toll-like receptor 2. Mol Microbiol 58:289-304.

189. Keestra AM, Godinez I, Xavier MN, Winter MG, Winter SE, Tsolis RM, Baumler AJ. 2011. Early MyD88-dependent induction of interleukin-17A expression during Salmonella colitis. Infect Immun 79:3131-40.

190. Keestra AM, Winter MG, Klein-Douwel D, Xavier MN, Winter SE, Kim A, Tsolis RM, Baumler AJ. 2011. A Salmonella virulence factor activates the NOD1/NOD2 signaling pathway. MBio 2.

191. Keestra AM, Winter MG, Auburger JJ, Frassle SP, Xavier MN, Winter SE, Kim A, Poon V, Ravesloot MM, Waldenmaier JF, Tsolis RM, Eigenheer RA, Baumler AJ. 2013. Manipulation of small Rho GTPases is a pathogen-induced process detected by NOD1. Nature 496:233-7.

192. Sellin ME, Muller AA, Felmy B, Dolowschiak T, Diard M, Tardivel A, Maslowski KM, Hardt WD. 2014. Epithelium-Intrinsic NAIP/NLRC4 Inflammasome Drives

Infected Enterocyte Expulsion to Restrict Salmonella Replication in the Intestinal Mucosa. Cell Host Microbe 16:237-48.

193. Knodler LA, Crowley SM, Sham HP, Yang H, Wrande M, Ma C, Ernst RK, Steele-Mortimer O, Celli J, Vallance BA. 2014. Noncanonical Inflammasome Activation of Caspase-4/Caspase-11 Mediates Epithelial Defenses against Enteric Bacterial Pathogens. Cell Host Microbe 16:249-56.

194. Zhang S, Santos RL, Tsolis RM, Stender S, Hardt WD, Baumler AJ, Adams LG. 2002. The Salmonella enterica serotype typhimurium effector proteins SipA, SopA, SopB, SopD, and SopE2 act in concert to induce diarrhea in calves. Infect Immun 70:3843-55.

195. Matsuda S, Haneda T, Saito H, Miki T, Okada N. 2019. Salmonella enterica Effectors SifA, SpvB, SseF, SseJ, and SteA Contribute to Type III Secretion System 1-Independent Inflammation in a Streptomycin-Pretreated Mouse Model of Colitis. Infect Immun 87.

196. Harris JC, Dupont HL, Hornick RB. 1972. Fecal leukocytes in diarrheal illness. Ann Intern Med 76:697-703.

197. Sekirov I, Gill N, Jogova M, Tam N, Robertson M, de Llanos R, Li Y, Finlay BB. 2010. Salmonella SPI-1-mediated neutrophil recruitment during enteric colitis is associated with reduction and alteration in intestinal microbiota. Gut Microbes 1:30-41.

198. Gill N, Ferreira RB, Antunes LC, Willing BP, Sekirov I, Al-Zahrani F, Hartmann M, Finlay BB. 2012. Neutrophil elastase alters the murine gut microbiota resulting in enhanced Salmonella colonization. PLoS One 7:e49646.

199. Lawley TD, Bouley DM, Hoy YE, Gerke C, Relman DA, Monack DM. 2008. Host transmission of Salmonella enterica serovar Typhimurium is controlled by virulence factors and indigenous intestinal microbiota. Infect Immun 76:403-16.

200. Crawford RW, Keestra AM, Winter SE, Xavier MN, Tsolis RM, Tolstikov V, Baumler AJ. 2012. Very long O-antigen chains enhance fitness during Salmonella-induced colitis by increasing bile resistance. PLoS Pathog 8:e1002918.

201. Sana TG, Flaugnatti N, Lugo KA, Lam LH, Jacobson A, Baylot V, Durand E, Journet L, Cascales E, Monack DM. 2016. Salmonella Typhimurium utilizes a T6SS-mediated antibacterial weapon to establish in the host gut. Proc Natl Acad Sci U S A 113:E5044-51.

202. Costa LF, Mol JP, Silva AP, Macedo AA, Silva TM, Alves GE, Winter S, Winter MG, Velazquez EM, Byndloss MX, Baumler AJ, Tsolis RM, Paixao TA, Santos

RL. 2016. Iron acquisition pathways and colonization of the inflamed intestine by Salmonella enterica serovar Typhimurium. Int J Med Microbiol 306:604-610.

203. Goetz DH, Holmes MA, Borregaard N, Bluhm ME, Raymond KN, Strong RK. 2002. The neutrophil lipocalin NGAL is a bacteriostatic agent that interferes with siderophore-mediated iron acquisition. Mol Cell 10:1033-43.

204. Flo TH, Smith KD, Sato S, Rodriguez DJ, Holmes MA, Strong RK, Akira S, Aderem A. 2004. Lipocalin 2 mediates an innate immune response to bacterial infection by sequestrating iron. Nature 432:917-21.

205. Raffatellu M, George MD, Akiyama Y, Hornsby MJ, Nuccio SP, Paixao TA, Butler BP, Chu H, Santos RL, Berger T, Mak TW, Tsolis RM, Bevins CL, Solnick JV, Dandekar S, Baumler AJ. 2009. Lipocalin-2 resistance confers an advantage to Salmonella enterica serotype Typhimurium for growth and survival in the inflamed intestine. Cell Host Microbe 5:476-86.

206. Chassaing B, Srinivasan G, Delgado MA, Young AN, Gewirtz AT, Vijay-Kumar M. 2012. Fecal lipocalin 2, a sensitive and broadly dynamic non-invasive biomarker for intestinal inflammation. PLoS One 7:e44328.

207. Hantke K, Nicholson G, Rabsch W, Winkelmann G. 2003. Salmochelins, siderophores of Salmonella enterica and uropathogenic Escherichia coli strains, are recognized by the outer membrane receptor IroN. Proc Natl Acad Sci U S A 100:3677-82.

208. Fischbach MA, Lin H, Zhou L, Yu Y, Abergel RJ, Liu DR, Raymond KN, Wanner BL, Strong RK, Walsh CT, Aderem A, Smith KD. 2006. The pathogen-associated iroA gene cluster mediates bacterial evasion of lipocalin 2. Proc Natl Acad Sci U S A 103:16502-7.

209. Behnsen J, Jellbauer S, Wong CP, Edwards RA, George MD, Ouyang W, Raffatellu M. 2014. The cytokine IL-22 promotes pathogen colonization by suppressing related commensal bacteria. Immunity 40:262-73.

210. Patzer SI, Baquero MR, Bravo D, Moreno F, Hantke K. 2003. The colicin G, H and X determinants encode microcins M and H47, which might utilize the catecholate siderophore receptors FepA, Cir, Fiu and IroN. Microbiology-Sgm 149:2557-2570.

211. Sassone-Corsi M, Nuccio SP, Liu H, Hernandez D, Vu CT, Takahashi AA, Edwards RA, Raffatellu M. 2016. Microcins mediate competition among Enterobacteriaceae in the inflamed gut. Nature 540:280-283.

212. Nedialkova LP, Denzler R, Koeppel MB, Diehl M, Ring D, Wille T, Gerlach RG, Stecher B. 2014. Inflammation fuels colicin Ib-dependent competition of

Salmonella serovar Typhimurium and E. coli in enterobacterial blooms. PLoS Pathog 10:e1003844.

213. Nuccio SP, Baumler AJ. 2014. Comparative analysis of Salmonella genomes identifies a metabolic network for escalating growth in the inflamed gut. mBio 5:e00929-14.

214. Seif Y, Kavvas E, Lachance JC, Yurkovich JT, Nuccio SP, Fang X, Catoiu E, Raffatellu M, Palsson BO, Monk JM. 2018. Genome-scale metabolic reconstructions of multiple Salmonella strains reveal serovar-specific metabolic traits. Nat Commun 9:3771.

215. Wheeler NE, Gardner PP, Barquist L. 2018. Machine learning identifies signatures of host adaptation in the bacterial pathogen Salmonella enterica. PLoS Genet 14:e1007333.

216. Raffatellu M, Wilson RP, Winter SE, Baumler AJ. 2008. Clinical pathogenesis of typhoid fever. Journal of Infection in Developing Countries 2:260-266.

217. Rakov AV, Mastriani E, Liu SL, Schifferli DM. 2019. Association of Salmonella virulence factor alleles with intestinal and invasive serovars. BMC Genomics 20:429.

218. Parkhill J, Dougan G, James KD, Thomson NR, Pickard D, Wain J, Churcher C, Mungall KL, Bentley SD, Holden MT, Sebaihia M, Baker S, Basham D, Brooks K, Chillingworth T, Connerton P, Cronin A, Davis P, Davies RM, Dowd L, White N, Farrar J, Feltwell T, Hamlin N, Haque A, Hien TT, Holroyd S, Jagels K, Krogh A, Larsen TS, Leather S, Moule S, O'Gaora P, Parry C, Quail M, Rutherford K, Simmonds M, Skelton J, Stevens K, Whitehead S, Barrell BG. 2001. Complete genome sequence of a multiple drug resistant Salmonella enterica serovar Typhi CT18. Nature 413:848-52.

219. Deng W, Liou SR, Plunkett G, 3rd, Mayhew GF, Rose DJ, Burland V, Kodoyianni V, Schwartz DC, Blattner FR. 2003. Comparative genomics of Salmonella enterica serovar Typhi strains Ty2 and CT18. J Bacteriol 185:2330-7.

220. Thomson NR, Clayton DJ, Windhorst D, Vernikos G, Davidson S, Churcher C, Quail MA, Stevens M, Jones MA, Watson M, Barron A, Layton A, Pickard D, Kingsley RA, Bignell A, Clark L, Harris B, Ormond D, Abdellah Z, Brooks K, Cherevach I, Chillingworth T, Woodward J, Norberczak H, Lord A, Arrowsmith C, Jagels K, Moule S, Mungall K, Sanders M, Whitehead S, Chabalgoity JA, Maskell D, Humphrey T, Roberts M, Barrow PA, Dougan G, Parkhill J. 2008. Comparative genome analysis of Salmonella Enteritidis PT4 and Salmonella Gallinarum 287/91 provides insights into evolutionary and host adaptation pathways. Genome Res 18:1624-37.

221. Holt KE, Thomson NR, Wain J, Langridge GC, Hasan R, Bhutta ZA, Quail MA, Norbertczak H, Walker D, Simmonds M, White B, Bason N, Mungall K, Dougan G, Parkhill J. 2009. Pseudogene accumulation in the evolutionary histories of Salmonella enterica serovars Paratyphi A and Typhi. BMC Genomics 10:36.

222. Liu WQ, Feng Y, Wang Y, Zou QH, Chen F, Guo JT, Peng YH, Jin Y, Li YG, Hu SN, Johnston RN, Liu GR, Liu SL. 2009. Salmonella paratyphi C: genetic divergence from Salmonella choleraesuis and pathogenic convergence with Salmonella typhi. PLoS One 4:e4510.

223. Langridge GC, Fookes M, Connor TR, Feltwell T, Feasey N, Parsons BN, Seth-Smith HM, Barquist L, Stedman A, Humphrey T, Wigley P, Peters SE, Maskell DJ, Corander J, Chabalgoity JA, Barrow P, Parkhill J, Dougan G, Thomson NR. 2015. Patterns of genome evolution that have accompanied host adaptation in Salmonella. Proc Natl Acad Sci U S A 112:863-8.

224. Matthews TD, Schmieder R, Silva GG, Busch J, Cassman N, Dutilh BE, Green D, Matlock B, Heffernan B, Olsen GJ, Farris Hanna L, Schifferli DM, Maloy S, Dinsdale EA, Edwards RA. 2015. Genomic Comparison of the Closely-Related Salmonella enterica Serovars Enteritidis, Dublin and Gallinarum. PLoS One 10:e0126883.

225. Key FM, Posth C, Esquivel-Gomez LR, Hubler R, Spyrou MA, Neumann GU, Furtwangler A, Sabin S, Burri M, Wissgott A, Lankapalli AK, Vagene AJ, Meyer M, Nagel S, Tukhbatova R, Khokhlov A, Chizhevsky A, Hansen S, Belinsky AB, Kalmykov A, Kantorovich AR, Maslov VE, Stockhammer PW, Vai S, Zavattaro M, Riga A, Caramelli D, Skeates R, Beckett J, Gradoli MG, Steuri N, Hafner A, Ramstein M, Siebke I, Losch S, Erdal YS, Alikhan NF, Zhou Z, Achtman M, Bos K, Reinhold S, Haak W, Kuhnert D, Herbig A, Krause J. 2020. Emergence of human-adapted Salmonella enterica is linked to the Neolithization process. Nat Ecol Evol 4:324-333.

226. Hu Y, Wang Z, Qiang B, Xu Y, Chen X, Li Q, Jiao X. 2019. Loss and Gain in the Evolution of the Salmonella enterica Serovar Gallinarum Biovar Pullorum Genome. mSphere 4.

227. Maier L, Vyas R, Cordova CD, Lindsay H, Schmidt TS, Brugiroux S, Periaswamy B, Bauer R, Sturm A, Schreiber F, von Mering C, Robinson MD, Stecher B, Hardt WD. 2013. Microbiota-derived hydrogen fuels Salmonella typhimurium invasion of the gut ecosystem. Cell Host Microbe 14:641-51.

228. Rivera-Chavez F, Winter SE, Lopez CA, Xavier MN, Winter MG, Nuccio SP, Russell JM, Laughlin RC, Lawhon SD, Sterzenbach T, Bevins CL, Tsolis RM, Harshey R, Adams LG, Baumler AJ. 2013. Salmonella uses energy taxis to benefit from intestinal inflammation. PLoS Pathog 9:e1003267.

229. Faber F, Thiennimitr P, Spiga L, Byndloss MX, Litvak Y, Lawhon S, Andrews-Polymenis HL, Winter SE, Baumler AJ. 2017. Respiration of Microbiota-Derived 1,2-propanediol Drives Salmonella Expansion during Colitis. PLoS Pathog 13:e1006129.

230. Thiennimitr P, Winter SE, Winter MG, Xavier MN, Tolstikov V, Huseby DL, Sterzenbach T, Tsolis RM, Roth JR, Baumler AJ. 2011. Intestinal inflammation allows Salmonella to use ethanolamine to compete with the microbiota. Proc Natl Acad Sci U S A 108:17480-5.

231. Spiga L, Winter MG, Furtado de Carvalho T, Zhu W, Hughes ER, Gillis CC, Behrendt CL, Kim J, Chessa D, Andrews-Polymenis HL, Beiting DP, Santos RL, Hooper LV, Winter SE. 2017. An Oxidative Central Metabolism Enables Salmonella to Utilize Microbiota-Derived Succinate. Cell Host Microbe 22:291-301 e6.

232. Campbell JW, Morgan-Kiss RM, Cronan JE, Jr. 2003. A new Escherichia coli metabolic competency: growth on fatty acids by a novel anaerobic beta-oxidation pathway. Mol Microbiol 47:793-805.

233. Bronner DN, Faber F, Olsan EE, Byndloss MX, Sayed NA, Xu G, Yoo W, Kim D, Ryu S, Lebrilla CB, Baumler AJ. 2018. Genetic Ablation of Butyrate Utilization Attenuates Gastrointestinal Salmonella Disease. Cell Host Microbe 23:266-273 e4.

234. Schoneich C. 2005. Methionine oxidation by reactive oxygen species: reaction mechanisms and relevance to Alzheimer's disease. Biochimica et biophysica acta 1703:111-9.

235. Balagam B, Richardson DE. 2008. The mechanism of carbon dioxide catalysis in the hydrogen peroxide N-oxidation of amines. Inorganic chemistry 47:1173-8.

236. Heinzinger NK, Fujimoto SY, Clark MA, Moreno MS, Barrett EL. 1995. Sequence analysis of the phs operon in Salmonella typhimurium and the contribution of thiosulfate reduction to anaerobic energy metabolism. J Bacteriol 177:2813-20.

237. Rizzatti G, Lopetuso LR, Gibiino G, Binda C, Gasbarrini A. 2017. Proteobacteria: A Common Factor in Human Diseases. Biomed Res Int 2017:9351507.

238. Zhu W, Miyata N, Winter MG, Arenales A, Hughes ER, Spiga L, Kim J, Sifuentes-Dominguez L, Starokadomskyy P, Gopal P, Byndloss MX, Santos RL, Burstein E, Winter SE. 2019. Editing of the gut microbiota reduces carcinogenesis in mouse models of colitis-associated colorectal cancer. J Exp Med 216:2378-2393.

239. Bakken JS, Borody T, Brandt LJ, Brill JV, Demarco DC, Franzos MA, Kelly C, Khoruts A, Louie T, Martinelli LP, Moore TA, Russell G, Surawicz C, Fecal

Microbiota Transplantation W. 2011. Treating Clostridium difficile infection with fecal microbiota transplantation. Clin Gastroenterol Hepatol 9:1044-9.

240. Buffie CG, Bucci V, Stein RR, McKenney PT, Ling L, Gobourne A, No D, Liu H, Kinnebrew M, Viale A, Littmann E, van den Brink MR, Jenq RR, Taur Y, Sander C, Cross JR, Toussaint NC, Xavier JB, Pamer EG. 2015. Precision microbiome reconstitution restores bile acid mediated resistance to Clostridium difficile. Nature 517:205-8.

241. Khan KJ, Ullman TA, Ford AC, Abreu MT, Abadir A, Marshall JK, Talley NJ, Moayyedi P. 2011. Antibiotic therapy in inflammatory bowel disease: a systematic review and meta-analysis. Am J Gastroenterol 106:661-73.

242. Hildebrand H, Malmborg P, Askling J, Ekbom A, Montgomery SM. 2008. Early-life exposures associated with antibiotic use and risk of subsequent Crohn's disease. Scand J Gastroenterol 43:961-6.

243. Hviid A, Svanstrom H, Frisch M. 2011. Antibiotic use and inflammatory bowel diseases in childhood. Gut 60:49-54.

244. Zou Y, Wu L, Xu W, Zhou X, Ye K, Xiong H, Song C, Xie Y. 2020. Correlation between antibiotic use in childhood and subsequent inflammatory bowel disease: a systematic review and meta-analysis. Scand J Gastroenterol 55:301-311.

245. Xu J, Chen N, Wu Z, Song Y, Zhang Y, Wu N, Zhang F, Ren X, Liu Y. 2018. 5-Aminosalicylic Acid Alters the Gut Bacterial Microbiota in Patients With Ulcerative Colitis. Front Microbiol 9:1274.

246. Donohoe DR, Garge N, Zhang X, Sun W, O'Connell TM, Bunger MK, Bultman SJ. 2011. The microbiome and butyrate regulate energy metabolism and autophagy in the mammalian colon. Cell Metab 13:517-26.

247. Donohoe DR, Wali A, Brylawski BP, Bultman SJ. 2012. Microbial regulation of glucose metabolism and cell-cycle progression in mammalian colonocytes. PloS one 7:e46589.

248. Kelly CJ, Zheng L, Campbell EL, Saeedi B, Scholz CC, Bayless AJ, Wilson KE, Glover LE, Kominsky DJ, Magnuson A, Weir TL, Ehrentraut SF, Pickel C, Kuhn KA, Lanis JM, Nguyen V, Taylor CT, Colgan SP. 2015. Crosstalk between Microbiota-Derived Short-Chain Fatty Acids and Intestinal Epithelial HIF Augments Tissue Barrier Function. Cell Host Microbe 17:662-71.

249. Pereira IA, Ramos AR, Grein F, Marques MC, da Silva SM, Venceslau SS. 2011. A comparative genomic analysis of energy metabolism in sulfate reducing bacteria and archaea. Front Microbiol 2:69.

250. Furne J, Springfield J, Koenig T, DeMaster E, Levitt MD. 2001. Oxidation of hydrogen sulfide and methanethiol to thiosulfate by rat tissues: a specialized function of the colonic mucosa. Biochem Pharmacol 62:255-9.

251. Levitt MD, Furne J, Springfield J, Suarez F, DeMaster E. 1999. Detoxification of hydrogen sulfide and methanethiol in the cecal mucosa. J Clin Invest 104:1107-14.

252. Palmer RM, Ashton DS, Moncada S. 1988. Vascular endothelial cells synthesize nitric oxide from L-arginine. Nature 333:664-6.

253. De Groote MA, Granger D, Xu Y, Campbell G, Prince R, Fang FC. 1995. Genetic and redox determinants of nitric oxide cytotoxicity in a Salmonella typhimurium model. Proc Natl Acad Sci U S A 92:6399-403.

254. Szabo C, Ischiropoulos H, Radi R. 2007. Peroxynitrite: biochemistry, pathophysiology and development of therapeutics. Nat Rev Drug Discov 6:662-80.

Tables

Table 1.1: Microbiome vocabulary

Term	Definition
Colonization resistance	Mechanisms executed by microbiota-nourishing immunity that prevent engraftment of a specific microorganism through competition and habitat filtering
Communicable disease	Disease caused by an infectious agent that is transmitted from one animal or person to another, through direct contact, or indirectly through fomites or vectors
Dominant taxa	Dominant taxa are the most abundant taxa in a community, exerting a strong influence on other taxa
Dysbiosis	A state of abnormal competition or habitat filtering
Ecosystem engineering	The process by which a keystone species modifies a habitat, thereby strongly effecting other organisms
Facultative anaerobic bacteria	Bacteria that can grow in the presence of (and often can respire) oxygen at atmospheric levels but can grow fermentatively when oxygen is absent
Foundation species	A species that provides the foundation for a habitat by physically modifying the environment, thereby structuring communities of other organisms
Habitat filters	Factors that select for microbial traits licensing growth and survival in a host habitat patch

Habitat patch	The dynamic environment on a host surface where the microbiota assembles
Historical contingency	Dependence of the taxa composition on the order and timing of species arrival during microbiota assembly
Homeostasis	The outcome of normal competition and normal habitat filtering, which in turn generates microbiota resistance and microbiota resilience
Keystone species	A species that has a disproportionally large effect on its habitat relative to its abundance within the microbial community
Microbiome	The microbiota and its host environment
Microbiota	Host-associated microbial communities
Microbiota-nourishing immunity	A subdivision of the immune system, composed of the microbiota and host-derived habitat filters, which confers colonization resistance on body surfaces
Microbiota resilience	The ability of the microbiota to return to a healthy equilibrium state after perturbation
Microbiota resistance	Temporal stability in the taxa composition of mature host-associated microbial communities
Niche modification	A mechanism that uses microbiota-mediated habitat filtering to prevent engraftment of microorganisms that harbor inadequate trait combinations

Niche preemption	A mechanism that uses direct competition for critical resources with members of the microbiota to prevent engraftment of similar microorganisms
Non-communicable disease	Medical condition that is not caused by an infectious agent but is due to an underlying defect in host physiology that is not transmissible
Nutrient-niche	An ecological position defined by criticsl resources that support growth of a suitable occupant
Obligate anaerobic bacteria	Bacteria that cannot respire oxygen and cannot grow under atmospheric oxygen concentrations
Opportunistic infection	Infection with opportunistic pathogen
Opportunistic pathogens	Microbes associated with disease in immunocompromised members of a host species
Pathogens (or frank pathogens)	Microbes associated with communicable diseases in immunocompetent members of a host species
Priority effects	The ability of resident microbes to prevent engraftment of new microorganisms through niche preemption and/or niche modification
Sterilizing Immunity	The part of our immune system that preserves tissue sterility by detecting and distinguishing microbial intruders from self and subsequently triggering innate and adaptive immune responses aimed at removing the intruder from tissue

Virulence factors	Molecules produced by pathogens to overcome host defenses and cause disease

Figures

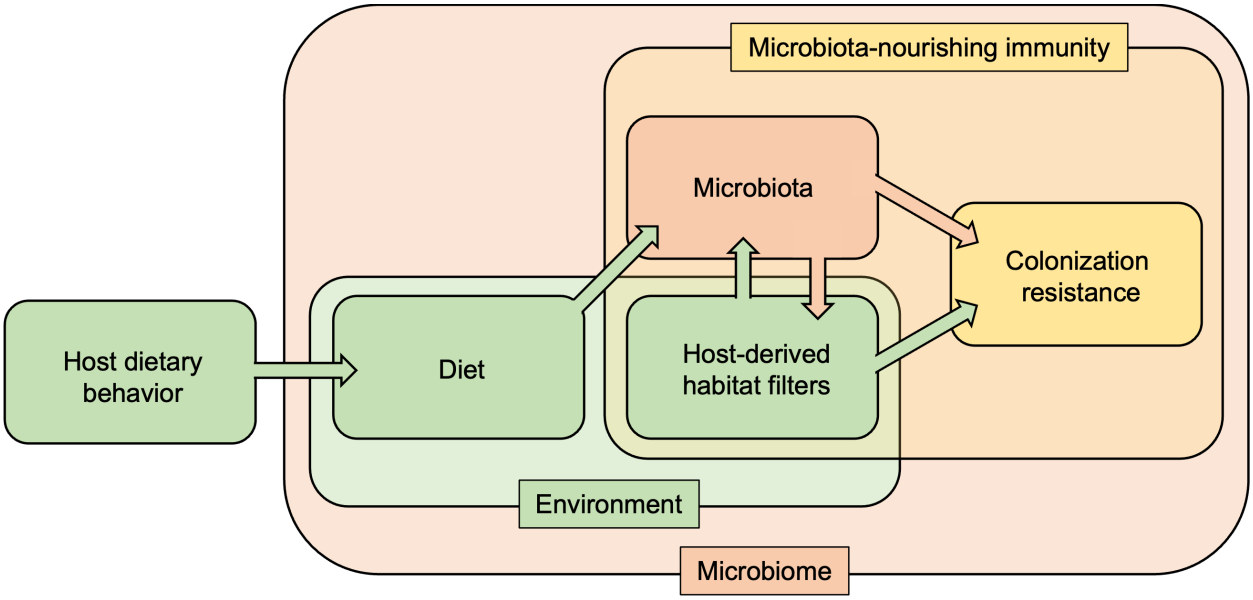

Figure 1.1: Composition of the term microbiome. The microbiome is defined as the microbiota and its environment. The latter is determined by host-derived habitat filters and the diet, which is controlled by host behavior. Host-derived habitat filters shape the size, species composition and biogeography of the microbiota and in turn the microbiota contributes to host nutrition and immune education. Microbiota-nourishing immunity is composed of the microbiota and host-derived habitat filters, which form a host-microbe chimera that functions in conferring colonization resistance.

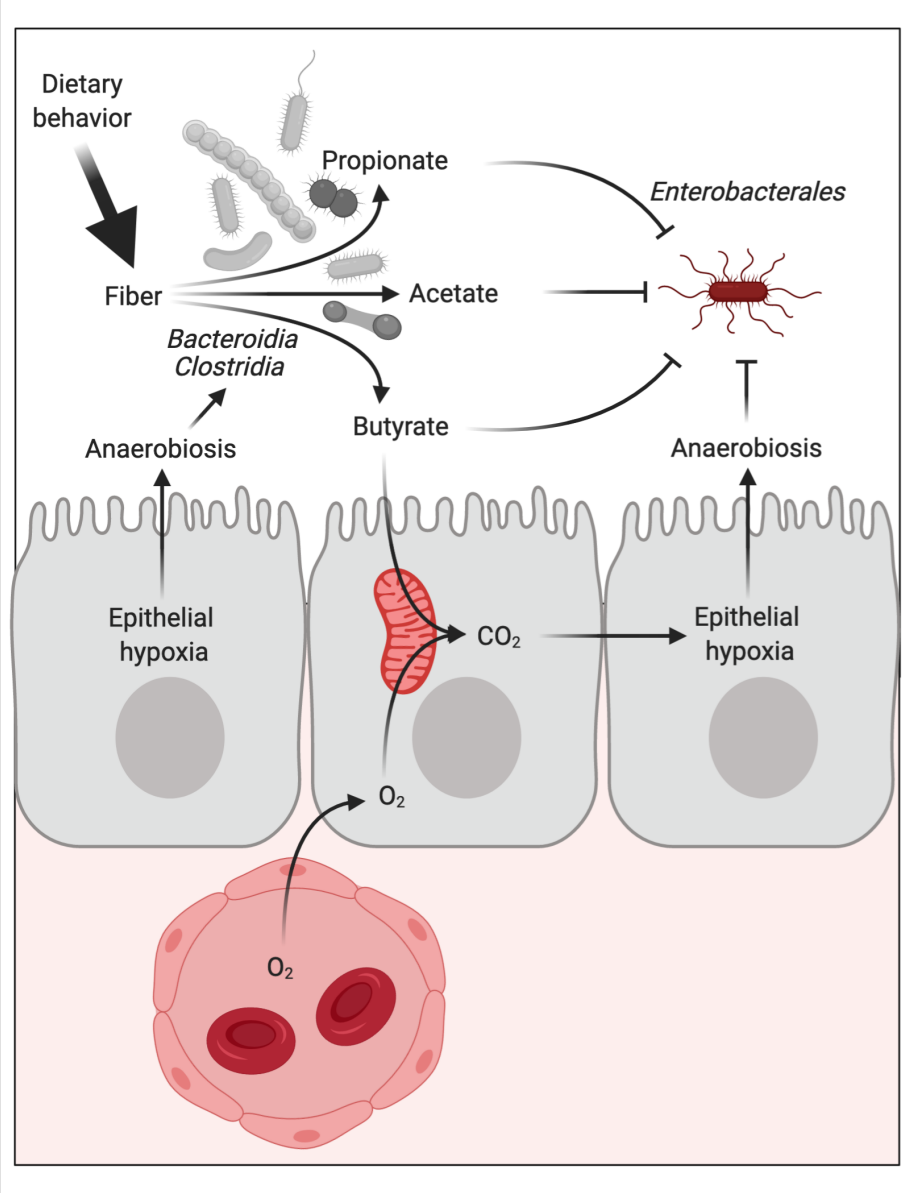

Figure 1.2: Habitat filtering in the adult colon. Epithelial hypoxia and dietary fiber filter the habitat in the large intestine to license growth of obligate anaerobic fiber eaters, which drives a dominance of the classes *Clostridia* and *Bacteroidia* in the fecal microbiota. Facultative anaerobic bacteria, such as members of the *Enterobacterales*, remain minority species because epithelial hypoxia limits critical resources they require for overcoming growth inhibition by short-chain fatty acids (acetate, butyrate and propionate). Created with BioRender.com

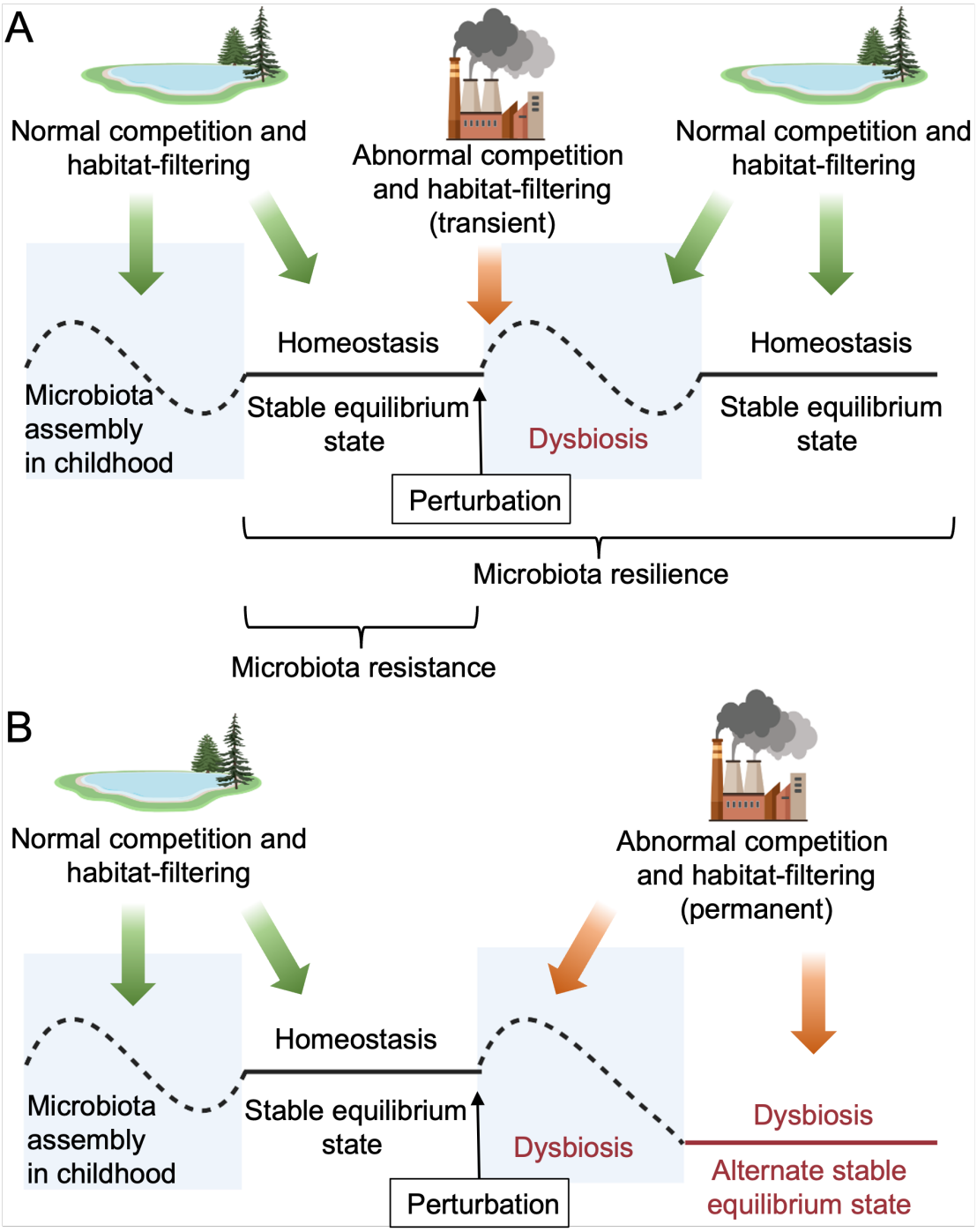

Figure 1.3: Normal competition and habitat filtering promote homeostasis, microbiota resistance and microbiota resilience. (A) After birth, the microbiota exhibits fluctuations as it assembles to fill nutrient-niches created by competition and habitat filtering. Once microbiota assembly is complete, a state of normal competition

and habitat filtering maintains homeostasis, characterized by a stable equilibrium state in which the microbiota composition remains invariable over time, a phenomenon termed microbiota resistance. A brief perturbation, such as a disruption of the microbiota with antibiotics, leads to a transient state of abnormal competition and habitat filtering, which causes dysbiotic fluctuation in the microbiota composition. However, once normal competition and habitat filtering resume, the microbiota reassembles to reach an equilibrium state that is functionally similar to that of the community prior to the perturbation. The ability of the microbiota to return to homeostasis after a perturbation is termed microbiota resilience. (B) A lasting perturbation, which can be caused for example by chronic intestinal inflammation, triggers a permanent state of abnormal competition and habitat filtering. As new nutrient-niches created by abnormal competition and habitat filtering are filled, the microbiota composition shifts permanently to reach an alternate equilibrium state. Through this process, abnormal competition and habitat filtering maintain a perpetual state of dysbiosis. Created with BioRender.com

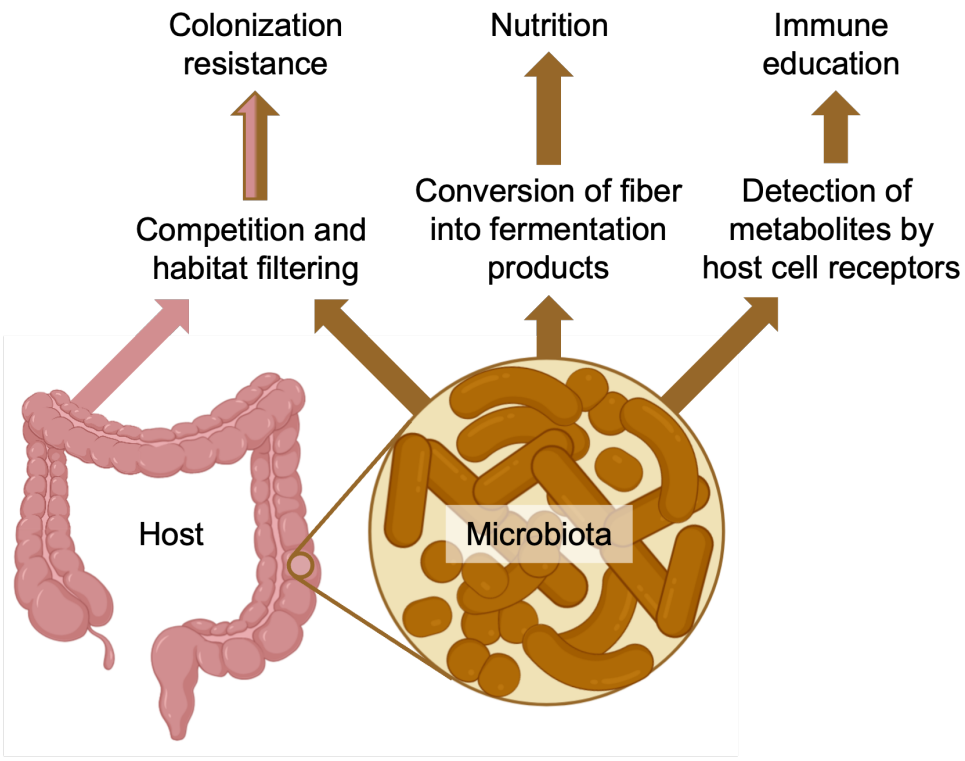

Figure 1.4: Functions of the gut microbiota. Nutrients (e.g. fiber) that evade absorption and degradation by host enzymes in the small intestine enter the colon where they are converted into fermentation products by the gut microbiota. This metabolic activity of the gut microbiota has been likened to the function of an organ that contributes to host nutrition and immune education. Host-derived habitat filters and the microbiota form a host microbe chimera that performs a third function, termed colonization resistance, which prevents harmful microbes from entering the body. Created with BioRender.com

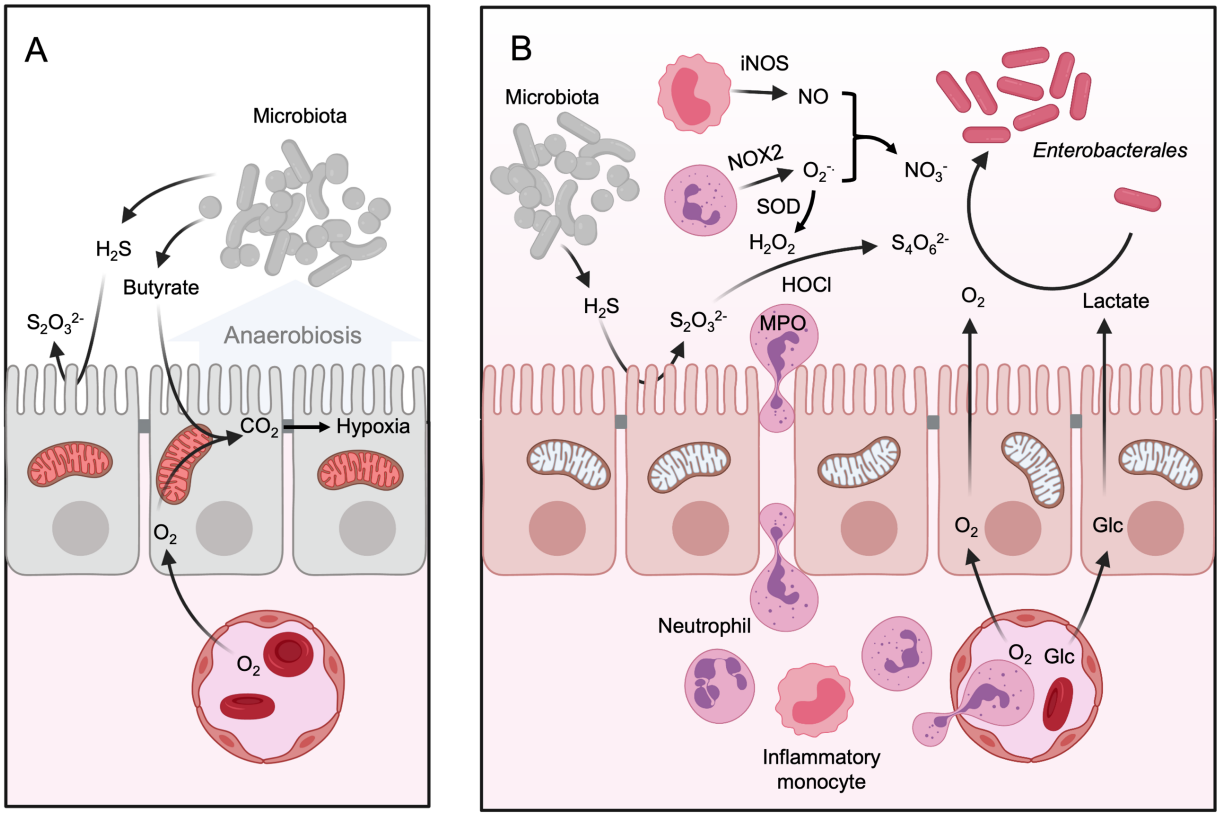

Fig. 1.5: Intestinal inflammation creates a state of abnormal habitat filtering. (A) During homeostasis, microbiota-derived butyrate maintains high oxygen (O_2) consumption in the colonic epithelium through mitochondrial oxidative phosphorylation (246-248). The resulting epithelial hypoxia limits diffusion of oxygen into the gut lumen to preserve anaerobiosis, which maintains a dominance of obligate anaerobic bacteria in the gut microbiota (89). Sulfate-reducing bacteria generate hydrogen sulfide (H_2S) (249), which is detoxified by epithelial sulfide oxidases to thiosulfate ($S_2O_3^{2-}$) (250, 251). (B) During intestinal inflammation, neutrophils and inflammatory monocytes migrate into the intestinal lumen. Inflammatory monocytes are the dominant source of inducible nitric oxide synthase (iNOS), which generates nitric oxide (NO) (252). Nitric oxide can react with superoxide ($O_2^{\cdot-}$) produced by phagocyte NADPH oxidase (NOX2) to form

peroxynitrite (253), which decomposes to nitrate (NO_3^-) in the gut lumen (254). Superoxide is converted by superoxide dismutase (SOD) to hydrogen peroxide (H_2O_2), which is converted to hypochloric acid (HOCl) by neutrophil myeloperoxidase (MPO). These reactive oxygen species oxidize thiosulfate to tetrathionate ($S_4O_6^{2-}$) (10). Intestinal inflammation reduces mitochondrial bioenergetics in the colonic epithelium, thereby reducing epithelial oxygen consumption (154). The resulting loss of epithelial hypoxia increases diffusion of oxygen into the intestinal lumen to disrupt anaerobiosis. Catabolism of glucose (Glc) by host cells through aerobic glycolysis increases the luminal concentration of host-derived lactate (59). Through these mechanisms, intestinal inflammation elevates the availability of oxygen, lactate, nitrate and tetrathionate in the colonic lumen to create a state of abnormal habitat filtering that drives an expansion of facultative anaerobic *Enterobacterales*, which is a microbial signature of dysbiosis in the fecal microbiota (36, 37). Created with BioRender.com

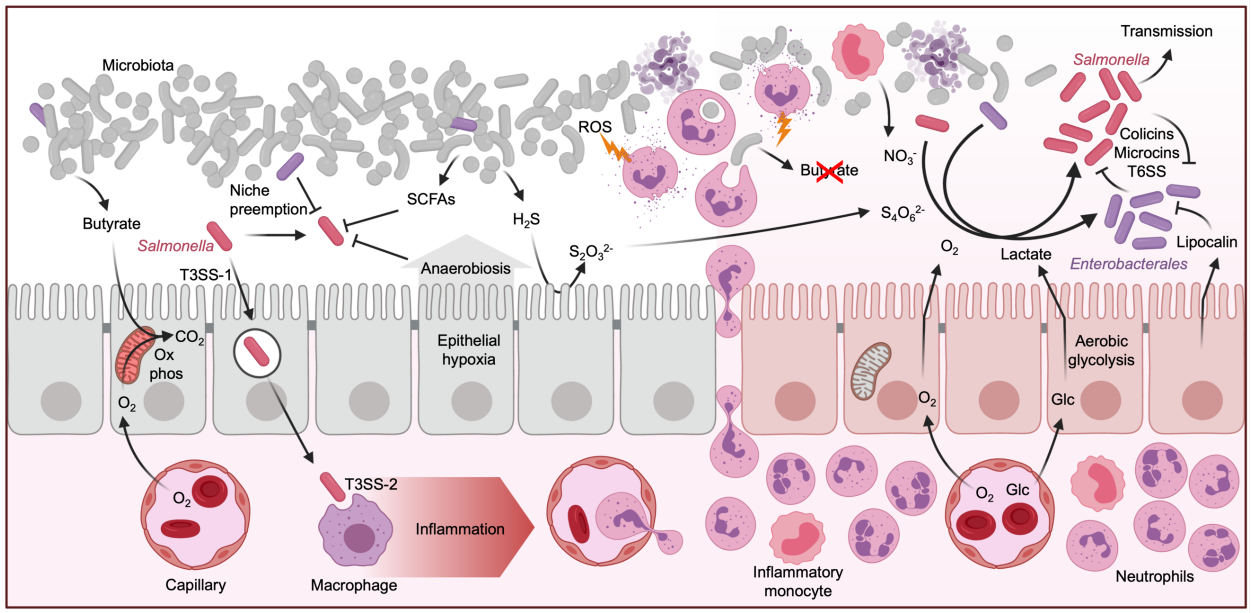

Fig. 1.6: *S.* Typhimurium uses its virulence factors for ecosystem engineering.

During homeostasis, conversion of microbiota-derived butyrate to carbon dioxide (CO_2) through mitochondrial oxidative phosphorylation (Ox phos) results in high epithelial oxygen (O_2) consumption, which maintains epithelial hypoxia. Epithelial cells detoxify microbiota-derived hydrogen sulfide (H_2S) by conversion into thiosulfate ($S_2O_3^{2-}$). Upon entry, *S.* Typhimurium uses its virulence factors to invade the intestinal epithelium (T3SS-1) and survive in macrophages in host tissue (T3SS-2). However, prior to the development of host responses, anaerobiosis and niche preemption by endogenous *Enterobacterales* limit access of the luminal *S.* Typhimurium population to resources critical for overcoming growth inhibition by short-chain fatty acids (SCFA's). As a result, the luminal *S.* Typhimurium population drops, which can lead to a pathogen extinction if the challenge dose is low. In the meantime, the virulence factor-mediated tissue invasion is detected by the innate immune system, which results in orchestration of an inflammatory response characterized by cellular infiltrates that are dominated by

neutrophils. The inflammatory response eventually clears the subpopulation of the pathogen that resides in tissue, but it also induces migration of phagocytes into the intestinal lumen. Luminal phagocytes release reactive oxygen species (ROS) and reactive nitrogen species that generate host-derived electron acceptors, including tetrathionate ($S_4O_6^{2-}$) and nitrate (NO_3^-). Luminal neutrophils also deplete butyrate-producing *Clostridia* from the gut microbiota, which reduces mitochondrial bioenergetics in the intestinal epithelium. The consequent shift in epithelial energy metabolism to aerobic glycolysis, the conversion of glucose (Glc) into lactate, is associated with elevated epithelial release of oxygen and lactate. In turn, these changes in the luminal environment create a state of abnormal habitat filtering, thereby providing *S.* Typhimurium with critical resources (nitrate, tetrathionate, oxygen and lactate) to expand in the gut microbiota, which is required for pathogen transmission by the fecal oral route. The new nutrient-niche created by virulence factor-induced inflammation also supports growth of endogenous *Enterobacterales*, provided they can overcome growth inhibition by lipocalin-2 (Lipocalin), an antimicrobial protein released by epithelial cells during intestinal inflammation. Through this chain of events, virulence factor-mediated ecosystem engineering creates a new nutrient-niche in which *S.* Typhimurium and endogenous *Enterobacterales* battle for supremacy using their antimicrobial weaponry, including colicins, microcins and type VI secretion systems (T6SS). Created with BioRender.com

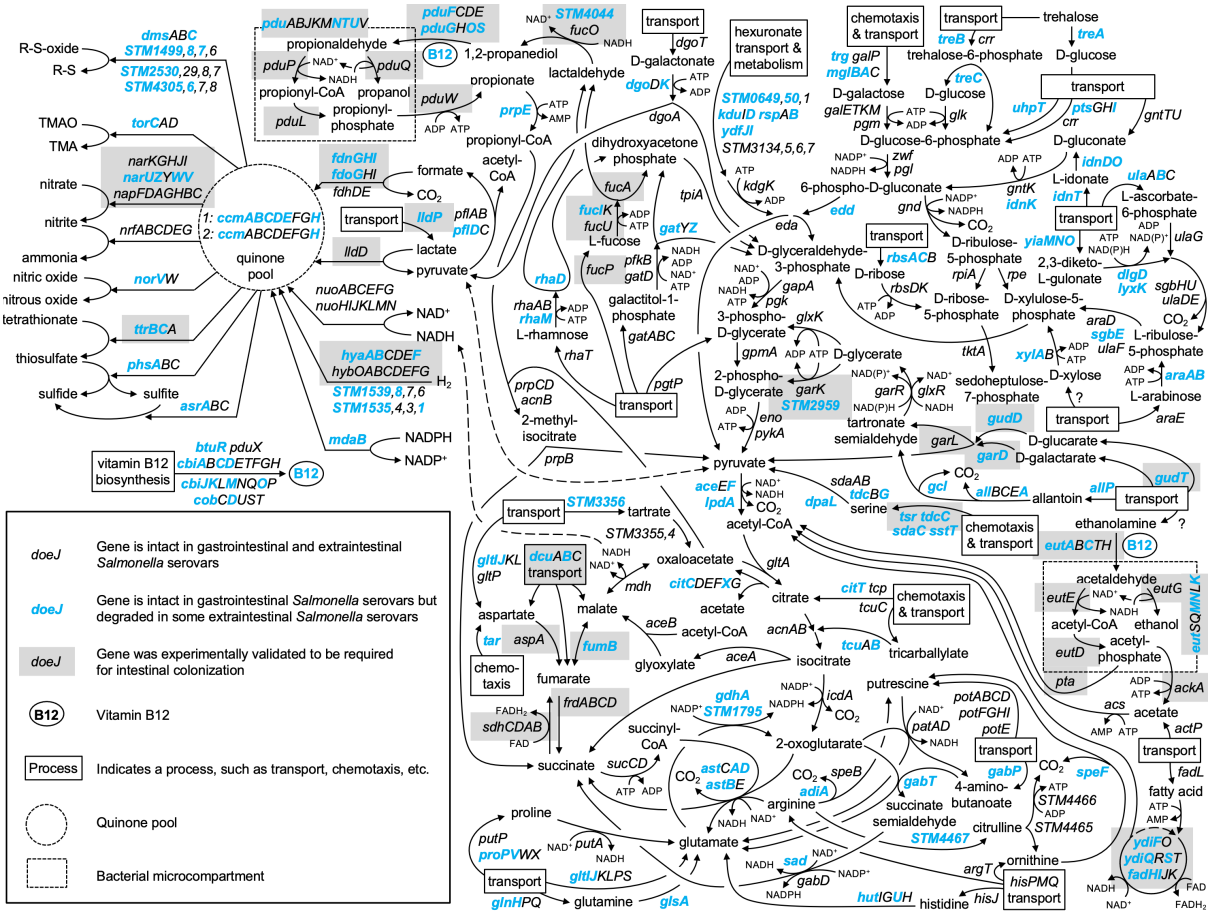

Figure 1.7: Reconstruction of a metabolic network required for growth in an engineered nutrient-niche. Whole genome comparison of 5 genomes representing extraintestinal *Salmonella* serovars and 10 genomes representing gastrointestinal *Salmonella* serovars reveals metabolic pathways gastrointestinal pathogens use to fuel their growth in the inflamed gut (213). The graphic shows pathways that are degrading in genomes of extraintestinal *Salmonella* serovars (genes in blue font) but are intact in genomes of gastrointestinal *Salmonella* serovars. The metabolic network predicted by this *in silico* analysis provides a window into the nutrient-niche that is engineered by *S.* Typhimurium virulence factors in the gut. Modified from (213) with permission.

Chapter 2: Re-engineering of the intestinal environment by *Salmonella* breaks colonization resistance in the presence of a compositionally intact microbiota

Andrew W. L. Rogers[1], Lauren C. Radlinski[1], Henry Nguyen[1], Connor R. Tiffany[1], Thaynara Parente Carvalho[1], Hugo L. P. Masson[1], Michael L. Goodson[2], Lalita Bechtold[1], Kohei Yamazaki[1,3], Megan J. Liou[1,4], Brittany M. Miller[1,5], Scott P. Mahan[1], Briana M. Young[1,] Aurore M. Demars[1], Sophie R. Gretler[1,] Anaïs B. Larabi[1], Jee-Yon Lee[1], Derek J. Bays[6], Renee M. Tsolis[1], and Andreas J. Bäumler[1,#]

Affiliations:

[1] Department of Medical Microbiology and Immunology, School of Medicine, University of California at Davis, One Shields Ave; Davis CA 95616, USA

[2] Department of Anatomy, Physiology and Cell Biology, School of Veterinary Medicine, University of California, Davis, CA, USA

[3] Laboratory of Veterinary Public Health, School of Veterinary Medicine, Kitasato University, Aomori, Japan.

[4] Current address: Department of Microbiology, Perelman School of Medicine, University of Pennsylvania, Philadelphia, PA, USA.

[5] Current address: Division of Gastroenterology and Hepatology, Perelman School of Medicine, University of Pennsylvania, Philadelphia, PA, USA.

[6] Department of Internal Medicine, Division of Infectious Diseases, School of Medicine, University of California at Davis, One Shields Ave; Sacramento CA 95817, USA

Published in:

Cell Host & Microbe. (Published date August 23rd, 2024)

https://doi.org/10.1016/j.chom.2024.07.025

Reprinted with permission from Elsevier.

Summary

The gut microbiota prevents harmful microbes from entering the body, a function known as colonization resistance. The enteric pathogen *Salmonella enterica* serovar (*S.*) Typhimurium uses its virulence factors to break colonization resistance through unknown mechanisms. Using metabolite profiling and genetic analysis we show that the initial rise in luminal pathogen abundance was powered by a combination of aerobic respiration and mixed acid fermentation of simple sugars, such as glucose, which resulted in their depletion from the metabolome. The initial rise in the abundance of the pathogen in the feces coincided with a reduction in the cecal concentrations of acetate and butyrate and an increase in epithelial oxygenation. Notably, these changes in the host environment preceded changes in the microbiota composition. We conclude that changes in the host environment can weaken colonization resistance even in the absence of overt compositional changes in the gut microbiota.

Introduction

Salmonella enterica serovar (*S.*) Typhimurium is an invasive enteric pathogen that causes an inflammatory diarrhea in immunocompetent individuals(1). The pathogen uses a type III secretion system (T3SS-1) encoded by *Salmonella* pathogenicity island 1 (SPI1)(2) to invade the intestinal epithelium(3). A second type III secretion system (T3SS-2) encoded by SPI2(4) enables the pathogen to survive in tissue(5), in part by avoiding NADPH phagocyte oxidase-dependent killing(6-8). T3SS-1-mediated entry and T3SS-2-mediated survival in tissue trigger acute intestinal inflammation(9), an aspect of host-pathogen interaction that can be modeled in streptomycin pretreated mice (mouse colitis model)(10). In streptomycin pretreated mice, T3SS-1 and T3SS-2 contribute to inflammation in the cecum and colon(11), a host response that prevents microbiota recovery after antibiotic treatment(12, 13) by driving the recruitment of phagocytes into the intestinal lumen(14). Streptomycin pretreated, genetically susceptible mice have been used extensively to study virulence factors of the pathogen and mucosal immune responses to infection(15).

However, streptomycin pretreatment disrupts microbiota-mediated colonization resistance(16), thereby reducing the utility of the mouse colitis model for studying how *S.* Typhimurium overcomes this non-specific host defense. A streptomycin-mediated microbiota disruption depletes short-chain fatty acids(17), resulting in a metabolic reprogramming of the intestinal epithelium that increases the availability of oxygen and nitrate in the mucus layer(18). Furthermore, streptomycin treatment increases the concentrations of simple carbohydrates in cecal contents(19). Thus, when *S.* Typhimurium arrives in the cecum of a streptomycin pretreated mouse, the pathogen can

fuel its luminal growth using critical resources that are not available when the microbiota is intact. As a result, the pathways that allow *S.* Typhimurium to initially overcome microbiota-mediated colonization resistance remain incompletely understood. Here we determined how *S.* Typhimurium overcomes colonization resistance in mice with an intact microbiota and which resources drive an initial pathogen expansion.

Results

Salmonella virulence factors overcome microbiota-mediated growth inhibition

To establish the kinetics of fecal shedding when antibiotic-naïve mice are infected with *S.* Typhimurium, CBA mice from Jackson laboratories (CBA/J mice), which were routinely confirmed to be *Enterobacterales* free(20), were mock-infected or infected with 10^9 colony-forming units (CFU) of the *S.* Typhimurium wild type (strain IR715, a nalidixic acid-resistant derivative of isolate ATCC14028) by oral gavage. Fecal pellets were collected daily for 10 days to enumerate *S.* Typhimurium. Whereas pathogen numbers in the feces decreased initially, a notable increase was observed three days after infection and *S.* Typhimurium was subsequently shed at high numbers with the feces (**Fig. 2.1A**).

To contrast the kinetics to the commonly used mouse colitis model(15), CBA/J mice received a single dose of streptomycin and were infected the next day with 10^9 CFU of the *S.* Typhimurium wild type. Notably, the initial decrease in *S.* Typhimurium numbers observed two days after infection in antibiotic-naïve CBA/J mice was not observed in streptomycin-pretreated CBA/J mice (**Fig. 2.1A**), implicating the gut microbiota in the initial control of pathogen growth.

To determine whether the marked rise in *S.* Typhimurium numbers recovered from feces of antibiotic-naïve CBA/J mice three days after infection required inflammation triggered by virulence factors of the pathogen, the experiment was repeated with an isogenic *S.* Typhimurium strain that was rendered avirulent by engineering mutations in *invA*, encoding a component of T3SS-1, and *spiB*, encoding a component of T3SS-2. When *Enterobacterales*-free CBA/J mice were infected with 10^9 CFU of an avirulent *invA*

spiB mutant, a rise in *S.* Typhimurium numbers recovered from the feces was no longer observed three days after infection and the avirulent strain was recovered in low numbers from the feces throughout the experiment (**Fig. 2.1A**). Collectively, these data suggested that an intact microbiota reduces pathogen load in the feces during the initial two days after infection, but the pathogen uses its virulence factors to overcome this growth inhibition by three days after infection, presumably because virulence factor-induced intestinal inflammation triggers changes in the intestinal growth environment.

A rise in absolute pathogen abundance is linked to a depletion of simple sugars

Previous work shows that virulence factor-induced inflammation drives respiration using cytochrome *bd* II oxidase, encoded by *cyxA*, and nitrate reductases encoded by *napA*, *narZ*, and *narG* (13). Consistent with this idea, a *S.* Typhimurium *napA narZ narG cyxA* mutant exhibited reduced fitness compared to the *S.* Typhimurium wild type 10 days after inoculating antibiotic-naïve CBA/J mice with a 1:1 mixture of both strains (**Fig. 2.1B**). However, cytochrome *bd* II oxidase-mediated aerobic respiration and anaerobic nitrate respiration did not confer a fitness advantage three days after infection. These data suggested that virulence factors enabled *S.* Typhimurium to overcome microbiota-mediated growth inhibition three days after infection (**Fig. 2.1A**) through an unknown mechanism.

To determine which resources the pathogen initially relies on to overcome microbiota-mediated growth inhibition, we determined which metabolites were depleted from the cecal metabolome at days three and four after *S.* Typhimurium infection.

Antibiotic-naïve CBA/J mice were mock-infected or infected with 10^9 CFU of the *S.* Typhimurium wild type by oral gavage. Cecal contents collected three or four days after *S.* Typhimurium infection were analyzed by metabolite profiling. Principal component analysis of the samples showed a distinct clustering of metabolite profiles from samples collected four days after *S.* Typhimurium infection compared to samples collected from mock-infected mice (**Fig. 2.1C**), indicating that *S.* Typhimurium infection changes the composition of the murine cecal metabolome either directly, or indirectly by triggering inflammation. The 95% confidence interval of metabolite profiles from samples collected three days after *S.* Typhimurium infection overlapped with the other two treatment groups. Notably, all features significantly decreased in samples collected four days after *S.* Typhimurium infection compared to mock-infection were also significantly decreased in samples collected three days after *S.* Typhimurium infection.

The metabolic footprint *S.* Typhimurium produced four days after infection featured a depletion of simple sugars from cecal contents, including depletion of tri- and disaccharides (e.g., maltotriose, maltose, sucrose, cellobiose, and sophorose), hexoses (e.g., glucose, 3,6-anhydro-D-galactose, and glucose-1-phosphate), pentoses (e.g., ribose, xylulose, and xylose), trioses (e.g., dihydroxyacetone), amino sugars (e.g., UDP-*N*-acetylglucosamine), sugar acids (e.g., galacturonic acid, glucuronic acid, and glyceric acid), and sugar alcohols (e.g., sorbitol, lactitol, and galactinol) (**Fig 2.1D**).

Mixed acid fermentation drives an *S.* Typhimurium expansion in the feces

We reasoned that *S.* Typhimurium might reduce the cecal concentration of sugars either directly by catabolizing them or indirectly by triggering inflammation. Pathways for catabolizing simple sugars converge on phosphoenolpyruvate and pyruvate. In the absence of respiratory electron acceptors, such as oxygen or nitrate, these metabolites are then broken down by *S.* Typhimurium through mixed acid fermentation in a set of reactions that yield the fermentation products lactate, acetate, succinate, formate, ethanol, carbon dioxide and hydrogen (**Fig. 2.S1A**)(21). To test the hypothesis that *S.* Typhimurium catabolism reduces the cecal concentration of sugars, we determined whether *S.* Typhimurium uses mixed acid fermentation to overcome growth inhibition by the microbiota three days after infection. Since bacterial growth is limited by the availability of adenosine triphosphate (ATP)(22), we prioritized mutating the energy-producing steps of mixed acid fermentation. One branch of mixed acid fermentation involves conversion of phosphoenolpyruvate to fumarate through the reductive tricarboxylic acid (TCA) cycle(21). Fumarate reductase encoded by *frdABCD* functions in energy production (i.e., fumarate respiration) by transferring electrons from the quinone pool to fumarate, which is reduced to succinate (**Fig. 2.S1A**). Consistent with a previous report(23), fumarate respiration conferred a clear fitness advantage at days five, seven and ten after *S.* Typhimurium infection, but the contribution of this pathway to growth at three days after infection was less prominent (**Fig. 2.1E**).

A second branch of mixed acid fermentation is initiated by the enzyme pyruvate formate lyase, which converts pyruvate to formate and acetyl-coenzyme A (CoA). Acetyl-CoA is further catabolized to acetate by phosphate acetyltransferase (Pta) and acetate kinase (AckA), which yields ATP through substrate level phosphorylation (**Fig. 2.S1A**). A

S. Typhimurium *ackA pta* mutant exhibited reduced fitness compared to wild-type *S.* Typhimurium at three days after infection (**Fig. 2.1F**). However, interpretation of this phenotype is complicated by the fact that a *S.* Typhimurium *ackA pta* mutant is also defective for acetyl-phosphate signaling, which could contribute to growth attenuation(24). We therefore also tested a mutant lacking alcohol dehydrogenase (AdhE), because to maintain redox balance when sugars are fermented to acetate, a fraction of acetyl-CoA must be converted to ethanol by this enzyme(21). A *S.* Typhimurium *adhE* mutant exhibited a discernable fitness defect at three days after infection (**Fig. 2.1G**). The finding that both an *ackA pta* mutant and an *adhE* mutant exhibited prominent growth defects three days after infection (**Fig. 2.1F and 2.1G**) suggested that this branch of mixed acid fermentation enhanced *S.* Typhimurium growth when virulence factors enabled the pathogen to overcome microbiota-mediated growth inhibition (**Fig. 2.1A**).

Glucose utilization contributes to virulence factor-dependent pathogen expansion

Next, we determined whether fermentation of specific sugars contributes to a rise in the absolute abundance of *S.* Typhimurium in the feces three days after infection. Metabolite profiling suggested that the abundance of glucose was highest in cecal contents compared to other simple sugars (**Fig. 2.S1B**). Since glucose is also the preferred carbon source of *S.* Typhimurium, we constructed a mutant defective in glucose transport/metabolism (**Fig. 2.1A**). To this end, we mutated *ptsG*, encoding a component of the enzyme II complex of the phosphoenolpyruvate-dependent glucose-specific phosphotransferase system (PTS), *glk*, encoding glucokinase, and *manXYZ*, encoding a

PTS transporter with broad specificity for mannose, glucose, 2-deoxyglucose, *N*-acetylglucosamine, *N*-acetylmannosamine and galactosamine. These mutations were chosen, because previous work shows that a *S.* Typhimurium *ptsG glk manXYZ* mutant is unable to utilize glucose as a carbon source(25). Importantly, inactivation of *ptsG*, *glk*, and *manXYZ* prevents accumulation of phosphorylated intermediates (**Fig. 2.S1A**), which can have toxic effects(26). A *S.* Typhimurium *ptsG glk manXYZ* mutant exhibited reduced fitness compared to wild-type *S.* Typhimurium at three days after infection as indicated by reduced recovery from the feces of mice infected with a 1:1 mixture of both strains (**Fig. 2.2A**). These data suggested that glucose was one of the sugars contributing to a rise in the absolute abundance of the pathogen three days after infection.

Next, we tested whether other simple sugars that become depleted during *S.* Typhimurium infection also contribute to growth of the pathogen. Among the metabolites depleted during *S.* Typhimurium infection were the acidic sugars galacturonic acid and glucuronic acid (**Fig. 2.S1B**), which are degraded through the Entner–Doudoroff pathway. We thus tested whether inactivation of this pathway through mutations in *edd*, encoding 6-phosphogluconate dehydratase, and *eda*, encoding 2-keto-3-deoxy-6-phosphogluconate aldolase, would reduce fitness of *S.* Typhimurium. A *S.* Typhimurium *edd eda* mutant exhibited reduced fitness compared the *S.* Typhimurium wild type at three days after infection (**Fig. 2.S1C**), thus further supporting the idea that utilization of simple sugars supports an initial pathogen expansion.

Next, we wanted to determine whether enhanced pathogen growth is triggered by an increased availability of glucose. *S.* Typhimurium initiates infection by invading Peyer's patches in the ileum(27), which triggers ileitis(28). Ileitis is known to induce malabsorption

in the small intestine, which decreases glucose absorption(29, 30). We thus hypothesized that *S.* Typhimurium-induced inflammation in the small intestine causes malabsorption to increase the amount of dietary glucose entering the large intestine. Expression of *Lcn2*, encoding the proinflammatory marker lipocalin-2, was significantly increased in RNA isolated from preparations of ileal epithelial cells three days after *S.* Typhimurium infection (**Fig. 2.2B**), which was indicative of inflammation. Glucose is primarily absorbed by epithelial cells via the sodium-dependent glucose co-transporter (SGLT1)(30). Transcript levels of *Sglt1* were significantly reduced in RNA isolated from preparations of ileal epithelial cells three days after *S.* Typhimurium infection compared to samples from mock-infected mice (**Fig. 2.2C**). A similar reduction in mRNA levels were also observed for *Glut2*, encoding a transport protein that facilitates diffusion of glucose across cell membranes (**Fig. 2.2D**). Next, antibiotic-naïve CBA/J mice were mock infected or infected with the *S.* Typhimurium wild type and received a bolus of glucose by oral gavage 3 days after infection. *S.* Typhimurium infection reduced blood glucose levels compared to mock-infection (**Fig. 2.2E and 2.2F**), indicative of either reduced glucose absorption or increased glucose tolerance.

The hypothesis that *S.* Typhimurium virulence factors trigger glucose malabsorption predicted that inhibition of host glucose transport would rescue growth of an avirulent *S.* Typhimurium *invA spiB* mutant (**Fig. 2.1A**). To test this prediction, antibiotic-naïve CBA/J mice were infected with an *S.* Typhimurium *invA spiB* mutant. Two days after infection, mice were mock-treated or treated with sotagliflozin, a sodium-glucose co-transporter 1 and 2 inhibitor, by oral gavage followed 30 minutes later by feeding a bolus of glucose by the same route. Sotagliflozin treatment did not increase

growth of an avirulent *S.* Typhimurium *invA spiB* mutant (**Fig. 2.2G**), which did not support the hypothesis that virulence factor-induced glucose malabsorption enables *S.* Typhimurium wild type to overcome microbiota-mediated growth inhibition three days after infection. Next, we measured absolute glucose levels in cecal contents of mice by a colorimetric assay. Consistent with results from metabolite profiling (**Fig. 2.1D and Fig. 2.S1B**), the concentration of glucose was reduced in cecal contents three days after infection with the *S.* Typhimurium wild type compared to mock-infected mice (**Fig. 2.2H**). This depletion of glucose during *S.* Typhimurium infection was dependent on virulence factors of the pathogen because it was no longer observed in animals infected with an avirulent *S.* Typhimurium *invA spiB* mutant. We hypothesized that glucose consumption by the pathogen would mask an increase in glucose availability triggered by malabsorption in the ileum. We thus reasoned that an increase in cecal glucose concentration would be observed when mice are infected with a *S.* Typhimurium *ptsG glk manXYZ* mutant, which has intact virulence factors to trigger inflammation, but lacks the ability to deplete glucose (**Fig. 2.S1A**). The concentration of glucose was no longer reduced in cecal contents three days after infection with a *S.* Typhimurium *ptsG glk manXYZ* mutant compared to mock-infected mice (**Fig. 2.2H**). These data supported the idea that a reduction in the cecal glucose concentration three days after infection with the *S.* Typhimurium wild type was causatively linked to glucose consumption by the pathogen. However, compared to mock-infected mice, glucose levels were not increased in ceca of mice infected with a *ptsG glk manXYZ* mutant, thus refuting the idea that malabsorption in the ileum increases the concentration of glucose in the cecum during *S.* Typhimurium infection.

In summary, two lines of evidence refuted the hypothesis that virulence factor-induced inflammation in the small intestine increased glucose availability in the cecum by causing glucose malabsorption (**Fig 2.2G and 2.2H**). Instead, the most parsimonious explanation for our observations was that virulence factors triggered an unknown change in the cecal environment to stimulate pathogen growth. In turn, enhanced pathogen growth resulted in the depletion of simple sugars, such as glucose.

Initial pathogen growth is not linked to compositional microbiota changes

Having established that depletion of glucose is a consequence of pathogen expansion, we wanted to determine which virulence factor-induced changes in the host environment caused a rise in the absolute luminal abundance of *S.* Typhimurium three days after infection. Since virulence factors trigger colitis(13), we first wanted to determine whether this host response is already overt at three days after infection. *S.* Typhimurium infection increased transcript levels of genes encoding proinflammatory cytokines, including *Il17a* (**Fig. 2.3A**), *Mip2* (**Fig. 2.3B**), *Kc* (**Fig. 2.3C**), and *Lcn2* (**Fig. 2.3D**), in RNA isolated from the cecal mucosa three days after infection. Furthermore, blinded scoring of histological sections prepared from tissue samples collected from the cecum three days after *S.* Typhimurium infection revealed severe acute inflammatory changes (**Fig. 2.3E and 2.3F**). Notably, the severity of inflammatory changes was similar at three and ten days after infection. These data suggested that overt intestinal inflammation was already detectable at three days after *S.* Typhimurium infection.

Since intestinal inflammation is known to change the microbiota composition during *S.* Typhimurium infection(12, 13), we next investigated how compositional changes developed over time. To this end, we performed 16S ribosomal RNA amplicon sequencing (microbiota profiling) on fecal samples collected from mice before, and at days three, five, seven and ten after *S.* Typhimurium infection. Principle coordinate analysis suggested that compared to samples collected prior to infection, the microbiota composition became progressively more divergent at later time points after *S.* Typhimurium infection (**Fig. 2.4A**). Comparing the distance between microbial communities using weighted unique fraction metric (UniFrac) revealed that the composition of the fecal microbiota in samples collected at days five, seven and ten after *S.* Typhimurium infection was significantly different from fecal microbial collected prior to infection (**Fig. 2.4B**). However, weighted UniFrac distance of the fecal microbiota collected at three days after *S.* Typhimurium infection was not significantly different from microbiota collected prior to infection.

Consistent with a previous report(13), a significant reduction in the relative abundance of *Clostridia* species was observed 10 days after infection (**Fig. 2.4C**). Random forest analysis predicted that differences in the relative abundance of *Clostridia* were the largest predictor of variation between treatment groups (**Fig. 2.4D**). The number of amplicon sequence variants (ASVs) belonging to the class *Clostridia* that exhibited a reduced relative abundance increased progressively over time, with more than 200 *Clostridia* ASVs showing a significant reduction 10 days after infection compared to pre-infection samples (**Fig. 2.4E**). On the *Clostridia* family level, the most striking reduction in the relative abundance was observed for members of the families *Lachnospiraceae* and *Oscillospiraceae* at 10 days after infection (**Fig. 2.4F**). However, at three days after

infection, neither the relative abundance of *Clostridia* (**Fig. 2.4C**) nor the relative abundances of individual *Clostridia* families (**Fig. 2.4F**) were significantly reduced compared to the community composition prior to infection. In summary, microbiota profiling suggested that compared to pre-infection samples, statistically significant compositional changes were not observed three days after infection.

Reactive nitrogen species impair microbiota metabolism to change the host environment.

To investigate whether inflammation alters microbiota function three days after *S.* Typhimurium infection, we determined concentrations of short-chain fatty acids, the main fermentation products of the gut microbiota, in cecal contents using gas chromatography/mass spectrometry (GC/MS). Whereas the concentration of propionate in cecal contents of mice collected three days after *S.* Typhimurium infection did not change compared to cecal contents collected from mock-infected mice, acetate and butyrate levels were significantly higher in cecal contents of mock-infected mice (**Fig. 2.5A**). *S.* Typhimurium did not deplete butyrate using anaerobic β-oxidation, because reduced cecal butyrate levels were still observed in mice three days after infection with a *S.* Typhimurium *fadD ydiQRSTD* mutant (**Fig. 2.5B**). Short-chain fatty acids are known to contribute to colonization resistance against *S.* Typhimurium by mediating a pH-dependent growth inhibition of the pathogen(17, 31). To determine whether the observed reduction in short-chain fatty acid levels can accelerate growth of *S.* Typhimurium *in vitro*, feces from naïve CBA/J mice were diluted in saline containing short-chain fatty acids

levels that either resembled conditions encountered prior to infection (i.e., 40 mM acetate, 3 mM propionate, and 7.5 mM butyrate) or conditions encountered 3 days after infection (i.e., 20 mM acetate, 3 mM propionate, and 2 mM butyrate). Fecal slurries were then sterile filtered, buffered to pH 5.8, inoculated with *S.* Typhimurium and cultured under microaerophilic conditions (1% oxygen) in a hypoxia chamber. Fecal slurries containing short-chain fatty acid levels that resembled conditions encountered 3 days after infection increased *S.* Typhimurium growth compared to fecal slurries containing short-chain fatty acid levels that resembled conditions encountered prior to infection (**Fig. 2.5C**).

We next investigated whether *S.* Typhimurium-induced intestinal inflammation (**Fig. 2.3**) impairs microbiota metabolism to reduce concentrations of acetate and butyrate by three days after infection (**Fig. 2.5A**). Inhibition of nitric oxide production using the inducible nitric oxide (iNOS) inhibitor aminoguanidine, but not treatment with the NADPH oxidase inhibitor apocynin, restored acetate and butyrate levels three days after *S.* Typhimurium infection (**Fig. 2.5D**). Expression of *Nos2*, the gene encoding iNOS, was significantly elevated in the cecal mucosa by day three after *S.* Typhimurium infection (**Fig. 2.5E**). Compared to mock-treated mice, an increase in acetate and butyrate levels in aminoguanidine-treated mice (**Fig. 2.5D**) was associated with reduced numbers of *S.* Typhimurium recovered from the feces three days after infection (**Fig. 2.5F**), but this difference did not reach statistical significance. However, analysis of short-chain fatty acid levels from five independent experiments revealed that colonization levels of the *S.* Typhimurium wild type were inversely correlated to the cecal concentrations of butyrate ($P = 0.011$) and acetate ($P = 0.014$) (**Fig. 2.5G**). Concentrations of butyrate and acetate explained only a fraction of the changes in *S.* Typhimurium colonization levels (i.e., the

R^2 values were 0.108 and 0.101, respectively), which suggested that mechanisms in addition to reduced short-chain fatty acid levels might contribute to a more efficient utilization of glucose by the pathogen.

CydAB-mediated respiration fuels pathogen growth three days after infection.

We initially considered that nitric oxide resistance of *S.* Typhimurium may provide the pathogen with an advantage over nitric oxide sensitive obligately anaerobic bacteria (**Table S1**). To test this idea, we constructed mutations in *S.* Typhimurium genes implicated in mediating resistance against nitric oxide, including *hmpA*, *norVW*, and *cydAB*(32-34). Neither inactivation of *hmpA* nor deletion of *norVW* reduced the numbers of *S.* Typhimurium recovered from feces three days after infection (**Fig. 2.6A and 2.6B**). In contrast, inactivation of *cydAB* markedly reduced the fitness of *S.* Typhimurium three days after infection (**Fig. 2.6C**). However, inactivation of *cydAB* did not markedly change the minimal inhibitory concentration of *S.* Typhimurium against nitric oxide released by diethethylenetriamine NONOate during anaerobic growth *in vitro* (**Table 2.S1**).

The *cydAB* genes encode cytochrome *bd* oxidase, which promotes aerobic respiration under microaerophilic conditions. We reasoned that instead of mediating nitric oxide resistance, cytochrome *bd* oxidase might promote growth by respiring oxygen. An inverse correlation of *S.* Typhimurium colonization levels with concentrations of acetate and butyrate (**Fig, 2.5G**) also pointed to a possible elevation of epithelial oxygenation, because short-chain fatty acids maintain epithelial hypoxia(18). To determine whether epithelial oxygenation is already elevated at three days after *S.* Typhimurium infection to increase oxygen availability in the lumen, we visualized epithelial oxygenation with

pimonidazole, a 2-nitroimidazole that is reductively activated specifically in hypoxic cells (< 1% oxygen)(35, 36). Anaerobiosis in the intestinal lumen is maintained by epithelial hypoxia(18), which was eliminated at three days after *S.* Typhimurium infection (**Fig. 2.6D and 2.6E**).

Short-chain fatty acids help uphold epithelial hypoxia(18, 37) by maintaining the regulatory T cell pool in the colonic mucosa(38-41), and because butyrate stimulates epithelial peroxisome proliferator-activated receptor gamma (PPAR-γ) signaling to activate mitochondrial oxygen consumption(18). Epithelial hypoxia can be lost when short-chain fatty acids are depleted(18, 37), or when epithelial injury during inflammation stimulates regenerative hyperplasia(42-44), which leads to reduced mitochondrial oxygen consumption in the intestinal epithelium. To determine whether a loss of epithelial hypoxia three days after *S.* Typhimurium infection involved a shift in epithelial energy metabolism(45), we determined transcript levels the PPAR-γ regulated gene *Angptl4*, the gene encoding PPAR-γ coactivator (PGC)-1alpha (*Pgc1a*), and genes encoding components of the electron transport chain, including *Ndufs1*, *Ndufv1*, *Uqcr*, *cox1*, and *Atp5g1*, in preparations of epithelial cells isolated from cecal tissue three days after infection with *S.* Typhimurium or mock infection. Transcript levels of *Angptl4*, *Pgc1a*, *Ndufs1*, *Ndufv1*, *Uqcr*, *cox1*, and *Atp5g1* were significantly reduced in RNA isolated from cecal epithelial cells three days after *S.* Typhimurium infection compared to mock infection, suggesting that an increased oxygen bioavailability in the intestinal lumen (**Fig. 2.6C**) was linked to reduced epithelial mitochondrial activity associated with reduced epithelial PPAR-γ signaling (**Fig 2.6F**).

The picture emerging from this work is that an expansion of *S.* Typhimurium in the feces three days after infection (**Fig. 2.1A**) depends on catabolism of simple sugars (**Fig. 2.1D, 2.2A and 2.S1C**), which is fueled by a combination of mixed acid fermentation (**Fig. 2.1F and 2.1G**) and respiration of oxygen (**Fig. 2.6C**), which becomes available when epithelial hypoxia diminishes (**Fig. 2.6D and 2.6E**).

Discussion

Based on the idea that the microbiome is composed of the microbiota and their genes(46), dysbiosis is commonly defined as a compositional change, including an absence of beneficial microbes, the presence of potentially harmful microorganisms, or a decrease in microbial diversity(47). This viewpoint focuses research on establishing links between compositional and functional changes in the gut microbiota(47). However, a weakening of a canonical microbiome function (i.e., colonization resistance) became apparent three days after *S.* Typhimurium infection, when significant compositional changes were absent. An alternative idea is that the microbiome comprises the microbiota and their host environment(48, 49). Our observation is better compatible with this alternative definition and its correlate that dysbiosis represents a change in the host environment(50, 51). Changes in the host environment were notable three days after *S.* Typhimurium infection, which included overt intestinal inflammation, elevated epithelial oxygenation, and a significant drop in the luminal concentrations of acetate and butyrate, which is considered a biomarker of dysbiosis(52). These changes in the host environment three days after *S.* Typhimurium infection were accompanied by enhanced pathogen growth, indicative of impaired colonization resistance, even though significant changes in the microbiota composition were still absent. Thus, *S.* Typhimurium can overcome colonization resistance by triggering changes in the host environment through metabolic reprogramming of the epithelium before changes in the microbiota composition become apparent. These data suggest that virulence factors break colonization resistance by acting on the host to increase oxygen availability, whereas changes in the microbiota composition at later stages of infection are secondary sequelae.

Short-chain fatty acids are the main metabolites produced by the gut microbiota through fermentation of carbohydrates. Production of acetate and butyrate by obligately anaerobic bacteria hinges upon acetyl-CoA production by pyruvate:ferredoxin oxidoreductase, an enzyme that is inhibited when the non-heme iron in its catalytic site reacts with nitric oxide(53, 54). Thus, a possible explanation for reduced levels of acetate and butyrate three days after *S.* Typhimurium infection is that nitric oxide inhibits enzymes involved in acetyl-CoA production by obligately anaerobic bacteria.

Pathogen growth correlated with a reduced concentration of several simple sugars in the cecal metabolome three days after *S.* Typhimurium infection. One possible explanation for this correlation was that the pathogen catabolized simple sugars to increase its luminal abundance. Notably, the relative abundance of glucose in the cecal metabolome was higher than that of most other simple sugars but was significantly reduced three days after *S.* Typhimurium infection. Glucose is a preferred carbon source of *S.* Typhimurium, which controls utilization of alternative carbon sources by catabolite repression(55, 56). A *S.* Typhimurium mutant deficient for glucose fermentation no longer reduced cecal glucose concentrations during infection, which causatively linked catabolism of glucose by *S.* Typhimurium to a depletion of this sugar in cecal contents three days after infection. Furthermore, the ability to catabolize glucose was required for pathogen growth three days after infection. Collectively, these data suggest that depletion of glucose from cecal contents three days after *S.* Typhimurium infection was a consequence of the pathogen using this carbon source to increase its abundance in the intestinal lumen.

The fermentative catabolism of simple carbohydrates by *S.* Typhimurium converges on a pathway known as mixed acid fermentation(21). Increased recovery of *S.* Typhimurium from feces three days after infection was dependent on the energy producing branches of mixed acid fermentation, which provided experimental support for the idea that sugar fermentation fueled luminal growth of the pathogen. In addition, *cydAB*-mediated aerobic respiration contributed to pathogen growth three days after infection. Sugar catabolism in *E. coli* and *S.* Typhimurium is known to involve a combination of mixed acid fermentation and aerobic respiration, except under extreme circumstances. Complete conversion of glucose into carbon dioxide only proceeds under atmospheric oxygen levels (i.e., 21% O_2) when culture flasks are vigorously agitated to improve the transfer of oxygen from gas to liquid(57). As oxygen availability is reduced below this level, the amount of acetate produced from glucose increases and reaches its maximum under anaerobic conditions(57). Epithelial hypoxia maintains the oxygen concentration in the murine cecum at approximately 0.6% O_2(58), which is close to anaerobiosis(57). When epithelial hypoxia is lost, oxygen levels in the cecal lumen can rise to tissue levels, which is approximately 4% O_2 in the cecal mucosa(58). In this environment, glucose is expected to be catabolized by a combination of aerobic respiration and mixed acid fermentation(57), with oxygen being the main factor determining whether growth of the pathogen is accelerated.

The picture emerging from this study and previous work is that in mice with an intact microbiota, *S.* Typhimurium uses its virulence factors to break colonization resistance by triggering changes in the host environment prior to changing the microbiota composition. These changes in the host environment trigger an initial bloom of the

pathogen, which is driven by catabolism of simple sugars, such as glucose, through a combination of aerobic respiration and mixed acid fermentation. We show that the initial growth on oxygen involves cytochrome *bd* oxidase. However, by day ten after infection, pathogen growth also depends on cytochrome *bd* II oxidase-dependent respiration of oxygen, respiration of nitrate and respiration of tetrathionate(13, 59). The environmental cues responsible for this change in the utilization of respiratory reductases remain unknown. The desired outcome might be an optimal utilization of growth-limiting resources, such as respiratory electron acceptors, to ensure that *S.* Typhimurium is continuously shed in high numbers with the feces, which in turn is required for fecal oral transmission of the pathogen(13, 60).

Acknowledgements

Plasmid pRE112 was a gift from Dieter Schifferli (Addgene plasmid # 43828 ; http://n2t.net/addgene:43828 ; RRID:Addgene 43828).

Sequencing library preparations and sequencing was carried out at the DNA Technologies and Expression Analysis Cores at the UC Davis Genome Center, supported by NIH Shared Instrumentation Grant 1S10OD010786-01.

Work in A.J.B.'s laboratory was supported by the Kenneth Rainin Foundation award #20230029 (A.J.B. and J.-Y.L.) and by Public Health Service Grants AI044170, AI096528, AI112445, AI112949, AI146432 and AI153069. D.J.B was supported by the National Center for Advancing Translational Sciences, National Institutes of Health, through grant number UL1 TR001860 and linked award KL2 TR001859. The content is solely the responsibility of the authors and does not necessarily represent the official views of the NIH.

Author contributions

A.W.L.R. study design, supervised personnel, performed mouse experiments and analyzed the data. C.R.T. analyzed the microbiota profiling data and supervised the analysis of metabolomics data. A.W.L.R., L.C.R., H.N., H.L.P.M., M.L.G., L.B., K.Y., M.J.L., B.M.M., S.P.M., B.M.Y., A.M.D., S.R.G., A.B.L., J.Y.L., and D.J.B. helped perform mouse experiments. A.W.L.R. generated gene deletion mutant bacteria for mouse experiments. H.L.P.M. performed measurements of short-chain fatty acid concentrations. L.C.R. contributed to the design of the experiments and validation of the manuscript.

A.J.B. was a major contributor in conceptualization, supervision and writing the manuscript.

Declarations of Interest

The authors declare no competing interests.

Figures

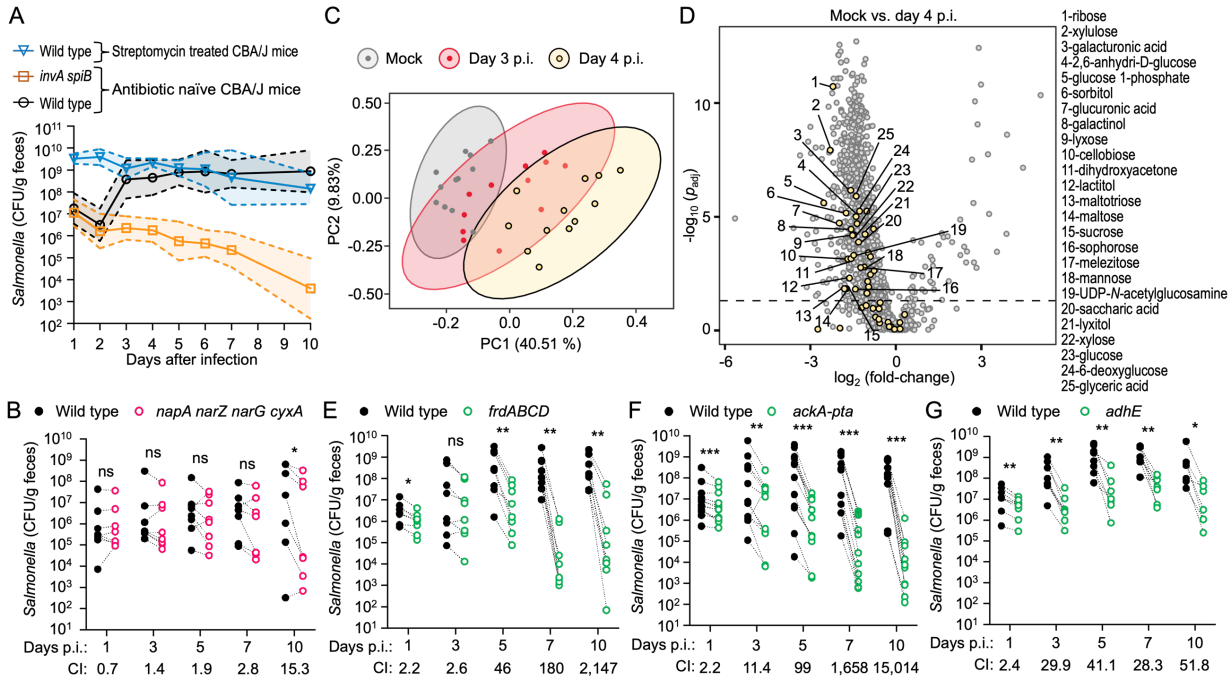

Figure 2.1: An initial rise in the absolute *S.* Typhimurium abundance is driven by mixed acid fermentation in mice with an intact microbiota.

(A) Groups (*n* = 8) of antibiotic-naïve, genetically resistant (CBA/J) mice were infected with 10^9 colony-forming units (CFU) of the *S.* Typhimurium wild type (WT) or an avirulent *invA spiB* mutant and the recovery of CFU from feces was recorded over time. To compare these data with findings from the mouse colitis model, CBA/J mice were pretreated with a single dose of streptomycin (20 mg/animal) and infected one day later with 10^9 CFU of the *S.* Typhimurium wild type. Solid lines indicate the geometric mean. Dotted lines indicate the geometric standard deviation. (B and E-G) CBA/J mice were infected with a 1:1 mixture of the indicated strains. The graphs show CFU of the *S.* Typhimurium WT and the respective mutant recovered from feces at the indicated days after infection (Days p.i.). WT and mutant CFU recovered from the same animal are connected by dotted lines.

The competitive index (CI) determined for each time point is the ratio of wild type to mutant bacteria. (B) Mice were infected with WT and a *napA narZ narG cyxA* mutant. (C and D) CBA/J mice were mock infected or infected with 10^9 CFU of the *S.* Typhimurium WT. Cecal contents were collected three days after infection (Day 3 p.i.) or four days after infection (Day 4 p.i.) for untargeted metabolomics analysis. (C) Principal component analysis of the cecal metabolome in the indicated groups of mice. (D) Volcano plot of metabolites with carbohydrates colored in yellow. (E) Mice were infected with the *S.* Typhimurium WT and a *frdABCD* mutant. (F) Mice were infected with the *S.* Typhimurium WT and an *ackA pta* mutant. (G) Mice were infected with the *S.* Typhimurium WT and an *adhE* mutant. (B, C and E-G) Each dot represents data from one animal (*n*). *, $P < 0.05$; **, $P < 0.01$; *****, $P < 0.001$; ns, $P > 0.05$.

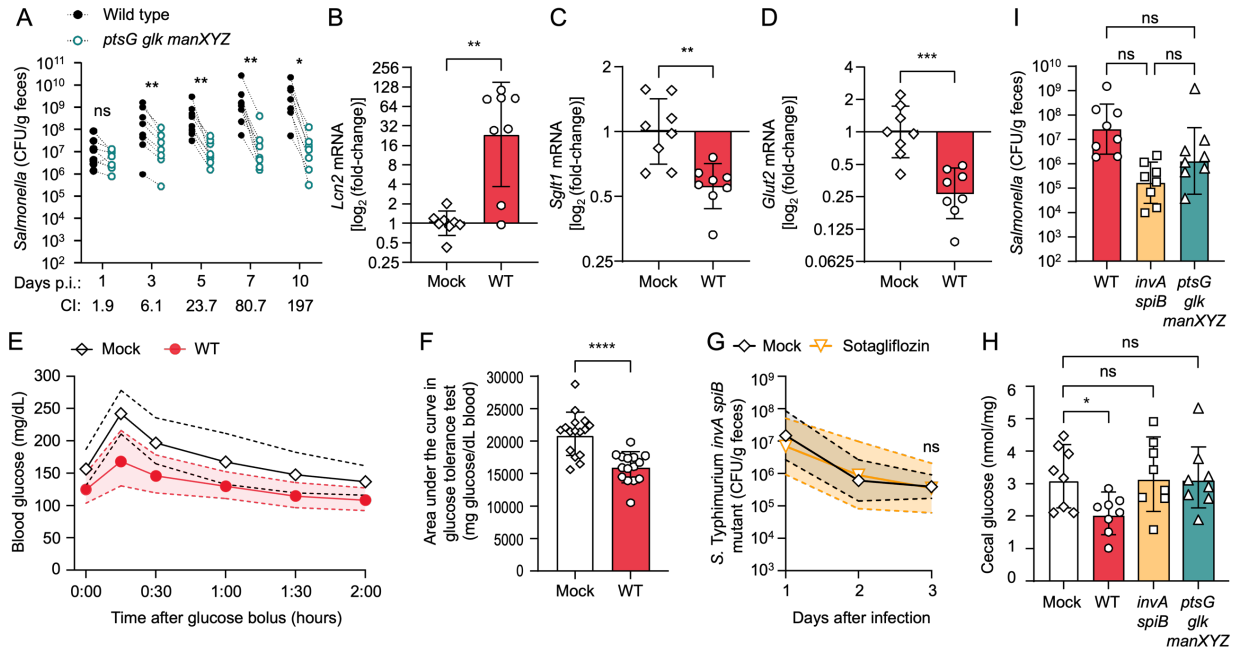

Figure 2.2: *S.* Typhimurium depletes cecal glucose by catabolizing the sugar to increase absolute pathogen abundance in the feces.

(A) Antibiotic-naïve, genetically resistant (CBA/J) mice were infected with a 1:1 mixture of the *S.* Typhimurium wild type (WT) and a mutant unable to catabolize glucose (*ptsG glk manXYZ* mutant). The graph shows colony-forming units (CFU) of each strain recovered from feces at the indicated days after infection (Days p.i.). WT and *ptsG glk manXYZ* mutant CFU recovered from the same animal are connected by dotted lines. The competitive index (CI) determined for each time point is the ratio of wild type to mutant bacteria. (B-D) CBA/J mice were mock infected or infected with the *S.* Typhimurium WT and ileal epithelial cells were collected three days later to isolate mRNA. Fold changes in transcript levels of *Lcn2* (B), *Sglt1* (C), and *Glut2* (D) were determined by quantitative real-time PCR. (E and F) CBA/J mice were mock infected (n = 16) or infected with the *S.* Typhimurium WT (n = 15) and received a bolus of glucose three days later. (E) Blood glucose levels were measured after the indicated time points after receiving the bolus of

glucose (glucose tolerance test). Data is from two independent experiments. (F) The graph shows the area under the curve of the glucose tolerance test. (G) Groups (*n* =8) of CBA/J mice were infected with an avirulent *S.* Typhimurium strain (*invA spiB* mutant). Two days after infection, mice were mock-treated or treated with sotagliflozin, followed 30 minutes later by feeding a bolus of glucose. The graph shows recovery of the *S.* Typhimurium *invA spiB* mutant from the feces at the indicated time points after infection. (H and I) CBA/J mice were mock infected or infected with the indicated *S.* Typhimurium strains. Data is from two independent experiments. (H) Concentrations of glucose in cecal contents was measured three days after infection. (I) CFU in feces were determined three days after infection (B-D, F, H and I) The graphs show geometric means ± geometric standard deviation. (E and G) Solid lines indicate the geometric mean. Dotted lines indicate the geometric standard deviation. Each symbol represents data from one animal. (A-D, F, H and I) Each dot represents data from one animal (*n*). *, $P < 0.05$; **, $P < 0.01$; *****, $P < 0.001$; ****, $P < 0.0001$; ns, $P > 0.05$.

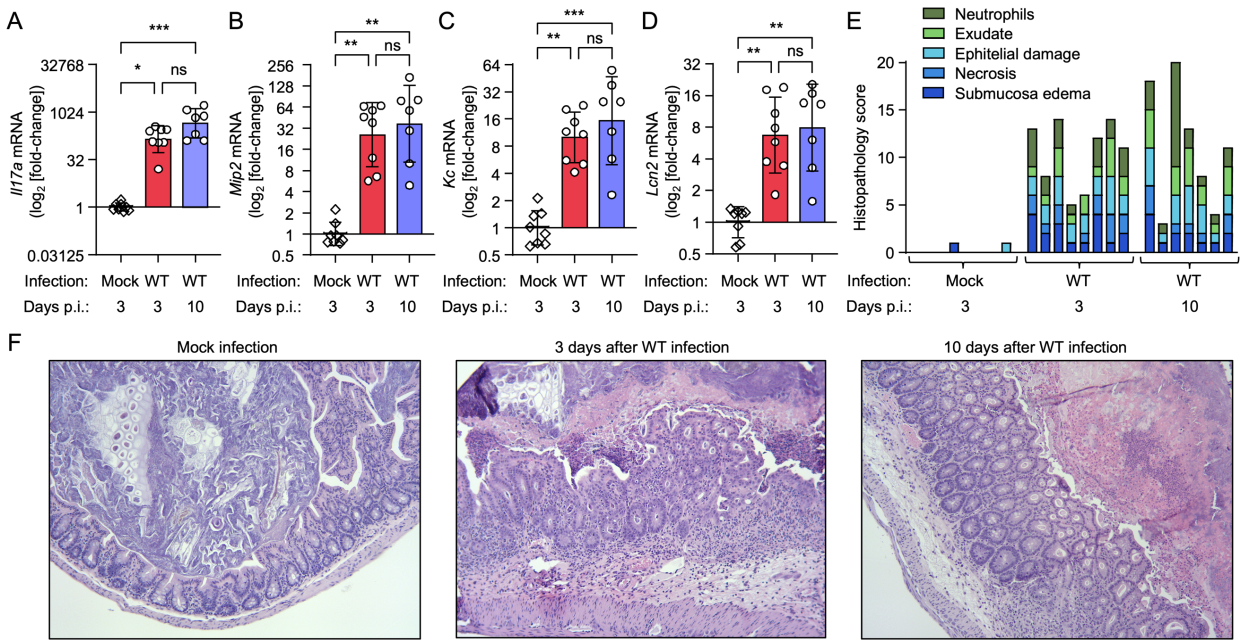

Figure 2.3: Intestinal inflammation elicited during *S.* Typhimurium infection.

Antibiotic-naïve, genetically resistant (CBA/J) mice were mock infected or infected with the *S.* Typhimurium wild type (WT) and the cecum was collected at the indicated time points to assess the severity of intestinal inflammation. Each dot (A-D) or bar (E) represents data from one animal (*n*). (A-D) RNA was extracted from cecal tissue and transcript levels of genetic markers of inflammation, including *Il17a* (A), *Mip2* (B), *Kc* (C), and *Lcn2* (D), were determined by quantitative real time PCR. Transcript levels are expressed as fold-changes compared to transcript levels detected in mock-infected animals. The graphs show geometric means ± geometric standard deviation. (E and F) Hematoxylin and eosin-stained histological sections from the cecum were blinded and analyzed by a veterinary pathologist. (E) Histopathology score for each animal (bars). (F) Representative images are shown. *, $P < 0.05$; **, $P < 0.01$; ***, $P < 0.005$; ns, $P > 0.05$.

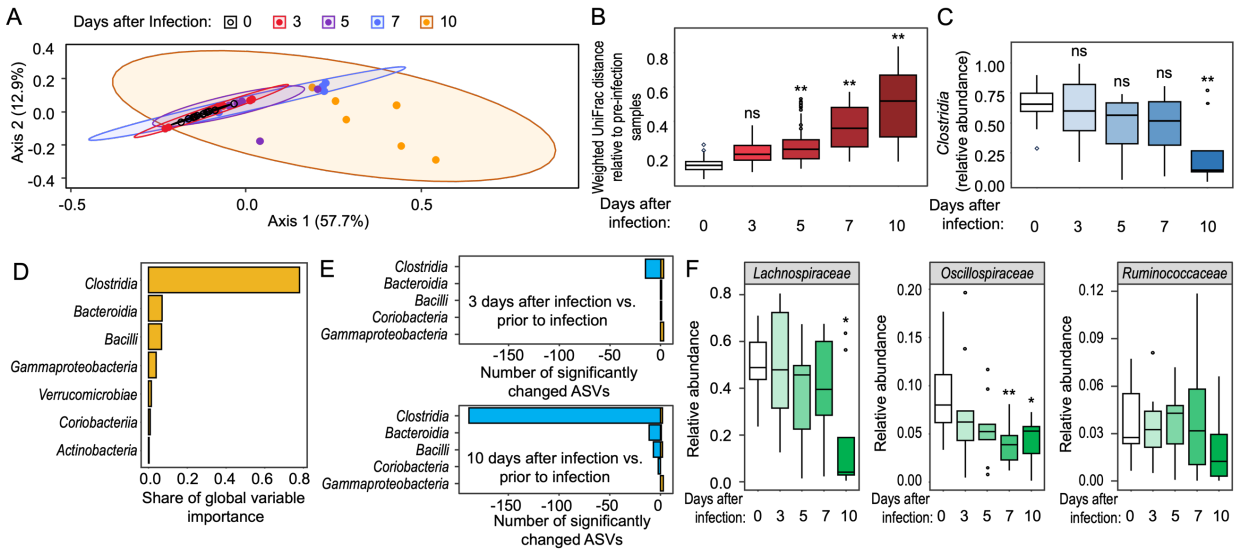

Figure 2.4: Kinetics of compositional changes in the fecal microbiota during *S.* Typhimurium infection.

Groups of antibiotic-naïve, genetically resistant (CBA/J) mice were infected with the *S.* Typhimurium wild type and fecal samples were collected for DNA extraction at the indicated time points. (day 0: *n* = 12; day 3: *n* = 10; day 5: *n* = 9; day 7: *n* = 8; day 10: *n* = 8) (A) PCoA plot showing variation of the mouse fecal microbiota composition by treatment group. Each dot represents data from one animal. (B) Comparison of distances between samples collected at the indicated time points after infection using weighted unique fraction metric (UniFrac). (C) Relative abundance of *Clostridia* ASVs detected from feces collected at the indicated time points after infection. (D) Identification of predictors of variation between samples on the class level using random forest analysis. (E) Bar plot displaying the number of significantly increased and decreased ASVs by class in feces collected three days after infection (top panel) or 10 days after infection (bottom panel) compared to feces collected prior to infection (FDR corrected *P* value =< 0.05). (F) Relative abundance of ASVs belonging to the indicated *Clostridia* families in feces

collected at the indicated time points after infection. (B, C, and F) The box plots represent the first to third quartiles, and the line indicates the median value. *, $P < 0.05$; **, $P < 0.01$; ns, $P > 0.05$.

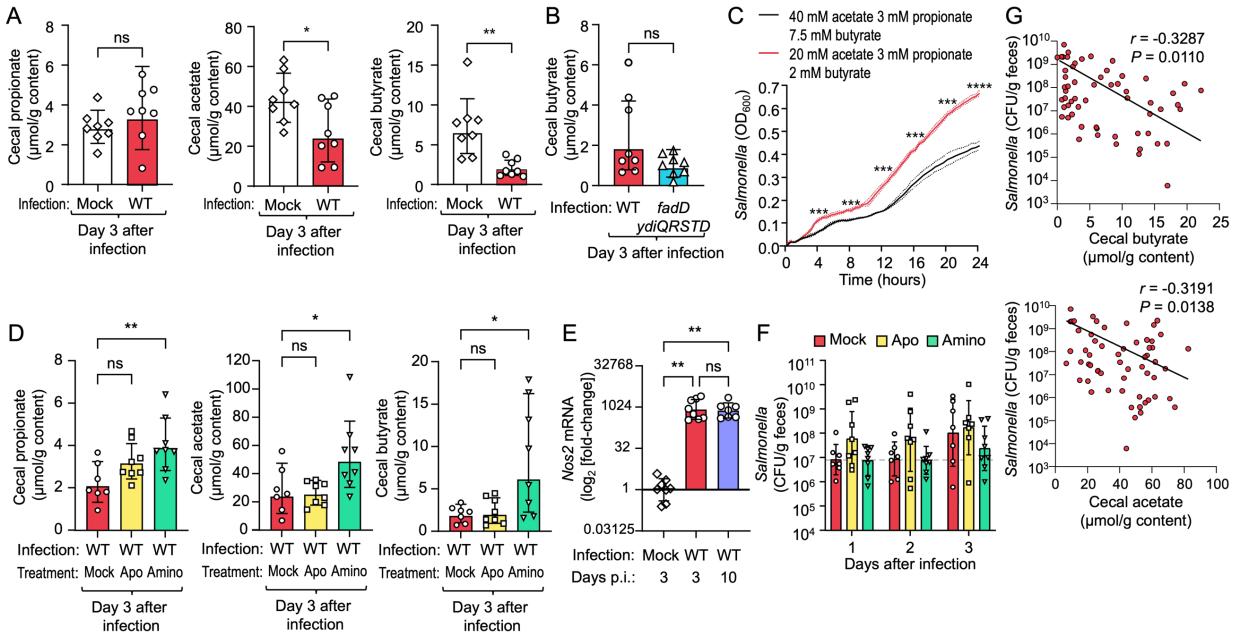

Figure 2.5: Reactive nitrogen species reduce concentrations of microbiota-derived acetate and butyrate three days after infection with *S.* Typhimurium.

(A, B, D-F) Antibiotic-naïve, genetically resistant (CBA/J) mice were mock infected (A and E), infected with the *S.* Typhimurium wild type (WT) (A, B, D-F), or infected with a *S.* Typhimurium *fadD ydiQRSTD* mutant (B) and cecal contents were collected at the indicated time points after infection. (A, B, and D) The graph shows the geometric mean concentration (bars) of the indicated short-chain fatty acids ± geometric standard deviation. (C) Growth of *S.* Typhimurium in fecal slurries containing short-chain fatty acid concentrations resembling conditions encountered prior to infection or 3 days after *S.* Typhimurium infection was monitored by measuring the optical density at 600 nm (OD_{600}) over time. Solid lines indicate the geometric mean of n = 4 repeats. Dotted lines indicate the geometric standard deviation. (D and F) Mice received regular drinking water (treatment: mock), or drinking water supplemented with 80 μg/mL apocynin (Apo) or 1 mg/mL aminoguanidine (Amino). (E) RNA was extracted from cecal tissue and transcript

levels of *Nos2* was determined by quantitative real time PCR. Transcript levels are expressed as fold-changes compared to transcript levels detected in mock-infected animals. The graphs show geometric means ± geometric standard deviation. (F) The graph shows the geometric mean of colony-forming units (CFU) recovered from feces of mice at the indicated time points after infection ± geometric standard deviation. (G) The relationship between *S.* Typhimurium wild type CFUs and the indicated cecal short-chain fatty acid levels at day 3 after infection were assessed by analyzing data from five independent experiments. (A, B, and D-G) Each symbol represents data from one animal and indicates *n*. *, $P < 0.05$; **, $P < 0.01$; ***, $P < 0.001$; ****, $P < 0.0001$; ns, $P > 0.05$.

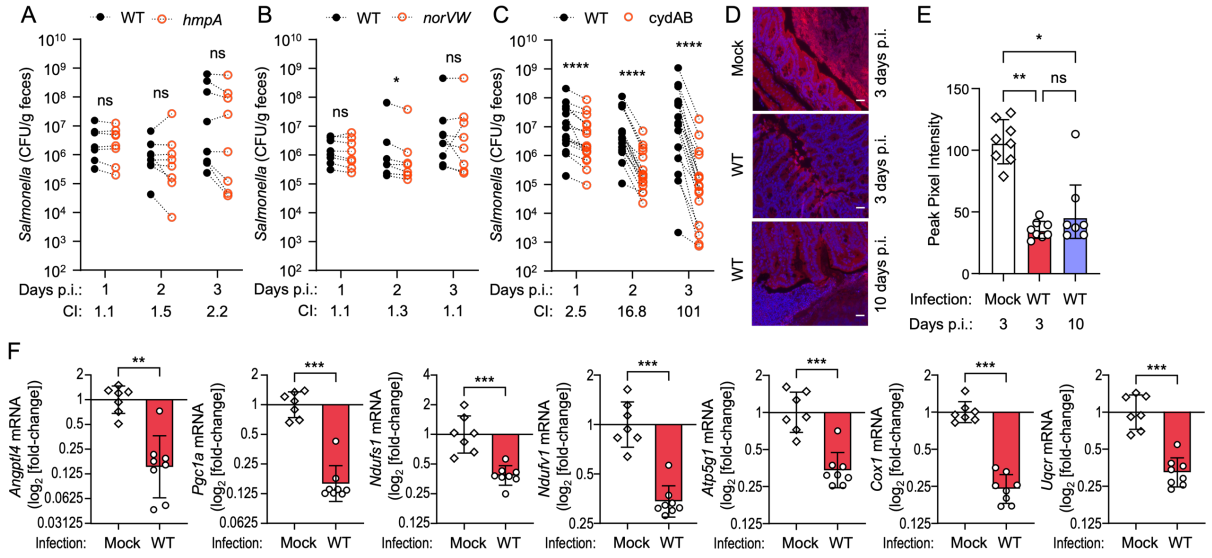

Figure 2.6: Loss of epithelial hypoxia drives *cydAB* mediated growth at 3 days after *S.* Typhimurium infection.

(A - C) CBA/J mice were infected with a 1:1 mixture of the indicated strains. The graphs show CFU of the *S.* Typhimurium WT and the respective mutant recovered from feces at the indicated days after infection (days p.i.). WT and mutant CFU recovered from the same animal are connected by dotted lines. The competitive index (CI) determined for each time point is the ratio of wild type to mutant bacteria. (D and E) CBA/J mice were mock infected or infected with the *S.* Typhimurium wild type (WT) and the cecum was collected three days later. One hour before euthanasia, mice were injected with pimonidazole HCl. (D) Binding of pimonidazole was detected using hypoxyprobe-1 primary antibody and a Cy-3 conjugated goat anti-mouse secondary antibody (red fluorescence) in histological sections from the cecum that were counterstained with DAPI nuclear stain (blue fluorescence). Representative images are shown with 100 μm scale bars. (E) Pimonidazole staining was quantified by measuring mean pixel intensities from the lumen to the border of the colonocytes, and into the tissue. The

graph shows the peak pixel intensity for each mouse (symbols) and the mean peak intensity for each group (bars) ± standard deviation. (F) CBA/J mice were mock infected or infected with the *S.* Typhimurium WT and cecal epithelial cells were collected three days later to isolate mRNA. Fold changes in transcript levels of the *Angptl4, Pgc1a, Ndufs1, Ndufv1, Atp5g1*, *cox1,* and *Uqcr* genes were determined by quantitative real-time PCR. (A-C, and E-F) Each symbol represents data from one animal and indicates *n*. *, $P < 0.05$; **, $P < 0.01$; ***, $P < 0.001$; ****, $P < 0.0001$; ns, $P > 0.05$.

Star Methods

Key Resources Table

REAGENT or RESOURCE	SOURCE	IDENTIFIER
Antibodies		
Mouse anti-pimonidazole monoclonal antibody MAb1	Hypoxyprobe	Hypoxyprobe™-1 Kit, HP1-1000, RRID: AB_2801307
Cyanine3-labeled goat anti-mouse IgG	Jackson ImmunoResearch	Cat# 115-165-003 RRID: AB_2338680
Bacterial and virus strains		
For bacterial strains used in this study see **Table S2**		
Biological samples		
Chemicals, peptides, and recombinant proteins		
4'-hydroxy-3'-methoxyacetophenone (apocynin)	Sigma Aldrich	Cat#: A10809
Aminoguanidine hydrochloride	TCI America	Cat#: A1129
Anhydrous pyridine	Sigma Aldrich	Cat#: 270970
N-tert-butyldimethylsilyl-N-methyltrifluoroacetamide with 1% tert-butyldimethylchlorosilate	Sigma Aldrich	Cat#: 375934
Lidocaine 2.5% and Prilocaine 2.5% Cream	Akorn	Cat#: 50383-667-30
Diethylenetriamine	Thermo Fisher Scientific	Cat#: 114312500
Diethylenetriamne NONOate	Cayman Chemical	Cat#: 82120
Dextrose 50%	Vetone	Cat#: 13985-067-00
Sotagliflozin	Cayman Chemical Company	Cat#: 19141
Tween 80	Thermo Fisher Scientific	Cat#: BP338-500
Difco LB Agar	BD Biosciences	Cat#: 244510
Difco LB Broth	BD Biosciences	Cat#: 244620
Difco Agar, Bacteriological	BD Biosciences	Cat#: 214530
Gifu Anaerobic Media	HiMedia	Cat#: M1801
Acetic-2,2,2-d_3 acid	C/D/N Isotopes	Cat#: D-0290
Sodium Propionate-d_5	C/D/N Isotopes	Cat#: D-5378
Sodium Butyrate-d_7	C/D/N Isotopes	Cat#: D-5372
Streptomycin sulfate, *Streptomyces* sp.	Merck Millipore	Cat#: 5711
Pimonidazole hydrochloride	Hydroxyprobe	Cat#: HP
Immuno-Mount	Epredia	Cat#: 9990402
Critical commercial assays		
Glucose Assay Kit	Abcam	Cat#: ab65333
QIAquick PCR Purification Kit	Qiagen	Cat#: 28106
QIAprep Spin Miniprep Kit	Qiagen	Cat#: 27106

DNeasy Poweroil Kit	Qiagen	Cat#: 12888
NEBuilder HiFi DNA Assembly Master Mix	New England Biolabs	Cat#: E2621L
Q5 Hot Start High-Fidelity 2X Master Mix	New England Biolabs	Cat#: M0493L
SYBR Green PCR Master Mix	Applied Biosciences	Cat#: 4309155
TRI Reagent	Molecular Research Center	Cat#: TR118
PureLink DNase	Invitrogen	Cat#: 12185010
EconoSpin Spin Column for RNA	Epoch Life Science	Cat#: 1940-250
UltraPure Distilled Water	Invitrogen	Cat#: 10977-015
MultiScribe Reverse Transcriptase	Applied Biosystems	Cat#: 4311235
RNase Inhibitor	Applied Biosystems	Cat#: N8080119
Random Hexamers	Invitrogen	Cat#: N8080127
Lysing Matrix C 2 mL Tubes	MP Biomedicals	Cat#: 6912050
KAPA2G Robust HotStart PCR Kit	Kapa Biossytems	Cat#: KK5522
AMPure XP SPRI Reagent	Beckman Coulter	Cat#: A63880
Qubit dsDNA High Sensitivity Quantification Kit	Invitrogen	Cat#: Q32851
Qubit 2.0 Fluorometer	Invtirogen	Cat#: Q32866
Microcon-10kDa Centrifugal Filter Unit	Merck Millipore	Cat#: MRCPRT010
True Metrix Self Monitoring Blood Glucose System Meter Kit	McKesson	Cat#: 06-RE4051-43
True Metrix Self Monitoring Blood Glucose Test Strips	McKesson	Cat#: 06-R3051-45
Wizard Genomic DNA Purification Kit	Promega	Cat#: A1120
Deposited data		
16S rRNA Gene amplicon sequencing data	This Study	BioProject Accession #: PRJNA1037532
Normalized metabolite spectra data	This Study	See **Supplementary File 1** for NIH Metabolomics Database sample identifiers
Experimental models: Cell lines		
Experimental models: Organisms/strains		
Mus musculus CBAJ	Jackson Labs	Cat#: 000656
Mus musculus C57BL/6J	Jackson Labs	Cat#: 000664
Oligonucleotides		
For PCR primers used in this study see **Table S3**		
For qRT-PCR primers used in this study see **Table S4**		
Recombinant DNA		
For plasmids used in this study see **Table S2**		
Software and algorithms		
NEBuilder Assembly Tool	New England Biolabs	https://nebuilder.neb.com/#!/
Prism v9.5.1	GraphPad Software	https://www.graphpad.com
Benchling 2023	Benchling	https://benchling.com
Microsoft Excel 2015	Microsoft	
QuantStudio Real-Time PCR System v1.3	Applied Biosystems	

omu	(61)	https://cran.r-project.org/web/packages/omu/
omuShiny		https://clostridia-enjoyer.shinyapps.io/omuShiny/
QIIME 1.8	(62)	http://qiime.org
Trimmomatic	(63)	http://www.usadellab.org/cms/index.php?page=trimmomatic
dada2	(64)	https://benjjneb.github.io/dada2/
Phyloseq	(65)	https://joey711.github.io/phyloseq/
RStudio v2022.7.2.576		http://www.rstudio.com/
msa	(66)	https://www.bioinf.jku.at/software/msa/
phangorn	(67)	https://cran.r-project.org/web/packages/phangorn/index.html
vegan		https://cran.r-project.org/web/packages/vegan/index.html
ggplot2	(68)	https://ggplot2.tidyverse.org.
deseq2	(69)	https://www.bioconductor.org/packages/release/bioc/html/DESeq2.html
AxioVision v4.8.1	Zeiss	
ImageJ	NIH	(70)
rstatix	Alboukadel Kassambara	https://rpkgs.datanovia.com/rstatix/
Other		
Vortex Genie 2	Scientific Industries	Cat#: SI-0236
Horizontal Microtube Holder	Scientific Industries	Cat#: SI-HP524
Mini-beadbeater-16	Biospec Products	Cat#: 607
ViiA 7 Real-Time PCR System	Applied Biosystems	
8890 Gas Chromatograph System	Agilent	
7000D Triple Quadrupole Mass Spectrometer	Agilent	
2100 Bioanalyzer	Agilent	
MiSeq System	Illumina	
O2 Control In Vitro Glove Box (hypoxia chamber)	Coy Laboratories	
Victor Nivo Multimode Microplate Reader	Perkin Elmer	Cat#: HH35000500

Resource Availability

Lead Contact

Further information and requests for resources and reagents should be directed to and will be fulfilled by the Lead Contact, Andreas J. Bäumler (ajbaumler@ucdavis.edu).

Materials Availability

Any unique materials generated in this study are available upon request from the Lead Contact.

Data and Code Availability

- Raw 16S rRNA amplicon sequencing is available under the BioProject accession number PRJNA1037532 through the NCBI BioProject database (https://www.ncbi.nlm.nih.gov/bioproject/).
- Source code for omuShiny can be found at https://github.com/connor-reid-tiffany/omuShiny, while the web app can be found at https://clostridia-enjoyer.shinyapps.io/omuShiny/.

Experimental Models and Subject Details

Animal Experiments

All experiments involving animals were approved by the Institutional Animal Care and Use Committee at the University of California, Davis. Upon arrival, 6-8 week-old male and female mice were randomly distributed into individually ventilated cages of four animals per cage, separated by sex. Animals were left undisturbed for at least a week to allow for acclimation to the vivarium. Mice were maintained on 5058 - PicoLab Mouse Diet 20 (LabDiet), an irradiated diet containing 20% protein and 9% fat. Rooms housing animals maintained a 12-hour light/dark cycle with lights on at 07:00 and off at 19:00. 70% ethanol was used to disinfect gloves and work surfaces between the handling of experimental groups. Clean, but not sterile, paper towels were used for the collection of freshly voided fecal pellets.

Streptomycin pre-treatment of C57BL/6J mice (Jackson Laboratories, Bar Harbor, ME) was performed 24 hours prior to *S.* Typhimurium infection by delivering 20 mg of streptomycin in 0.1 mL of sterile H_2O intragastrically. All *S.* Typhimurium infections were performed by delivering 1×10^9 CFU/mouse in 0.1 mL of LB broth intragastrically. The inoculum for single infections contained 1×10^{10} CFU/mL of a single strain of *S.* Typhimurium, while inoculums for competitive infections contained a 1:1 mixture of two strains of *S.* Typhimurium at a final concentration of 1×10^{10} CFU/mL. Mock infections were performed by delivering 0.1 mL of sterile LB by broth intragastrically. Freshly voided

fecal pellets were collected from Mock or *S.* Typhimurium-infected mice once daily beginning one day after infection and continuing until the animals were euthanized.

S. Typhimurium burden in the feces was determined by collecting freshly voided fecal pellets in 1.5 mL centrifuge tubes containing phosphate-buffered saline (PBS). Feces was kept on ice before being homogenized using a Vortex Genie 2 (Scientific Industries) equipped with a horizontal microtube holder (Scientific Industries). Homogenization was carried out at the maximum vortex intensity for 5 minutes or until complete homogenization of fecal pellets was achieved. *S.* Typhimurium in feces was enumerated by plating tenfold dilutions of fecal homogenate on LB agar (BD Biosciences) containing the appropriate antibiotics for selection. Antibiotic resistance profiles can be found in **Table S2**. Plates were incubated overnight at 37°C under atmospheric conditions. Competitive indices of competitive infections were calculated by enumerating wildtype and mutant *S.* Typhimurium, determining the ratio in the feces, and then dividing by the input ratio determined in the inoculum.

Oral glucose tolerance testing (oGTT) was performed on mock-infected or *S.* Typhimurium-infected mice at day 3 after infection. Mice were moved to fresh cages with water but without access to food at 07:00 to normalize baseline blood glucose concentrations by fasting. Mice were moved to fresh, individual cages without water at 6 hours after fasting (13:00) for the oGTT. A cream of 2.5% lidocaine and 2.5% prilocaine was administered to tail tips to minimize pain and discomfort before 1-2 mm of the tail tip was removed for blood collection. Baseline blood glucose measurements were performed before mice were given a bolus of 200 mg/mL glucose solution intragastrically at a dose equal to 2 g/kg body weight. Blood glucose measurements were performed at 15, 30, 60,

90, and 120 minutes after glucose bolus. Blood glucose measurements were performed in triplicate for each mouse at each timepoint by collecting blood from tail tips and using True Metrix Self Monitoring Blood Glucose System meters and test strips (McKesson, Richmond, VA) to quantify blood glucose concentrations.

The sodium-glucose co-transporter 1 and 2 (SGLT1 and SGLT2) inhibitor sotagliflozin was used to induce experimental glucose malabsorption in mice infected with an avirulent *S.* Typhimurium *invA spiB* mutant. Sotagliflozin was resuspended at a concentration of 7.5 mg/mL in a vehicle of 0.1% Tween 80. At 18:00 on day 2 after infection, mice were administered the sotagliflozin solution or vehicle only at a dose of 60 mg/kg by intragastric gavage. All mice received a bolus of 200 mg/mL glucose solution 30 minutes later by intragastric gavage at a dose of 2 g/kg body weight.

Aminoguanidine hydrochloride was administered in the drinking water to inhibit the activity of nitric oxide synthase. Aminoguanidine hydrochloride was dissolved in water to achieve a working concentration of 1 mg/mL. Apocynin (4'-hydroxy-3'-methoxyacetophenone) was administered in the drinking water to inhibit the activity of NADPH oxidase. Apocynin was first dissolved in 100% ethanol before further dilution in water to achieve a working concentration of 80 μg/mL apocynin. Water containing aminoguanidine hydrochloride or apocycnin was filter sterilized 0.2 μm vacuum filters. Mice received these drinking water solutions in water bottles ad libitum starting 3 days prior to infection with Wild type *S*. Typhimurium, and these treatments continued until the terminal timepoint of the experiment (day 3 after infection). Drinking water solutions were replaced every day with freshly made solutions.

Pimonidazole hydrochloride (PMDZ) was dissolved in DMSO to 100 mg/mL before further dilution in sterile PBS. 30-90 minutes prior to necropsy, this PMDZ solution was administered to mice by intraperitoneal injection at a dose of 100 mg/kg.

Bacterial Strains and Culture Conditions

E. coli and *S*. Typhimurium strains used in this study are listed in **Table S2**. *E. coli* and *S.* Typhimurium strains were cultured in Luria-Bertani (LB) broth (LB, BD Biosciences) or on LB plates unless otherwise indicated. Incubation of broth cultures and plates was carried out under atmospheric conditions at 37°C for at 16-20 hours. Agar plates and liquid media were supplemented with antibiotics used at the following concentrations when required: carbenicillin (Carb), 100 μg/mL; chloramphenicol (Cm), 30 μg/mL; kanamycin (Kan), 100 μg/mL.

Method Details

Construction of suicide vectors for allelic exchange

All plasmids used for targeted mutagenesis of *S.* Typhimurium by allelic exchange were generated using the suicide vector pRE112 as the backbone(71). To generate plasmids for targeted mutagenesis of specific *S.* Typhimurium genes, DNA fragments containing ~500 bp of the upstream and downstream regions of the target genes were seamlessly assembled into pRE112. The NEBuilder Assembly Tool (New England

Biolabs) web application was used to generate primers used for the amplification of the upstream and downstream regions of the target genes by PCR. The sequence of pRE112 was used as the vector backbone with the linearization method being specified as PCR amplification by the primers pRE_linear_F and pRE_linear_R listed in **Table S3**. The upstream and downstream regions were specified as separate fragments. The following settings were used for primer design by NEBuilder Assembly Tool (New England Biolabs): Product/Kit = #E2621 NEBuilder HiFi DNA Assembly Master Mix, Minimum Overlap = 20 nt, Minimum Overlap Tm = 48°C, Circularize = Yes, PCR Polymerase/Kit Q5 Hot Start High-Fidelity 2X Master Mix, PCR Primer Conc. = 500 nM, Min. Primer Length = 18 nt. Resulting primer sets used for the amplification of upstream and downstream regions of target genes are listed in **Table S3**. DNA fragments used in the assembly of suicide vectors were generated by PCR amplification from purified pRE112 or *S.* Typhimurium genomic DNA using Q5 Hot Start High-Fidelity 2X Master Mix (New England Biolabs). DNA assembly was performed using NEBuilder HiFi DNA Assembly Master Mix (New England Biolabs). Resulting plasmid assemblies were transformed into *E. coli* DH5α λ*pir* and confirmed by Sanger sequencing using the primers pRE_chk_F and pRE_chk_R listed in **Table S3**.

Generation of S. Typhimurium mutants by allelic exchange

Purified suicide vectors were transformed into the donor *E. coli* strain S17-1 λ*pir* and introduced into the genome of *S.* Typhimurium AJB715 by conjugation. Chromosomal integration of the vector by the first crossover event was selected for by plating on Cm

and Kan. Resulting merodiploid clones were cultured overnight in LB broth without Cm to allow for a second crossover event, and sucrose selection was used to identify clones lacking the suicide vector(72).

Fecal slurry growth assay

Freshly voided fecal pellets were collected from CBA/J mice and stored at -80°C before further processing. Fecal pellets from 8 male and 8 female mice were pooled together and resuspended to a concentration of 125 mg/mL in an aqueous solution of 50 mM 2-(N-morpholino)ethanesulfonic acid (MES) and 0.9 % NaCl. The fecal suspension was homogenized at room temperature for 10 minutes using a Vortex Genie 2 (Scientific Industries) at the maximum setting. The fecal suspension was centrifuged at 10,000 x g for 5 minutes to pellet particulate matter and the resulting supernatant was split into two equal volumes of 4 mL each. One volume was combined with 4 mL of an aqueous solution containing 50 mM 2-(N-morpholino)ethanesulfonic acid (MES), 0.9 % NaCl, 80 mM sodium acetate, 6 mM sodium propionate, and 15 mM sodium butyrate. The final concentration of short-chain fatty acids in this fecal homogenate was 40 mM acetate, 3 mM propionate, and 7.5 mM butyrate in order to match the concentrations found in cecal contents of mock infected mice as measured by GC-MS. The second volume was combined with 4 mL of an aqueous solution containing 50 mM MES, 0.9 % NaCl, 40 mM sodium acetate, 6 mM sodium propionate, and 4 mM sodium butyrate. The final concentration of short-chain fatty acids in this fecal homogenate was 20 mM acetate, 3 mM propionate, and 2 mM butyrate in order to match the concentrations found in cecal

contents of *S.* Typhimurium infected mice at 3 days after infection as measured by GC-MS. Both fecal homogenates were corrected to a pH of 5.8 using HCl and NaOH and sterilized by filtration through a 0.2 μm filters.

Growth curves of *S.* Typhimurium in fecal homogenates were performed in 96 well plates containing 200 μL of fecal homogenate per well. Uninoculated plates were placed in a hypoxia chamber (Coy Laboratories) overnight to equilibrate to the chamber conditions of 1% O_2 and 5% CO_2. An overnight culture of *S.* Typhimurium FF176 was washed once by pelleting 1 mL of cells at 10,000 x g for 2 minutes and resuspending in 1 mL of sterile PBS. Washed cells were moved into the hypoxia chamber and 2 μL of this resuspension was used inoculate wells containing fecal homogenate. 2 μL of sterile PBS was added to wells of uninoculated fecal homogenate to act as negative control wells. Inoculated 96 well plates were incubated in a Victor Nivo multimode microplate reader (Perkin Elmer) at 37°C contained within the hypoxia chamber. The optical density at 600 nm of the wells was measured every 30 minutes and the plates were shaken with a double orbital pattern.

Minimal inhibitory concentration assays

Minimal inhibitory concentration (MIC) assays for diethylenetriamine (DETA, Sigma Aldrich) and diethethylenetriamine NONOate (DETA NONOate, Cayman Chemical) were conducted on two species of Lachnospiraceae (*Enterocloster bolteae* and *Anaerostipes caccae*), one species of Oscillospiraceae (Anaerotruncus colohominis), and *S.* Typhimurium. DETA NONOate releases nitric oxide (NO) under neutral conditions with a

half-life of ~20 hours according to the manufacturer. DETA serves as the negative control for DETA NONOate, as the latter decomposes into DETA upon spontaneous release of NO. DETA was diluted in 0.01 M NaOH to 500 mM and allowed to reduce under anaerobic conditions for 48 hours. DETA NONOate stocks were prepared under anaerobic conditions by dissolving DETA NONOate in pre-reduced 0.01 M NaOH to a concentration of 500 mM and aliquoting in cryovials and storing at -80°C. DETA and DETA NONOate were diluted to 20 mM or 20 μM in Gifu anaerobic media broth (GAM, HiMEdia) immediately prior to use in MIC assays. All MIC assays for DETA and DETA NONOate were conducted under anaerobic conditions in an anaerobic chamber (Coy Laboratories) to compare the MICs for obligate anaerobic Clostridia and *S.* Typhimurium under identical conditions. MIC assays were performed in 96-well tissue culture plates (Corning). 100 μL of GAM broth was distributed to columns 3 to 12 of each plate, and 200 μL was distributed to column 1 to act as a sterile control. 200 μL of 20 mM or 20 μM DETA or DETA NONOate was distributed column 2, and 1:2 dilutions of these solutions were carried out in succession to column 11, resulting in a range of decreasing drug concentrations, with column 12 serving as a no-drug control condition. Clostridia species and *S*. Typhimurium were grown overnight in 5 mL of GAM broth at 37°C in an anaerobic chamber before 1:100 or 1:500 dilution in GAM broth, respectively. 100 μL of these bacterial suspensions were distributed into columns 2 to 12 of each MIC assay plate to achieve inoculum doses of 1×10^5 to 1×10^6 CFU/well. Every condition was assessed in quadruplicate. MIC assay plates were incubated in the anaerobic chamber at 37°C for 20 hours before visual inspection was used to determine the MIC. Wells containing no obvious turbidity (bacterial growth) were considered to contain inhibitory conditions, while wells containing obvious

turbidity were considered to contain sub- or non-inhibitory conditions. When replicate wells contained a mixture of turbidity and no turbidity, the condition was considered to be sub-inhibitory.

Histopathology

The distal segment of the cecum was fixed in 10% phosphate-buffered formalin for approximately 24 hours before being stored in 70% ethanol. Fixed tissues were embedded in paraffin and cut into 3-5 μm sections before being stained with hemotoxylin and eosin (HE) using standard histological techniques. Tissue sections were blinded prior to examination by light microscopy. A veterinary pathologist scored histopathological changes using the criteria listed in **Table S5**. Representative images were taken using a Zeiss Primo Star microscope.

Hypoxia staining and imaging

The Hydroxyprode kit was used for staining slides as previously described (18, 44). The distal segment of the cecum was fixed in 10% phosphate-buffered formalin for approximately 24 hours before being stored in 70% ethanol. Fixed tissues were embedded in paraffin and cut into 3-5 μm sections. Tissue sections were mounted on slides and prepared for staining by submerging in xylene (10 minutes, 2 times) and ethanol (95% for 3 minutes, 80% for 3 minutes, and 70% for 3 minutes). Slides were incubated with 20 mg/mL Proteinase K in TE buffer for 15 minutes at 37°C. Serum was

used to block slides at room temperature for 1 hour. Slides were incubated with the mouse IgG1 anti-PMDZ monoclonal antibody 4.3.11.3 (Hydroxyprobe) overnight at 4°C, and then incubated with Cyanine3-labeled goat anti-mouse IgG (Jackson ImmunoResearch) for 90 minutes at room temperature. Slides were washed 3 times in PBS between each incubation step. Dried slides were mounted with Immuno-Mount (Epredia).

Stained slides were randomized and blinded before imaging on a Zeiss AxioVision microcope with AxioVision 4.8.1 software (Zeiss) at 20X magnification. Three representative images were collected for each tissue section. ImageJ (NIH) was used to isolate the Texas Red channel from each image, and three representative slices of equal size containing the epithelium-lumen boundary were saved. The Plot Profile of each slice was exported for quantitative analysis. The peak pixel intensity of each slice (representing the epithelium-lumen boundary) was collected, unblinded, and used to compare the peak pixel intensities among groups.

RNA Isolation and quantitative real-time PCR

Murine enterocytes were isolated from freshly collected ileal or cecal tissue. Ileal tissue was defined as the last 10 cm of small intestine immediately proximal to the cecum. Tissue was cut longitudinally to expose the epithelial surface and then cut laterally into several pieces before being placed into ice-cold phosphate-buffered saline containing 0.5M ethylenediaminetetraacetic acid (EDTA) and 1.5 mM dithiothreitol (DTT) for 20 minutes. Tissue was then moved to phosphate-buffered saline containing 0.5M EDTA and incubated at 37°C for 10 minutes. Tubes containing tissue were vigorously shaken by

hand for approximately 30 seconds to release epithelial cells from the underlying tissue. Intact tissue was removed, and the resulting suspension of epithelial cells was centrifuged at 800 x g for 5 minutes at 4°C. Supernatant was aspirated and the cell pellet was moved to a 2 mL screw cap micro tube containing 1 mL of TRI Reagent (Molecular Research Center). Murine enterocytes were homogenized and lysed in a Mini-beadbeater-16 (Biospec Products). When enterocyte isolation was not required, murine cecal tissues were frozen in liquid nitrogen upon collection and stored at -80°C prior to homogenization. Frozen cecal tissues were transferred to Lysing Matrix C tubes containing 1 mL of TRI Reagent (Molecular Research Center) and homogenized in a Mini-beadbeater-16 (Biospec Products). Total RNA was collected from murine cecal tissue or isolated enterocytes in the aqueous phase after the addition of 200 μL chloroform by following the TRI Reagent method following the manufacturer's protocol. Total RNA was isolated from the aqueous phase and subjected to on-column PureLink DNase (Invitrogen) digestion in EconoSpin (Epoch Life Science) columns before elution in UltraPure distilled water (Invitrogen). 1 μg of isolated RNA was reverse transcribed with MultiScribe reverse transcriptase (Applied Biosystems) and random hexamers (Invitrogen) and RNase Inhibitor (Applied Biosystems) to form cDNA. Quantitative real-time PCR (qPCR) was performed using SYBR Green PCR master mix and the primers listed in **Table S4** on a ViiA 7 real-time PCR system (Applied Biosystems). The following parameters were used for reaction cycling: 50°C for 2 minutes, 95°C for 10 minutes, 40 cycles of 95°C for 15 seconds, and 60°C for 1 minute. QuantiStudio Real-Time PCR software v1.3 (Applied Biosystems) and the $2^{-\Delta\Delta Ct}$ method were used to calculate fold changes between

experimental groups. Ct values of each transcript were normalized to the beta-2 microglobulin (*B2m*) gene.

16S rRNA gene amplicon sequencing sample preparation, library preparation, and sequencing

Freshly voided fecal pellets were collected from mice prior to infection by *S.* Typhimurium and again at 3, 5, 7, and 10 days after infection and stored at -20°C. Nucleic acids were extracted using DNeasy Powersoil Kit (Qiagen) according to the manufacturer's protocol. DNA concentrations were determined using a Qubit 2.0 Fluorometer (Invitrogen) and samples were normalized to 20 ng/µL prior to library preparation. Primers 341F (**TCGTCGGCAGCGTCAGATGTGTATAAGAGACAG**(spacer)*TG*CCTACGGGNGGCWGCAG) and 806R (**GTCTCGTGGGCTCGGAGATGTGTATAAGAGACAG**(spacer)*CC*GGACTACNVGGGTWTCTAAT were used to amplify the V3-V4 domain of the 16S rRNA using a two step PCR procedure. In step one of the amplification procedure, both forward and reverse primers contained an Illumina tag sequence (bold), a variable length spacer (no spacer, A, CA, or GCA for 341F; no spacer, G, TG, ATG for 806R) to increase diversity and improve the quality of the sequencing run, a linker sequence (italicized), and the 16S target sequence (underlined). Each 25 µl PCR reaction contained 1 Unit Kapa2G Robust Hot Start Polymerase (Kapa Biosystems), 1.5 mM $MgCl_2$, 0.2 mM final concentration dNTP mix, 0.2 µM final concentration of each primer, 3 µl KAPA 5X Enhancer 1, and 1ul of DNA for

each sample. PCR conditions were: an initial incubation at 95°C for 3 min, followed by 28 cycles of 95°C for 30 s, 50°C for 30 s, 72°C for 30 s and a final extension of 72°C for 3 min. In step two, each sample was barcoded with a unique forward and reverse barcode combination using forward primers (**AATGATACGGCGACCACCGAGATCTACAC**NNNNNNNNTCGTCGGCAGCGTC) with an Illumina P5 adapter sequence (bold), a unique 8 nt barcode (N), a partial matching sequence of the forward adapter used in step one (underlined), and reverse primers (**CAAGCAGAAGACGGCATACGAGAT**NNNNNNNNGTCTCGTGGGCTCGG)) with an Illumina P7 adapter sequence (bold), unique 8 nt barcode (N), and a partial matching sequence of the reverse adapter used in step one (underlined). The PCR reaction in step two contained 1 Unit Kapa2G Robust Hot Start Polymerase (Kapa Biosystems), 1.5 mM $MgCl_2$, 0.2 mM final concentration dNTP mix, 0.2 μM final concentration of each uniquely barcoded primer and 1ul of the product from the PCR reaction in step one diluted at a 10:1 ratio in water. PCR conditions were: an initial incubation at 95°C for 3 min, followed by 8 cycles of 95°C for 30 s, 58°C for 30 s, 72°C for 30 s and a final extension of 72°C for 3 min.

The final product was quantified on the Qubit instrument using the Qubit High Sensitivity dsDNA kit (Invitrogen) and individual amplicons were pooled in equal concentrations. The pooled library was cleaned utilizing Ampure XP beads (Beckman Coulter) then checked for quality and proper amplicon size on an Agilent 2100 Bioanalyzer (Agilent Technologies). The library was quantified via qPCR followed by 300-bp paired-end sequencing using an Illumina MiSeq instrument (Illumina) in the Genome

Center DNA Technologies Core, University of California, Davis. Library preparation was performed by the UC Davis Host Microbe Systems Biology Core Facility.

16S rRNA gene amplicon sequencing analysis

Sequencing reads were demultiplexed using QIIME 1.8(62), and non-biological nucleotides were trimmed using Trimmomatic(63). 16S rRNA sequencing reads were subsequently processed and assembled into amplicon sequence variants (ASV) using dada2(64) in R. First, reads with more than 2 expected errors were removed. Dereplication and sample inference were then performed on forward and reverse reads, prior to merging. A sequence table was constructed from merged reads, and chimeric reads were subsequently removed. Taxonomy was assigned to reads to the genus level using the dada2 formatted rdp training dataset 14 which can be found here: https://zenodo.org/record/158955#.XJqlnxNKjUI. The R package phyloseq(65) was then used in downstream analysis of the data, including the generation of a phyloseq object, relative abundance bar plots, and the principle coordinate analysis plot. For the weighted unifrac analysis, the R package ms (66) was used to generate a multiple sequence alignment from the assembled reads with the following parameters: method = “ClustalW”, type = “dna”, order = “input”. The R package phangorn(67) was used to generate a maximum likelihood tree from the sequence alignment using a general time reversible (GTR) model with the following parameters: model = “GTR”, optInv = TRUE, optGamma = TRUE, rearrangement = “stochastic”, control = pml.control(trace = 0). The R package vegan

(https://vegandevs.github.io/vegan/authors.html#citation) was used to perform permanova analysis on weighted unifrac distances with default parameters and the R package ggplot2(68) was used to graph boxplots of the weighted unifrac distances. Differential abundance analysis of taxa was performed using the R package deseq2(69) with the parameters: test = “Wald”, fitType = “parametric”, cooksCutoff = FALSE. The R package omu(61) was then used to generate fold change frequency tables and differential abundance bar plots from the deseq2 modeled data. For differential abundance analysis of Clostridia, Lachnospiraceae, Oscilliospiraceae, and Ruminococcaceae, a Kruskal-Wallis one way ANOVA was performed using the R package rstatix (https://rpkgs.datanovia.com/rstatix/). A dunns post hoc test was then performed to do pairwise comparisons. Supervised random forest was performed by using the caret package (https://doi.org/10.18637/jss.v028.i05) in R with days post *S*. Typhimurium infection as the response variable in the model. Pseudo-random subsampling was performed to select 40 percent of the samples as training data, while the remaining 60 percent of samples were used for testing.

Metabolomics sample collection and GC-TOF mass spectrometry

Murine cecal contents were collected from mock infected mice or mice at day 3 or 4 after *S.* Typhimurium infection. Samples were collected in 2 mL cryovials and immediately frozen in liquid nitrogen before storage at -80°C. Frozen samples were transported on dry ice to the West Coast Metabolomics Center where they were processed for untargeted primary metabolite profiling by GC-TOF mass spectrometry.

Data were acquired using the following parameters. Column: Restek corporation Rtx-5Sil MS (30 m length × 0.25 mm internal diameter with 0.25-μm film made of 95% dimethyl/5%diphenylpolysiloxane). Mobile phase: Helium. Column temperature: 50–330°C. Flow rate: 1 mL min−1. Injection volume: 0.5 μL. Injection: 25 splitless time into a multi-baffled glass liner. Injection temperature: 50°C ramped to 250°C by 12°C s−1. Oven temperature program: 50°C for 1 min, then ramped at 20 °C min−1 to 330°C, held constant for 5 minutes. The analytical GC column is protected by a 10-m long empty guard column which is cut by 20-cm intervals whenever the reference mixture QC samples indicate problems caused by column contaminations. This sequence of column cuts has been validated to have no detrimental effects with respect to peak shapes, absolute or relative metabolite retention times, or reproducibility of quantifications. Automatic liner exchanges are performed after each set of 10 injections which reduces sample carryover for highly lipophilic compounds such as free fatty acids. Mass spectrometry parameters are used as follows: a Leco Pegasus IV mass spectrometer is used with unit mass resolution at 17 spectra s−1 from 80–500 Da at − 70 eV ionization energy and 1800 V detector voltage with a 230°C transfer line and a 250°C ion source.

Metabolomics data processing

Raw data files are preprocessed directly after data acquisition and stored as ChromaTOF-specific *.peg files, as generic *.txt result files and additionally as generic ANDI MS *.cdf files. ChromaTOF vs. 2.32 is used for data preprocessing without smoothing, 3 s peak width, baseline subtraction just above the noise level, and automatic

mass spectral deconvolution and peak detection at signal/noise levels of 5:1 throughout the chromatogram. Apex masses are reported for use in the BinBase algorithm. Result *.txt files are exported to a data server with absolute spectra intensities and further processed by a filtering algorithm implemented in the metabolomics BinBase database. The BinBase algorithm (rtx5) used the settings: validity of chromatogram (< 10 peaks with intensity > 107 counts s−1), unbiased retention index marker detection (MS similarity > 800, validity of intensity range for high m/z marker ions), and retention index calculation by 5th order polynomial regression. Spectra are cut to 5% base peak abundance and matched to database entries from most to least abundant spectra using the following matching filters: retention index window ± 2000 units (equivalent to about ± 2 s retention time), validation of unique ions and apex masses (unique ion must be included in apexing masses and present at > 3% of base peak abundance), mass spectrum similarity must fit criteria dependent on peak purity and signal/noise ratios and a final isomer filter. Failed spectra are automatically entered as new database entries if s/n > 25, purity < 1.0, and presence in the biological study design class was > 80%. All thresholds reflect settings for ChromaTOF v. 2.32. Quantification is reported as peak height using the unique ion as default unless a different quantification ion is manually set in the BinBase administration software BinView. A quantification report table is produced for all database entries that are positively detected in more than 10% of the samples of a study design class (as defined in the miniX database) for unidentified metabolites. A subsequent post-processing module is employed to automatically replace missing values from the *.cdf files. Replaced values are labeled as ‘low confidence’ by color coding, and for each metabolite, the number of high-confidence peak detections is recorded as well as the ratio

of the average height of replaced values to high-confidence peak detections. These ratios and numbers are used for manual curation of automatic report data sets to data sets released for submission. These data were then normalized to the mTIC value (sum of the peak heights of the known metabolites).

Quantification of glucose in murine cecal contents

Murine cecal contents were collected from mock infected or *S.* Typhimurium infected mice at day 3 after infection. Samples were collected in 1.5 mL microcentrifuge tubes containing 200 µL of Assay Buffer from the Glucose Assay Kit (Abcam) and stored on ice before being homogenized using a Vortex Genie 2 (Scientific Industries) equipped with a horizontal microtube holder (Scientific Industries). Homogenization was carried out at the maximum vortex intensity for 5 minutes or until complete homogenization of cecal contents was achieved. Samples were then centrifuged at 10,000 x g for 5 minutes at 4°C to pellet particulate matter. Samples were deproteinized by centrifuging 150 µL of supernatant in Microcon-10 kDa centrifugal filter units (Merck Millipore) at 10,000 x g for 60 minutes at 4°C. Deproteinized sample supernatants were stored at -20°C until further processing. Quantification of glucose in the sample supernatants was performed using the Glucose Assay Kit (Abcam) according to the manufacturer's instructions. Glucose concentration results were normalized by starting sample weights.

Quantification of short-chain fatty acids GC-MS

Murine cecal contents were collected in 600 µL of PBS and kept on ice before being homogenized using a Vortex Genie 2 (Scientific Industries) equipped with a horizontal microtube holder (Scientific Industries). Homogenization was carried out at the maximum vortex intensity for 5 minutes or until complete homogenization of cecal contents was achieved. Samples were then centrifuged at 6,000 x g for 10 min to pellet particulate matter. For each sample, 100 µL of supernatant was combined with 10 µL of a solution containing deuterated acetate, propionate, and butyrate (C/D/N isotopes) so that each deuterated metabolite was at a final concentration of 100 µM. Samples were dried without heat in a vacuum dryer and then stored at -80°C until use. Dried extracts were then solubilized by sonication in 0.1 ml anhydrous pyridine (Sigma Aldrich) and then incubated for 20 min at 80°C. An equal amount of N-tert-butyldimethylsilyl-N-methyltrifluoroacetamide with 1% tert-butyldimethylchlorosilate (Sigma-Aldrich) was added, and the samples were incubated for 1 h at 80°C. Samples were centrifuged at 20,000 g for 1 min to remove leftover particles. 100 µL of the supernatant was transferred to an autosampler vial and analyzed by gas chromatography-mass spectrometry (GC-MS) using an Agilent 8890 Gas Chromatograph and Agilent 7000D Mass spectrometer. 1 µL of the sample was injected with a 1:50 split ratio at an injection temperature of 250°C on an HP 5ms Ultra Inert (2x15-m-length, 0.25-mm diameter, 0.25 µm film thickness) fused silica capillary column. Helium was used as the carrier gas with a constant flow of 1.2 mL/min. The gas chromatograph (GC) oven temperature started at 50°C for 20 min, rising to 90°C at 10°C/min and holding for 1 min, then raised to 310°C at 40°C/min with a final hold for 2 min. The interface was heated to 300°C. The ion source was used in electron ionization (EI) mode (70 V, 150 µA, 200°C). The dwell time for selected ion

monitoring (SIM) events was 50ms. Acetate, propionate, and butyrate were quantified using SIM, with the monitored m/z, and experimentally determined retention times detailed in **Supplementary Table 6**.

Efficient recovery of target metabolites was determined using deuterated compounds as internal standards. Quantification was based on external standards comprised of a series of dilutions of pure compounds, derivatized as described above at the same time as the samples.

Short-chain fatty acid values as determined by GC-MS were normalized by the weight of the respective input sample and converted to mmol/g concentrations prior to statistical analysis.

Quantification and Statistical Analysis

Statistical analysis was carried out using Graphpad PRISM unless otherwise noted. The Shapiro-Wilk test was used to determine if data was normally distributed prior to choosing a statistical test. Normally distributed data sets were analyzed by parametric tests while data sets without a normal distribution were analyzed by nonparametric tests. Populations were not assumed to have equal standard deviations. A *P* value of less than 0.05 was considered significant. The number of animals (*n*) used in experiments are indicated in the figure legends. The statistical tests used to analyze data generated from different measurements (e.g. CFU data, short-chain fatty acid measurements, etc.) are detailed below.

Following processing, metabolomics data were analyzed using our recently developed shiny application, omuShiny. Principal component analysis was performed on metabolite abundances that were performed by the omuShiny glog function (ln(x+1)). Ellipses denote a 95% confidence interval on a multivariate t distribution. Univariate statistics were performed using ANOVA on ln(x+1) transformed metabolite abundances followed by Tukey's post hoc test. P values were adjusted using the Benjamini-Hochberg method to correct for the false discovery rate. The results of these statistical analyses can be found in table format within **Supplementary File 1**. Volcano plots were derived from data generated by the univariate statical analysis in omuShiny.

Data sets consisting of CFU/g feces values were analyzed by nonparametric tests. Experiments involving one *S*. Typhimurium strain per animal were analyzed by using an unpaired Mann-Whitney test followed by Holm-Šídák's multiple comparison test to correct for multiple comparisons when 2 groups were compared. A Kruskal-Wallis test followed by Dunn's multiple comparisons test was used when three groups were compared. Competitive infections were analyzed by comparing WT CFUs to mutant CFUs at each indicated timepoint using a Wilcoxon matched-pairs signed rank test.

Quantitative real time PCR data was analyzed by nonparametric tests. A Mann-Whitney test was used when two groups were compared. A Kruskal-Wallis test followed by Dunn's multiple comparisons test was used when three or more groups were compared.

Cecal short-chain fatty acid concentrations were analyzed by Welch's t test to compare values between groups when 2 groups were compared. A Kruskal-Wallis test

followed by Dunn's multiple comparisons test was used when three groups were compared.

The relationship between *S.* Typhimurium Wildtype CFUs and cecal short-chain fatty acid levels at day 3 after infection were assessed by pooling matched wild type CFU-short-chain fatty acid concentration data from five independent experiments. Data were plotted and assessed by Pearson correlation coefficient, and nonlinear least squares regression was used to generate a line of best-fit.

Area under the curve (AUC) for the glucose tolerance test was determined for each animal between 0 and 2 hours after the bolus gavage with the baseline being set to Y = 0. An unpaired t test with Welch's correction was used to compare areas under the curve between groups.

Cecal glucose concentrations and matched cecal *S.* Typhimurium CFUs were compared using the Brown-Forsythe and Welch ANOVA tests followed by Dunnett's T3 multiple comparisons test.

Growth of *S.* Typhimurium in fecal slurries was analyzed by comparing optical densities at the indicated timepoints by an unpaired t test with Welch correction followed by Holm-Šídák's multiple comparison test to correct for multiple comparisons.

Histopathology scoring was analyzed by comparing the cumulative histopathology scores in each group using a Kruskal-Wallis test followed by Dunn's multiple comparisons test.

Peak pixel intensities at the lumen-epithelium border of pimonidazole-stained cecal tissue sections were compared using a Kruskal-Wallis test followed by Dunn's multiple comparison test.

References

1. Zhang S, Kingsley RA, Santos RL, Andrews-Polymenis H, Raffatellu M, Figueiredo J, Nunes J, Tsolis RM, Adams LG, Baumler AJ. 2003. Molecular pathogenesis of Salmonella enterica serotype typhimurium-induced diarrhea. Infect Immun 71:1-12.

2. Mills DM, Bajaj V, Lee CA. 1995. A 40 kb chromosomal fragment encoding Salmonella typhimurium invasion genes is absent from the corresponding region of the Escherichia coli K-12 chromosome. Mol Microbiol 15:749-59.

3. Galán JE, Curtiss III R. 1989. Cloning and molecular characterization of genes whose products allow *Salmonella typhimurium* to penetrate tissue culture cells. Proc Natl Acad Sci USA 86:6383-6387.

4. Ochman H, Soncini FC, Solomon F, Groisman EA. 1996. Identification of a pathogenicity island required for Salmonella survival in host cells. Proc Natl Acad Sci U S A 93:7800-4.

5. Hensel M, Shea JE, Gleeson C, Jones MD, Dalton E, Holden DW. 1995. Simultaneous identification of bacterial virulence genes by negative selection. Science 269:400-3.

6. Vazquez-Torres A, Xu Y, Jones-Carson J, Holden DW, Lucia SM, Dinauer MC, Mastroeni P, Fang FC. 2000. Salmonella pathogenicity island 2-dependent evasion of the phagocyte NADPH oxidase. Science 287:1655-8.

7. Grant AJ, Morgan FJ, McKinley TJ, Foster GL, Maskell DJ, Mastroeni P. 2012. Attenuated Salmonella Typhimurium lacking the pathogenicity island-2 type 3 secretion system grow to high bacterial numbers inside phagocytes in mice. PLoS Pathog 8:e1003070.

8. Hiyoshi H, English BC, Diaz-Ochoa VE, Wangdi T, Zhang LF, Sakaguchi M, Haneda T, Tsolis RM, Baumler AJ. 2022. Virulence factors perforate the pathogen-containing vacuole to signal efferocytosis. Cell Host Microbe 30:163-170 e6.

9. Tsolis RM, Adams LG, Ficht TA, Baumler AJ. 1999. Contribution of Salmonella typhimurium virulence factors to diarrheal disease in calves. Infect Immun 67:4879-85.

10. Barthel M, Hapfelmeier S, Quintanilla-Martinez L, Kremer M, Rohde M, Hogardt M, Pfeffer K, Russmann H, Hardt WD. 2003. Pretreatment of mice with

streptomycin provides a Salmonella enterica serovar Typhimurium colitis model that allows analysis of both pathogen and host. Infect Immun 71:2839-58.

11. Hapfelmeier S, Stecher B, Barthel M, Kremer M, Muller AJ, Heikenwalder M, Stallmach T, Hensel M, Pfeffer K, Akira S, Hardt WD. 2005. The Salmonella pathogenicity island (SPI)-2 and SPI-1 type III secretion systems allow Salmonella serovar typhimurium to trigger colitis via MyD88-dependent and MyD88-independent mechanisms. J Immunol 174:1675-85.

12. Stecher B, Robbiani R, Walker AW, Westendorf AM, Barthel M, Kremer M, Chaffron S, Macpherson AJ, Buer J, Parkhill J, Dougan G, von Mering C, Hardt WD. 2007. Salmonella enterica serovar typhimurium exploits inflammation to compete with the intestinal microbiota. PLoS Biol 5:2177-89.

13. Rivera-Chavez F, Zhang LF, Faber F, Lopez CA, Byndloss MX, Olsan EE, Xu G, Velazquez EM, Lebrilla CB, Winter SE, Baumler AJ. 2016. Depletion of Butyrate-Producing Clostridia from the Gut Microbiota Drives an Aerobic Luminal Expansion of Salmonella. Cell Host Microbe 19:443-54.

14. Sekirov I, Gill N, Jogova M, Tam N, Robertson M, de Llanos R, Li Y, Finlay BB. 2010. Salmonella SPI-1-mediated neutrophil recruitment during enteric colitis is associated with reduction and alteration in intestinal microbiota. Gut Microbes 1:30-41.

15. Kaiser P, Diard M, Stecher B, Hardt WD. 2012. The streptomycin mouse model for Salmonella diarrhea: functional analysis of the microbiota, the pathogen's virulence factors, and the host's mucosal immune response. Immunol Rev 245:56-83.

16. Bohnhoff M, Drake BL, Miller CP. 1954. Effect of streptomycin on susceptibility of intestinal tract to experimental Salmonella infection. Proc Soc Exp Biol Med 86:132-7.

17. Meynell GG. 1963. Antibacterial mechanisms of the mouse gut. II. The role of Eh and volatile fatty acids in the normal gut. British journal of experimental pathology 44:209-19.

18. Byndloss MX, Olsan EE, Rivera-Chávez F, Tiffany CR, Cevallos SA, Lokken KL, Torres TP, Byndloss AJ, Faber F, Gao Y, Litvak Y, Lopez CA, Xu G, Napoli E, Giulivi C, Tsolis RM, Revzin A, Lebrilla CB, Bäumler AJ. 2017. Microbiota-activated PPAR-g signaling inhibits dysbiotic Enterobacteriaceae expansion. Science 357:570-575.

19. Tiffany CR, Lee JY, Rogers AWL, Olsan EE, Morales P, Faber F, Baumler AJ. 2021. The metabolic footprint of Clostridia and Erysipelotrichia reveals their role in depleting sugar alcohols in the cecum. Microbiome 9:174.

20. Velazquez EM, Nguyen H, Heasley KT, Saechao CH, Gil LM, Rogers AWL, Miller BM, Rolston MR, Lopez CA, Litvak Y, Liou MJ, Faber F, Bronner DN, Tiffany CR, Byndloss MX, Byndloss AJ, Baumler AJ. 2019. Endogenous Enterobacteriaceae underlie variation in susceptibility to Salmonella infection. Nat Microbiol doi:10.1038/s41564-019-0407-8.

21. Clark DP. 1989. The fermentation pathways of Escherichia coli. FEMS Microbiol Rev 5:223-34.

22. Stouthamer AH. 1973. A theoretical study on the amount of ATP required for synthesis of microbial cell material. Antonie Van Leeuwenhoek 39:545-65.

23. Nguyen BD, Cuenca VM, Hartl J, Gul E, Bauer R, Meile S, Ruthi J, Margot C, Heeb L, Besser F, Escriva PP, Fetz C, Furter M, Laganenka L, Keller P, Fuchs L, Christen M, Porwollik S, McClelland M, Vorholt JA, Sauer U, Sunagawa S, Christen B, Hardt WD. 2020. Import of Aspartate and Malate by DcuABC Drives H(2)/Fumarate Respiration to Promote Initial Salmonella Gut-Lumen Colonization in Mice. Cell Host Microbe 27:922-936 e6.

24. Ren J, Sang Y, Qin R, Su Y, Cui Z, Mang Z, Li H, Lu S, Zhang J, Cheng S, Liu X, Li J, Lu J, Wu W, Zhao GP, Shao F, Yao YF. 2019. Metabolic intermediate acetyl phosphate modulates bacterial virulence via acetylation. Emerg Microbes Infect 8:55-69.

25. Bowden SD, Rowley G, Hinton JC, Thompson A. 2009. Glucose and glycolysis are required for the successful infection of macrophages and mice by Salmonella enterica serovar typhimurium. Infect Immun 77:3117-26.

26. Boulanger EF, Sabag-Daigle A, Thirugnanasambantham P, Gopalan V, Ahmer BMM. 2021. Sugar-Phosphate Toxicities. Microbiol Mol Biol Rev 85:e0012321.

27. Carter PB, Collins FM. 1974. The route of enteric infection in normal mice. J Exp Med 139:1189-1203.

28. Rydstrom A, Wick MJ. 2009. Monocyte and neutrophil recruitment during oral Salmonella infection is driven by MyD88-derived chemokines. Eur J Immunol 39:3019-30.

29. Stelzner M, Somasundaram S, Khakberdiev T. 2001. Systemic effects of acute terminal ileitis on uninflamed gut aggravate bile acid malabsorption. J Surg Res 99:359-64.

30. Palaniappan B, Sundaram S, Arthur S, Afroz S, Sundaram U. 2020. Inducible Nitric Oxide Regulates Na-Glucose Co-transport in a Spontaneous SAMP1/YitFc Mouse Model of Chronic Ileitis. Nutrients 12.

31. Sorbara MT, Dubin K, Littmann ER, Moody TU, Fontana E, Seok R, Leiner IM, Taur Y, Peled JU, van den Brink MRM, Litvak Y, Baumler AJ, Chaubard JL, Pickard AJ, Cross JR, Pamer EG. 2019. Inhibiting antibiotic-resistant Enterobacteriaceae by microbiota-mediated intracellular acidification. J Exp Med 216:84-98.

32. McLean S, Bowman LAH, Poole RK. 2010. Peroxynitrite stress is exacerbated by flavohaemoglobin-derived oxidative stress in Salmonella Typhimurium and is relieved by nitric oxide. Microbiology (Reading) 156:3556-3565.

33. Shepherd M, Achard ME, Idris A, Totsika M, Phan MD, Peters KM, Sarkar S, Ribeiro CA, Holyoake LV, Ladakis D, Ulett GC, Sweet MJ, Poole RK, McEwan AG, Schembri MA. 2016. The cytochrome bd-I respiratory oxidase augments survival of multidrug-resistant Escherichia coli during infection. Sci Rep 6:35285.

34. Mills PC, Rowley G, Spiro S, Hinton JCD, Richardson DJ. 2008. A combination of cytochrome c nitrite reductase (NrfA) and flavorubredoxin (NorV) protects Salmonella enterica serovar Typhimurium against killing by NO in anoxic environments. Microbiology (Reading) 154:1218-1228.

35. Terada N, Ohno N, Saitoh S, Ohno S. 2007. Immunohistochemical detection of hypoxia in mouse liver tissues treated with pimonidazole using "in vivo cryotechnique". Histochem Cell Biol 128:253-61.

36. Kizaka-Kondoh S, Konse-Nagasawa H. 2009. Significance of nitroimidazole compounds and hypoxia-inducible factor-1 for imaging tumor hypoxia. Cancer Sci 100:1366-73.

37. Kelly CJ, Zheng L, Campbell EL, Saeedi B, Scholz CC, Bayless AJ, Wilson KE, Glover LE, Kominsky DJ, Magnuson A, Weir TL, Ehrentraut SF, Pickel C, Kuhn KA, Lanis JM, Nguyen V, Taylor CT, Colgan SP. 2015. Crosstalk between Microbiota-Derived Short-Chain Fatty Acids and Intestinal Epithelial HIF Augments Tissue Barrier Function. Cell Host Microbe 17:662-71.

38. Atarashi K, Tanoue T, Shima T, Imaoka A, Kuwahara T, Momose Y, Cheng G, Yamasaki S, Saito T, Ohba Y, Taniguchi T, Takeda K, Hori S, Ivanov, II, Umesaki Y, Itoh K, Honda K. 2011. Induction of colonic regulatory T cells by indigenous Clostridium species. Science 331:337-41.

39. Furusawa Y, Obata Y, Fukuda S, Endo TA, Nakato G, Takahashi D, Nakanishi Y, Uetake C, Kato K, Kato T, Takahashi M, Fukuda NN, Murakami S, Miyauchi E, Hino S, Atarashi K, Onawa S, Fujimura Y, Lockett T, Clarke JM, Topping DL, Tomita M, Hori S, Ohara O, Morita T, Koseki H, Kikuchi J, Honda K, Hase K, Ohno H. 2013. Commensal microbe-derived butyrate induces the differentiation of colonic regulatory T cells. Nature 504:446-50.

40. Arpaia N, Campbell C, Fan X, Dikiy S, van der Veeken J, deRoos P, Liu H, Cross JR, Pfeffer K, Coffer PJ, Rudensky AY. 2013. Metabolites produced by commensal bacteria promote peripheral regulatory T-cell generation. Nature 504:451-5.

41. Smith PM, Howitt MR, Panikov N, Michaud M, Gallini CA, Bohlooly YM, Glickman JN, Garrett WS. 2013. The microbial metabolites, short-chain fatty acids, regulate colonic Treg cell homeostasis. Science 341:569-73.

42. Lopez CA, Miller BM, Rivera-Chávez F, Velazquez EM, Byndloss MX, Chávez-Arroyo A, Lokken KL, Tsolis RM, Winter SE, Bäumler AJ. 2016. Virulence factors enhance Citrobacter rodentium expansion through aerobic respiration. Science 353:1249-53.

43. Cevallos SA, Lee JY, Tiffany CR, Byndloss AJ, Johnston L, Byndloss MX, Baumler AJ. 2019. Increased Epithelial Oxygenation Links Colitis to an Expansion of Tumorigenic Bacteria. MBio 10.

44. Cevallos SA, Lee JY, Velazquez EM, Foegeding NJ, Shelton CD, Tiffany CR, Parry BH, Stull-Lane AR, Olsan EE, Savage HP, Nguyen H, Ghanaat SS, Byndloss AJ, Agu IO, Tsolis RM, Byndloss MX, Baumler AJ. 2021. 5-Aminosalicylic Acid Ameliorates Colitis and Checks Dysbiotic Escherichia coli Expansion by Activating PPAR-gamma Signaling in the Intestinal Epithelium. mBio 12.

45. Litvak Y, Byndloss MX, Baumler AJ. 2018. Colonocyte metabolism shapes the gut microbiota. Science 362:eaat9076.

46. Hooper LV, Gordon JI. 2001. Commensal host-bacterial relationships in the gut. Science 292:1115-8.

47. Petersen C, Round JL. 2014. Defining dysbiosis and its influence on host immunity and disease. Cell Microbiol 16:1024-33.

48. Tipton L, Darcy JL, Hynson NA. 2019. A Developing Symbiosis: Enabling Cross-Talk Between Ecologists and Microbiome Scientists. Front Microbiol 10:292.

49. Berg G, Rybakova D, Fischer D, Cernava T, Verges MC, Charles T, Chen X, Cocolin L, Eversole K, Corral GH, Kazou M, Kinkel L, Lange L, Lima N, Loy A, Macklin JA, Maguin E, Mauchline T, McClure R, Mitter B, Ryan M, Sarand I, Smidt H, Schelkle B, Roume H, Kiran GS, Selvin J, Souza RSC, van Overbeek L, Singh BK, Wagner M, Walsh A, Sessitsch A, Schloter M. 2020. Microbiome definition re-visited: old concepts and new challenges. Microbiome 8:103.

50. Rogers AWL, Tsolis RM, Baumler AJ. 2021. Salmonella versus the Microbiome. Microbiol Mol Biol Rev 85.

51. Lee JY, Tsolis RM, Baumler AJ. 2022. The microbiome and gut homeostasis. Science 377:eabp9960.

52. Niccolai E, Baldi S, Ricci F, Russo E, Nannini G, Menicatti M, Poli G, Taddei A, Bartolucci G, Calabro AS, Stingo FC, Amedei A. 2019. Evaluation and comparison of short chain fatty acids composition in gut diseases. World J Gastroenterol 25:5543-5558.

53. Woods LF, Wood JM, Gibbs PA. 1981. the involvement of Nitric Oxide in the inhibition of the phosphoroclastic system in Clostridium sporogenes by sodium nitrite. J Gen Microbiol 125:399-406.

54. Payne MJ, Glidewell C, Cammack R. 1990. Interactions of iron-thiol-nitrosyl compounds with the phosphoroclastic system of Clostridium sporogenes. J Gen Microbiol 136:2077-87.

55. Lee SK, Newman JD, Keasling JD. 2005. Catabolite repression of the propionate catabolic genes in Escherichia coli and Salmonella enterica: evidence for involvement of the cyclic AMP receptor protein. J Bacteriol 187:2793-800.

56. Kuroda M, Osaki N, Tsuda M, Tsuchiya T. 1992. Preferential utilization of glucose over melibiose, and vice versa, in a pts mutant of Salmonella typhimurium. Chem Pharm Bull (Tokyo) 40:1637-40.

57. Alexeeva S, Hellingwerf KJ, Teixeira de Mattos MJ. 2002. Quantitative assessment of oxygen availability: perceived aerobiosis and its effect on flux distribution in the respiratory chain of Escherichia coli. J Bacteriol 184:1402-6.

58. Friedman ES, Bittinger K, Esipova TV, Hou L, Chau L, Jiang J, Mesaros C, Lund PJ, Liang X, FitzGerald GA, Goulian M, Lee D, Garcia BA, Blair IA, Vinogradov SA, Wu GD. 2018. Microbes vs. chemistry in the origin of the anaerobic gut lumen. Proc Natl Acad Sci U S A 115:4170-4175.

59. Lopez CA, Winter SE, Rivera-Chavez F, Xavier MN, Poon V, Nuccio SP, Tsolis RM, Baumler AJ. 2012. Phage-mediated acquisition of a type III secreted effector protein boosts growth of salmonella by nitrate respiration. MBio 3:e00143-12.

60. Lawley TD, Bouley DM, Hoy YE, Gerke C, Relman DA, Monack DM. 2008. Host transmission of Salmonella enterica serovar Typhimurium is controlled by virulence factors and indigenous intestinal microbiota. Infect Immun 76:403-16.

61. Tiffany CR, Baumler AJ. 2019. omu, a Metabolomics Count Data Analysis Tool for Intuitive Figures and Convenient Metadata Collection. Microbiol Resour Announc 8.

62. Kuczynski J, Stombaugh J, Walters WA, Gonzalez A, Caporaso JG, Knight R. 2012. Using QIIME to analyze 16S rRNA gene sequences from microbial communities. Curr Protoc Microbiol Chapter 1:Unit 1E 5.

63. Bolger AM, Lohse M, Usadel B. 2014. Trimmomatic: a flexible trimmer for Illumina sequence data. Bioinformatics 30:2114-20.

64. Callahan BJ, McMurdie PJ, Rosen MJ, Han AW, Johnson AJ, Holmes SP. 2016. DADA2: High-resolution sample inference from Illumina amplicon data. Nat Methods 13:581-3.

65. McMurdie PJ, Holmes S. 2013. phyloseq: an R package for reproducible interactive analysis and graphics of microbiome census data. PLoS One 8:e61217.

66. Bodenhofer U, Bonatesta E, Horejs-Kainrath C, Hochreiter S. 2015. msa: an R package for multiple sequence alignment. Bioinformatics 31:3997-9.

67. Schliep KP. 2011. phangorn: phylogenetic analysis in R. Bioinformatics 27:592-3.

68. (ed). 2016. ggplot2 : Elegant Graphics for Data Analysis. Springer International Publishing : Imprint: Springer,, Cham. Accessed

69. Love MI, Huber W, Anders S. 2014. Moderated estimation of fold change and dispersion for RNA-seq data with DESeq2. Genome Biol 15:550.

70. Schneider CA, Rasband WS, Eliceiri KW. 2012. NIH Image to ImageJ: 25 years of image analysis. Nat Methods 9:671-5.

71. Edwards RA, Keller LH, Schifferli DM. 1998. Improved allelic exchange vectors and their use to analyze 987P fimbria gene expression. Gene 207:149-57.

72. Lawes M, Maloy S. 1995. MudSacI, a transposon with strong selectable and counterselectable markers: use for rapid mapping of chromosomal mutations in Salmonella typhimurium. J Bacteriol 177:1383-7.

Supplementary Figures

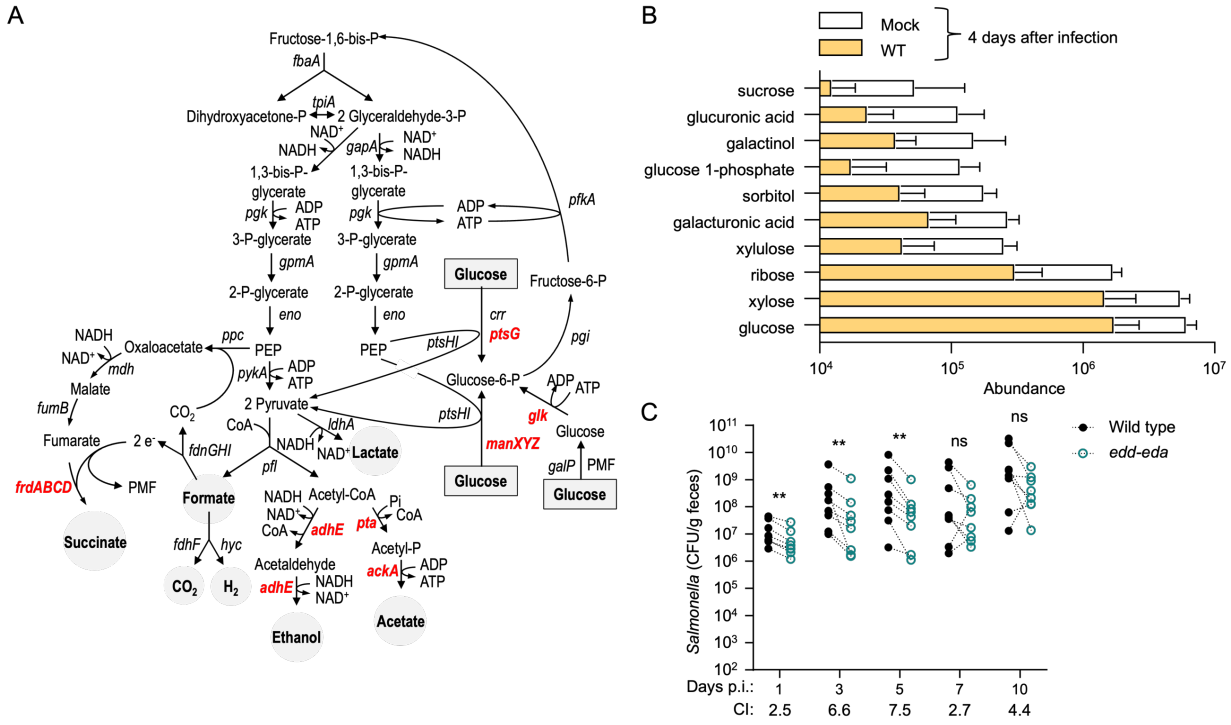

Figure 2.S1: Glucose catabolism by *S.* Typhimurium. Related to Figure 1.

(A) Schematic of pathways for glucose (gray rectangles) uptake and catabolism in *S.* Typhimurium. Genes mutated in this study are highlighted in red font. The end products of mixed-acid fermentation are marked by grey circles. PEP. Phosphoenolpyruvate; PMF, proton motive force; ATP, adenosine triphosphate; ADP, adenosine diphosphate; e^-, electron; CO_2, carbon dioxide; H_2, hydrogen; CoA, coenzyme A; NAD^+, Nicotinamide adenine dinucleotide; P, phosphate. (B) Antibiotic-naïve, genetically resistant (CBA/J) mice were mock infected or infected with 10^9 colony-forming units (CFU) of the *S.* Typhimurium WT. Cecal contents were collected four days after infection for untargeted metabolomics analysis. Shown is the geometric mean abundance of the indicated sugars in cecal contents of mock-infected mice (open bars) or *S.* Typhimurium-infected mice (yellow bars) ± geometric standard deviation. (C) CBA/J mice were infected with a 1:1

mixture of the indicated strains. The graphs shows CFU of the *S.* Typhimurium WT and the respective mutant recovered from feces at the indicated days after infection (Days p.i.). WT and mutant CFU recovered from the same animal are connected by dotted lines. The competitive index (CI) determined for each time point is the ratio of wild type to mutant bacteria.

Supplementary Tables

Table 2.S1: Resistance to nitric oxide of the indicated bacterial strains. Related to Figure 6.

	MIC	
Strain:	DETA (mM)	DETA NONOate (μM)
Enterocloster bolteae	>10	312.5
Anaerostipes caccae	2.5	10
Anaerotruncus colihominis	>10	5
S. Typhimurium	>10	5000
S. Typhimurium Δ*cydAB*	>10	5000
S. Typhimurium Δ*hmpA* Δ*norVW*	>10	1250
S. Typhimurium Δ*cydAB* Δ*hmpA* Δ*norVW*	>10	1250

Table 2.S2: Bacterial strains and plasmids used in this study. Related to STAR Methods.

Bacterial Strains		
Species and strain	**Genotype**	**Reference**
E. coli DH5α λ*pir*	F$^-$ *endA1 hsdR17* (*r*$^-$*m*$^+$) *supE44 thi-1 recA1 gyrA relA1* Δ(*lacZYA-argF*)*U189* Φ80l*acZ*Δ*M15* λ*pir*	(Pal et al., 2005)
E. coli S17-1 λ*pir*	zxx::RP4 2-(Tet^R::Mu) (Kan^R::Tn7) λ*pir recA1 thi pro hsdR* (*r*$^-$*m*$^+$)	(Simon et al., 1983)
S. Typhimurium IR715	ATCC14028 Nal^R (Nal^R)	(Stojiljkovic et al., 1995)
S. Typhimurium FF176	ATCC14028 Nal^R *phoN*::Tn*10dCam* (Nal^R, Cm^R)	(Faber et al., 2016)
S. Typhimurium AJB715	ATCC14028 Nal^R *phoN*::KSAC (Nal^R, Kan^R)	(Kingsley et al., 2003)
S. Typhimurium FF183	ATCC14028 Nal^R Δ*invA* Δ*spiB phoN*::Tn*10dCam* (Nal^R, Cm^R)	(Faber et al., 2017)
S. Typhimurium FF459	ATCC14028 Nal^R Δ*invA* Δ*spiB phoN*::KSAC (Nal^R, Kan^R)	(Walker et al., 2021)
S. Typhimurium FR104	ATCC14028 Nal^R Nal^R *cyxA*::pPT48 Δ*napA* Δ*narZ narG*:: pCAL18 (Nal^R, Carb^R, Cm^R)	(Rivera-Chavez et al., 2016)
S. Typhimurium AWLR36	ATCC14028 Nal^R Δ*ackA-pta phoN*::KSAC (Nal^R, Kan^R)	This Study
S. Typhimurium AWLR222	ATCC14028 Nal^R Δ*adhE phoN*::KSAC (Nal^R, Kan^R)	This Study
S. Typhimurium WJ29	ATCC14028 Nal^R Δ*frdABCD phoN*::KSAC (Nal^R, Kan^R)	(Woongjae Yoo, 2022)
S. Typhimurium AWLR228	ATCC14028 Nal^R Δ*ptsG* Δ*glk* Δ*manXYZ phoN*::KSAC (Nal^R, Kan^R)	This Study
S. Typhimurium AWLR204	ATCC14028 Nal^R Δ*edd-eda phoN*::KSAC (Nal^R, Kan^R)	This Study
S. Typhimurium LR179	ATCC14028 Nal^R Δ*cydAB phoN*::KSAC (Nal^R, Kan^R)	This Study

S. Typhimurium AWLR243	ATCC14028 Nal^R Δ*hmpA phoN*::KSAC (Nal^R, Kan^R)	This Study
S. Typhimurium AWLR244	ATCC14028 Nal^R Δ*norVW phoN*::KSAC (Nal^R, Kan^R)	This Study
S. Typhimurium AWLR245	ATCC14028 Nal^R Δ*hmpA* Δ*norVW phoN*::KSAC (Nal^R, Kan^R)	This Study
S. Typhimurium AWLR246	ATCC14028 Nal^R Δ*cydAB* Δ*hmpA* Δ*norVW phoN*::KSAC (Nal^R, Kan^R)	This Study
S. Typhimurium FF355	ATCC14028 Nal^R Δ*fadD* Δ*ydiQRSTD phoN*::KSAC (Nal^R, Kan^R)	This Study
Enterocloster bolteae	Wild type	(Atarashi et al., 2013)
Anaerostipes caccae	Wild type	(Atarashi et al., 2013)
Anaerotruncus colohominis	Wild type	(Atarashi et al., 2013)
S. Typhimurium AWLR204	ATCC14028 Nal^R Δ*edd-eda phoN*::KSAC (Nal^R, Kan^R)	This Study
Plasmids		
Name	**Genotype**	**Reference**
pRE112	*sacB1 cat ori*R6K *mobRP4*	(Edwards et al., 1998)
pAWLR43	pRE112 with upstream and downstream regions of *S.* Typhimurium *ackA-pta* forming a deletion mutant allele	This Study
pAWLR142	pRE112 containing upstream and downstream regions of *S.* Typhimurium *adhE* forming a deletion mutant allele	This Study
pAWLR148	pRE112 containing upstream and downstream regions of *S.* Typhimurium *glk* forming a deletion mutant allele	This Study
pAWLR150	pRE112 containing upstream and downstream regions of *S.* Typhimurium *ptsG* forming a deletion mutant allele	This Study
pAWLR152	pRE112 containing upstream and downstream regions of *S.* Typhimurium *manXYZ* forming a deletion mutant allele	This Study

pAWLR139	pRE112 containing upstream and downstream regions of *S.* Typhimurium *edd-eda* forming a deletion mutant allele	This Study
LR173	pRE112 containing upstream and downstream regions of *S.* Typhimurium *cydAB* forming a deletion mutant allele	This Study
pAWLR164	pRE112 containing upstream and downstream regions of *S.* Typhimurium *hmpA* forming a deletion mutant allele	This Study
pAWLR165	pRE112 containing upstream and downstream regions of *S.* Typhimurium *norVW* forming a deletion mutant allele	This Study

Table 2.S3: Primers used for targeted mutagenesis in this study. Related to STAR Methods.

Primers used for Targeted Mutagenesis		
Target	**Sequence**	**Reference**
ackA-pta	5'-TTCATGGCCATATCAATGACAGGCGGCATAAATCGTATG-3' 5'-TTTACTGTTACATGGAAGTACCTATTTATGATACGTG-3' 5'-CTTCCATGTAACAGTAAAAGCTAATGCCG-3' 5'-AATTCATGCAGTTCACTTAATTCATCAGCCCTGGTC-3'	This Study
adhE	5'-CATTCATGGCCATATCAATGAAAATCAAAAAGCGGTTG-3' 5'-TAACGAATTACATAATGCTCTCCTGATAATG-3' 5'-GAGCATTATGTAATTCGTTATCTGTTTTAGCATG-3' 5'-GGAATTCATGCAGTTCACTTCAAATTAGATATTCCAGTACTTTG-3'	This Study
ptsG	5'-CATTCATGGCCATATCAATGATCGATTATTAGTCGAGACC-3' 5'-TTACTGCTTACATAATTGAGAGTGCTCC-3' 5'-CTCAATTATGTAAGCAGTAATGATGTTGG-3' 5'-GGAATTCATGCAGTTCACTTTCGAATTTGAAGTGAACG-3'	This Study
glk	5'-CATTCATGGCCATATCAATGACGTAACGTGACGCAGCC-3' 5'-TAGAAGAATGTAAGCCAGATGGTGGCATAAAC-3' 5'-ATCTGGCTTACATTCTTCTACTGCTCCGCTAAAGTCAAAATAAG-3' 5'-GGAATTCATGCAGTTCACTTCGCAGATGGCGAGACCGG-3'	This Study
manXYZ	5'-CATTCATGGCCATATCAATGAAATTGAGGGATCCATTAATAATTC-3' 5'-AACAGCCTTACACTTGCTACCTCCTTTATTATTG-3' 5'-GTAGCAAGTGTAAGGCTGTTGTACACTAC-3' 5'-GGAATTCATGCAGTTCACTTAGAAGTTTATATATTTTTTCCAGATC-3'	This Study
edd-eda	5'-CATTCATGGCCATATCAATGGTCATGGCCTGTTCGGCG-3' 5'-AGCCTCTATGTAAGCCGTTAAATGCCCGATG-3' 5'-TAACGGCTTACATAGAGGCTCCTGAAATTTATC-3' 5'-GGAATTCATGCAGTTCACTTTTGATCTGAGCTACTCCG-3'	This Study

cydAB	5'-CATTCATGGCCATATCAATGCGGGGCAGTAAAAAACGC-3' 5'-GGTTCAGCGTCATCATGACTCCTTGCTCATC-3' 5'-AGTCATGATGACGCTGAACCTGATGACCTG-3' 5'-GGAATTCATGCAGTTCACTTAACCGTGACGGGTCCCAG-3'	This Study
hmpA	5'-CATTCATGGCCATATCAATGTAACCTTCAGCGTATTTG-3' 5'-GTTGCAATTACATACGTGCTTCCTTTATG-3' 5'-AGCACGTATGTAATTGCAACAAATCCTCTGAAAAAACGGG-3' 5'-GGAATTCATGCAGTTCACTTACCAGATAACCGGCGCCG-3'	This Study
norVW	5'-CATTCATGGCCATATCAATGCTGTCCGGGAATTAACCC-3' 5'-CACAGGCTTACATAACCACCTCAATTCATTC-3' 5'-GGTGGTTATGTAAGCCTGTGATGCCGGATG-3' 5'-GGAATTCATGCAGTTCACTTGCTATGAGGGCGAGGCCG-3'	This Study
pRE112 (pRE_linear_F)	5'-AAGTGAACTGCATGAATTC-3'	This Study
pRE112 (pRE_linear_R)	5'- CATTGATATGGCCATGAATG -3'	This Study
pRE112 (pRE_chk_F)	5'-CGTAAAATCGTGTTGAGGCC-3'	This Study
pRE112 (pRE_chk_R)	5'-AGCTTCTTCTAGAGGTACCGC-3'	This Study

Table 2.S4: Primers used in this study. Related to STAR Methods.

Primers used for qRT-PCR			
Target gene	**Sequence**	**Organism**	**Reference**
β2m	5'-GGTCTTTCTGGTGCTTGTCTCA-3' 5'-GTTCGGCTTCCCATTCTCC-3'	*Mus musculus*	(Matouskova et al., 2014)
IL-17a	5'-GCTCCAGAAGGCCCTCAGA-3' 5'-AGCTTTCCCTCCGCATTGA-3'	*Mus musculus*	(Godinez et al., 2008)
Cxcl1 (mKc)	5'-TGCACCCAAACCGAAGTCAT-3' 5'-TTGTCAGAAGCCAGCGTTCAC-3'	*Mus musculus*	(Godinez et al., 2008)
Cxcl2 (Mip2)	5'-AGTGAACTGCGCTGTCAATGC-3' 5'-AGGCAAACTTTTTGACCGCC-3'	*Mus musculus*	(Godinez et al., 2008)
Lcn2	5'-ACATTTGTTCCAAGCTCCAGGGC-3' 5'-CATGGCGAACTGGTTGTAGTCCG-3'	*Mus musculus*	(Godinez et al., 2008)
Sglt1	5'-CTCATGCCTAATGGACTGCGA-3' 5'-GCCAATCAGCACGAGGATGA-3'	*Mus musculus*	This Study
Glut2	5'-ATTCTTTGGTGGGTGGCTCG-3' 5'-CCAGTCCTGAAATTAGCCCACAA-3'	*Mus musculus*	This Study
Nos2	5'-TTGGGTCTTGTTCACTCCACGG-3' 5'-CCTCTTTCAGGTCACTTTGGTAGG-3'	*Mus musculus*	(Godinez et al., 2008)
Angptl4	5'-AGGCTGGACAGTTAATTCAGAGG-3' 5'-ATGCTATGCTATGCACCTTCTCCAGAC-3'	*Mus musculus*	(Lee et al., 2020)
Pgc1α	5'-CCCTGCCATTGTTAAGACC-3' 5'-TGCTGCTGTTCCTGTTTTC-3'	*Mus musculus*	(Lee et al., 2020)
Ndufs1	5'-AGCCGGCAGCCATCATGTTA-3' 5'-AGTTACTTGCTGCTGTGCCA-3'	*Mus musculus*	(Lee et al., 2020)
Ndufv1	5'-TTTCTCGGCGGGTTGGTTC-3' 5'-GGTTGGTAAAGATCCGGTCTTC-3'	*Mus musculus*	(Lee et al., 2020)
Atp5g1	5'-AGTTGGTGTGGCTGGATCA-3' 5'-GCTGCTTGAGAGATGGGTTC-3'	*Mus musculus*	(Lee et al., 2020)
Cox1	5'-TGCTAGCCGCAGGCATTAC-3' 5'-GGGTGCCCAAAGAATCAGAAC-3'	*Mus musculus*	(Lee et al., 2020)
Uqcr	5'-TGCCGAGGCCTCAGACACAG-3' 5'-TCCAAGGCATAAGAATAAGGTTT-3'	*Mus musculus*	(Lee et al., 2020)

Table 2.S5: Histopathology scoring matrix. Scoring criteria for examination of H&E-stained cecal and colonic sections. Related to STAR Methods.

Score	Submucosal edema	Necrosis	Neutrophils	Epithelial damage	Exudate
0	Absent	Absent	0 – 5	Absent	Absent
1	Slight (<10%)	Slight Necrosis	6 – 20	Desquamation	Slight accumulation
2	Mild (10%-20%)	Mild necrosis	21 - 50	Mild erosion	Mild accumulation
3	Moderate (20%-40%)	Moderate necrosis	51 - 100	Marked erosion	Moderate accumulation
4	Severe (>40%)	Severe necrosis	>100	Ulceration	Severe accumulation

Table 2.S6: Experimentally determined analyte retention times. Related to STAR Methods.

Analyte	Retention time (minutes)	Quantifier ion (m/z)	Qualifier 1 (m/z)	Qualifier 2 (m/z)
Acetate	9.513	117	118	159
Propionate	19.073	131	132	173
Butyrate	24.685	145	146	187
Acetate-d3	9.364	120	122	162
Propionate-d5	18.693	136	137	178
Butyrate-d7	24.503	152	153	194

Supplementary References

1. Pal D, Venkova-Canova T, Srivastava P, Chattoraj DK. 2005. Multipartite regulation of rctB, the replication initiator gene of Vibrio cholerae chromosome II. J Bacteriol 187:7167-75.

2. Simon R, Priefer U, Puhler A. 1983. A Broad Host Range Mobilization System for Invivo Genetic-Engineering - Transposon Mutagenesis in Gram-Negative Bacteria. Bio-Technology 1:784-791.

3. Stojiljkovic I, Baumler AJ, Heffron F. 1995. Ethanolamine utilization in Salmonella typhimurium: nucleotide sequence, protein expression, and mutational analysis of the cchA cchB eutE eutJ eutG eutH gene cluster. J Bacteriol 177:1357-66.

4. Faber F, Tran L, Byndloss MX, Lopez CA, Velazquez EM, Kerrinnes T, Nuccio SP, Wangdi T, Fiehn O, Tsolis RM, Baumler AJ. 2016. Host-mediated sugar oxidation promotes post-antibiotic pathogen expansion. Nature 534:697-9.

5. Kingsley RA, Humphries AD, Weening EH, De Zoete MR, Winter S, Papaconstantinopoulou A, Dougan G, Baumler AJ. 2003. Molecular and phenotypic analysis of the CS54 island of Salmonella enterica serotype typhimurium: identification of intestinal colonization and persistence determinants. Infect Immun 71:629-40.

6. Faber F, Thiennimitr P, Spiga L, Byndloss MX, Litvak Y, Lawhon S, Andrews-Polymenis HL, Winter SE, Baumler AJ. 2017. Respiration of Microbiota-Derived 1,2-propanediol Drives Salmonella Expansion during Colitis. PLoS Pathog 13:e1006129.

7. Walker GT, Yang G, Tsai JY, Rodriguez JL, English BC, Faber F, Souvannaseng L, Butler BP, Tsolis RM. 2021. Malaria parasite infection compromises colonization resistance to an enteric pathogen by reducing gastric acidity. Sci Adv 7.

8. Rivera-Chavez F, Zhang LF, Faber F, Lopez CA, Byndloss MX, Olsan EE, Xu G, Velazquez EM, Lebrilla CB, Winter SE, Baumler AJ. 2016. Depletion of Butyrate-Producing Clostridia from the Gut Microbiota Drives an Aerobic Luminal Expansion of Salmonella. Cell Host Microbe 19:443-54.

9. Woongjae Yoo JKZ, Nicolas G. Shealy, Teresa P. Torres, Julia D. Thomas, Catherine D. Shelton, Nora J. Foegeding, Erin E. Olsan, View ORCID ProfileMariana X. Byndloss. 2022. Microbiota-derived aspartate drives pathogenic Enterobacteriaceae expansion in the inflamed gut. bioRxiv doi:https://doi.org/10.1101/2022.02.14.480453

10. Atarashi K, Tanoue T, Oshima K, Suda W, Nagano Y, Nishikawa H, Fukuda S, Saito T, Narushima S, Hase K, Kim S, Fritz JV, Wilmes P, Ueha S, Matsushima K, Ohno H, Olle B, Sakaguchi S, Taniguchi T, Morita H, Hattori M, Honda K. 2013. Treg induction by a rationally selected mixture of Clostridia strains from the human microbiota. Nature 500:232-6.

11. Edwards RA, Keller LH, Schifferli DM. 1998. Improved allelic exchange vectors and their use to analyze 987P fimbria gene expression. Gene 207:149-57.

12. Matouskova P, Bartikova H, Bousova I, Hanusova V, Szotakova B, Skalova L. 2014. Reference genes for real-time PCR quantification of messenger RNAs and microRNAs in mouse model of obesity. PLoS One 9:e86033.

13. Godinez I, Haneda T, Raffatellu M, George MD, Paixao TA, Rolan HG, Santos RL, Dandekar S, Tsolis RM, Baumler AJ. 2008. T cells help to amplify inflammatory responses induced by Salmonella enterica serotype Typhimurium in the intestinal mucosa. Infect Immun 76:2008-17.

14. Lee JY, Cevallos SA, Byndloss MX, Tiffany CR, Olsan EE, Butler BP, Young BM, Rogers AWL, Nguyen H, Kim K, Choi SW, Bae E, Lee JH, Min UG, Lee DC, Baumler AJ. 2020. High-Fat Diet and Antibiotics Cooperatively Impair Mitochondrial Bioenergetics to Trigger Dysbiosis that Exacerbates Pre-inflammatory Bowel Disease. Cell Host Microbe 28:273-284.

Chapter 3: New insights gained from *Salmonella* Typhimurium infection in the antibiotic-naïve mouse model

Andrew W.L. Rogers

Salmonella Typhimurium as a Model Invader of the Gut Ecosystem

It is estimated that there are as many microbial cells inhabiting the average human body as there human cells that make up that body (1). Of those ~10^{13} microbial cells, the overwhelming majority of them reside in the large intestine (1). The microbial community that inhabits this site makes significant contributions to health and disease, and therefore represents an important field of study. One role of the gut microbiota is to confer colonization resistance against invading organisms, including pathogens. This function of the microbiota first became widely recognized with the development and widespread usage of antibiotic therapies in the 1940s (2). It was quickly observed that antibiotic treatment could result in patient susceptibility to secondary gastrointestinal infections (3). Researchers at the University of Chicago leveraged this observation in order to study gastrointestinal colonization resistance in the laboratory. They found that an oral dose of streptomycin given the day prior to oral *Salmonella enterica* infection rendered mice completely susceptible to colonization by low dose challenges, and thus, the use of *Salmonella enterica* as a model invader of the large intestine began.

Even at these early stages of *Salmonella*-driven colonization resistance research, the streptomycin-pretreatment model was compared with infections of antibiotic-naïve mice, revealing microbiota-derived short-chain fatty acids as important mediators of resistance to *Salmonella* engraftment (4-6). The streptomycin pre-treatment model has proven to be a convenient, reproducible method of studying *Salmonella*-induced colitis in mice that limits experimental variability, but its utility in studying the contribution of the endogenous gut microbiota to colonization resistance is limited, as ablation of those very

microbes is inherent to the model. Unfortunately, infecting antibiotic-naïve mice with even very high oral doses of *Salmonella* has historically been a challenging endeavor in the laboratory, as microbiota-mediated colonization resistance is often strong enough to render mice completely resistant to infection (7). Even when *Salmonella* infection takes hold, variations in microbiota composition can cause a level of variability in the data that makes hypothesis testing quite challenging (8). Together, these inherent difficulties of the antibiotic-naïve model have contributed to the dominance of the streptomycin pre-treatment model in the *Salmonella* gut pathogenesis field. The discovery in 2019 that endogenous Enterobacteriaceae are central mediators of colonization resistance to *Salmonella* Typhimurium (*S.* Typhimurium), coupled to the observation that specific pathogen-free (SPF) mice from The Jackson Laboratory lack endogenous Enterobacteriaceae, led to our increased focus on using the antibiotic-naïve mouse model of oral *Salmonella* infection to study microbiota-mediated colonization resistance (8).

Pathogen Kinetics as an Approach to Studying Colonization Resistance

With a model in place that allows for the study of colonization resistance in the context of *S.* Typhimurium encountering an unperturbed microbiota, we reasoned that the best proxy for colonization resistance would be pathogen burden in the feces, with declining pathogen burden indicating successful colonization resistance, and increasing pathogen burden indicating failed colonization resistance. What we found is that daily enumeration of *S.* Typhimurium in the feces of infected animals was indeed a useful strategy for tracking microbiota-mediated colonization resistance. Previous studies had

chosen arbitrary timepoints after infection for pathogen enumeration but had failed to track *S.* typhimurium burden on a daily basis. By simply observing daily infection kinetics in the antibiotic-naïve mouse model, we were able to determine that colonization resistance is intact one day after infection and is overcome by *S.* Typhimurium's virulence strategy by day 3 (**Fig. 2.1A**). In fact, the entirety of my findings stem from these initial observations of *S*. Typhimurium infection kinetics during the early stages of infection, as we were able to focus on day 3 after infection as the crucial moment of colonization resistance failure.

Microbiota Function vs. Microbiota Composition

A previous study from our research group showed that oral *S.* Typhimurium infection induces restructuring of microbiota composition, including a hallmark reduction in the abundance of bacteria belonging to the class Clostridia (9). Due to this correlation, we interpreted this to mean that these alterations of microbial community structure were necessary for the expansion of the pathogen in the large intestine. This hypothesis was proven false by the antibiotic-naive infection model when microbiota profiling by 16S rRNA amplicon sequencing indicated that microbiota alterations were not statistically significant at the time of *S.* Typhimurium expansion (**Fig. 2.4B**). In contrast, levels of the short-chain fatty acids acetate and butyrate were significantly decreased at day 3 after infection, implying that the metabolic output of the microbiota, and therefore its function, had been altered by *S.* Typhimurium-induced inflammation.

Microbiota composition can be a useful diagnostic for identifying the presence of abnormal habitat filtering in the gastrointestinal tract and has informed our working definition of “good” versus “bad” gut health. A state of homeostasis is often associated with a dominance of obligate anaerobes, while a state of dysbiosis can be identified by an overabundance of facultative anaerobes like members of the family Enterobacteriaceae (10). The observation that *S.* Typhimurium subverts colonization resistance while obligate anaerobes still dominate the large intestinal community challenges this generalization and suggests that colonization resistance cannot be fully predicted by microbiota composition alone. Cecal short-chain fatty acid concentrations were chosen as a readout for microbiota function as these are the primary fermentation products produced by obligate anaerobes and have previously been found to contribute to inhibition of *S.* Typhimurium in the gut (4-6, 11). While these weak acids were found to be negatively correlated with *S.* Typhimurium burden at day 3 after infection, the association was only moderate, implying that this aspect of microbiota function is only partially predictive of colonization resistance.

Our observation that *S.* Typhimurium expansion at day 3 after infection requires a switch in host epithelial metabolism that grants the pathogen access to aerobic respiration (**Fig. 2.6**) suggests that host processes may be stronger determinants of colonization resistance than microbial activities. However, this conclusion can be challenged by the fact that cecal butyrate concentrations are drastically depleted at day 3 after *S.* Typhimurium infection, and butyrate is known to support epithelial hypoxia both as an agonist for the nuclear hormone receptor PPAR-γ, and as a substrate for mitochondrial β-

oxidation (12, 13). In this example, microbiota function and host processes may be inextricably linked. In support of host processes overriding microbiota function in the maintenance of colonization resistance, a recent study found that even short dietary shifts to a high-fat meal induced increased bile acid secretion by the host. In turn, elevated bile acids allowed for the expansion of bile-resistant *Escherichia coli* (*E. coli*) and *S.* Typhimurium, demonstrating that host-derived environmental conditions are key in supporting or negating colonization resistance (14).

Taken together, these findings highlight host-mediated habitat filters as prerequisite conditions for microbiota-mediated colonization resistance or the lack thereof. While assessment of microbiota composition can indicate chronic aberrations in host-dependent habitat filtering (i.e. dysbiosis), readouts of microbiota function may represent alternative proxies for colonization resistance capacity in the short-term. The lesson that *S*. Typhimurium teaches us about colonization resistance is that the most relevant factors to measure as predictors of colonization resistance are host-derived habitat filters, with the state of epithelial metabolism and bile acid concentrations representing prime examples.

Short-Chain Fatty Acids as a Colonization Resistance Factor

Two independent investigations of colonization resistance to *S.* Typhimurium in the murine large intestine carried out in the 1960s identified short-chain fatty acids as important inhibitors of *S.* Typhimurium colonization (4-6). Another study from 2018 specifically identified propionate produced by *Bacteroides* species as a key determinant

of *S.* Typhimurium colonization (11). In both cases, inhibition by of *S.* Typhimurium by short-chain fatty acids was shown to be pH-dependent, as these weak acids become membrane-permeable in their protonated forms, allowing them to diffuse into the bacterial cytosol. This uncontrolled diffusion of short-chain fatty acids into the relatively neutral or basic cytosol leads to dissociation of the acids, and subsequent acidification of the intracellular environment (11, 15). Cytosolic acidification has been found to limit the benefit that Enterobacteriaceae gain from respiratory metabolism, as the generation of a proton motive force is negated by the free diffusion of protons that is mediated by protonated weak acids (15). This inhibitory effect of short-chain fatty acids on facultative anaerobic Enterobacteriaceae serves to shut down a major metabolic strategy of this bacterial family, as respiration of oxygen and alternative electron acceptors confers a competitive advantage in an environment otherwise dominated by obligate anaerobes (15, 16).

My work shows that the short-chain fatty acids acetate and butyrate are depleted in the cecum on day 3 after *S.* Typhimurium infection (**Fig. 2.5A**), but rescue of acetate and butyrate levels by inhibition of inducible nitric oxide synthase (iNOS) via the administration of aminoguanidine did not significantly inhibit the ability of the pathogen to expand (**Fig. 2.5D**). Combining cecal short-chain fatty acid concentrations and matched *S.* Typhimurium burdens at day 3 after infection from five independent experiments allowed us to test for a relationship between these variables (**Fig. 2.5G**). In agreement with the observation that *S.* Typhimurium expands in the presence of rescued short-chain fatty acid levels, we found only a weak negative correlation between *S.* Typhimurium

infection outcome on day 3 after infection and cecal short-chain fatty acid concentrations, in opposition to previous findings that short-chain fatty acids mediate colonization resistance to *S*. Typhimurium.

This discrepancy in the apparent impact of short-chain fatty acids on colonization resistance among *S.* Typhimurium studies requires further scrutiny. When comparing our findings to the studies carried out in the 1960s, we do find agreement in the fact that when all other conditions are equal, increased short-chain fatty acid concentrations slow the growth of *S.* Typhimurium (**Fig. 2.5C**) (4-6). Combined with the observation that *S.* Typhimurium still manages to expand in the presence of pre-infection concentrations of short-chain fatty acids (**Fig. 2.5D**), we hypothesize that *S.* Typhimurium possesses innate metabolic strategies for overcoming this inhibition in vivo. Further study will be required to test that hypothesis, and the antibiotic-naïve infection model is likely to be useful in that endeavor.

Propionate has been found to effectively inhibit *S*. Typhimurium expansion in an antibiotic-naïve mouse model of oral infection on day 2 after infection, which is precisely when we observe microbiota-mediated colonization resistance having the largest effect on S. Typhimurium colonization (**Fig. 2.1A**) (11). The same study observed that levels of cecal propionate of approximately 15 μmol/g feces was sufficient to inhibit *S.* Typhimurium expansion, but levels at or below 5 μmol/g feces enabled *S*. Typhimurium expansion at day 3 after infection (11). Notably, we never detected propionate at levels above 5 μmol/g cecal contents in our study (**Fig. 2.5A**), and *Bacteroides* species were found at

conspicuously low levels in the microbiota (data not shown). This observation indicates that compositional variations between large intestinal microbiotas can have a significant effect on colonization resistance to pathogens like *S.* Typhimurium and suggests that the CBA/J mice used for the study in Chapter 2 may be of limited use when assessing the contribution of short-chain fatty acids to gastrointestinal colonization resistance.

Clostridia Facilitate Exploitative Competition Between Enterobacteriaceae

The metabolite landscape of the *S.* Typhimurium-infected cecum features hundreds of differentially abundant metabolites compared to uninfected animals (**Fig. 2.1A**). We chose to focus on the depletion of simple sugars from the cecum as we hypothesized that the pathogen may be directly consuming them to fuel its growth, thereby leading to their decreased abundance. We found that this was indeed the case, as we could provide rigorous evidence that *S*. Typhimurium utilizes glucose when overcoming colonization resistance at day after infection (**Fig. 2.2A, 2.2I, 2.2H**), suggesting that at least a subset of the differentially abundant metabolites of the infected murine cecum represent the metabolic footprint of the pathogen.

The use of untargeted metabolomics has proven to be a powerful tool in identifying the ecological niches of gut microbiota members, which we term metabolic footprinting (17, 18). The use of this approach has previously allowed us to identify simple sugar depletion form the murine cecum as part of the metabolic footprint of bacteria belonging to the class Clostridia (18). Streptomycin treatment, which has a substantial negative

effect on Clostridia abundance, leads to an increase in free simple carbohydrates in the cecum (18). Conversely, colonization of mice with a consortium of 17 species of Clostridia leads to a depletion of those same classes of sugars (18). Interestingly, we find that the only members of the microbiota that decrease in abundance at day 3 after *S.* Typhimurium infection belong to the class Clostridia, and that depletion of Clostridia explains the major differences in the cecal microbial communities between pre- and post-infection samples (**Fig. 2.4C-F**). Taken together, these observations implicate Clostridia as primary consumers of simple sugars in the large intestine. The inhibition of Clostridia metabolism by nitric oxide, as evidenced by the sharp depletion of cecal butyrate at day 3 after *S.* Typhimurium infection, may underlie the ability of *S.* Typhimurium to access simple carbohydrates.

Many studies to date have identified competition for carbohydrates as playing a major role in driving competition between endogenous and invading Enterobacteriaceae, such as *E. coli* or *S.* Typhimurium (19-21). However, the literature also provides evidence that Clostridia play a key role in this inter-Enterobacteriaceae conflict by providing a metabolic landscape in which carbohydrate resources are scarce. A study using a consortium of microbes designed to maximize metabolic capabilities using the fewest possible bacterial species found that *E. coli* was able to limit the engraftment of *S.* Typhimurium in gnotobiotic mice in a manner that pivoted around the utilization of the sugar alcohol galactitol by both species of Enterobacteriaceae (21). When a species of Clostridia, specifically a member of the family Lachnospiraceae, was excluded from the

defined microbiota, simple sugars became abundant in the large intestinal environment, providing a context in which both *E. coli* and *S.* Typhimurium could co-exist (21).

The sum of these observations tells us that ecological theory stemming from the study of macroorganisms also applies to the microorganisms in the gastrointestinal tract. Competition for carbohydrates between species of Enterobacteriaceae is expected, as these organisms are phylogenetically related and share common metabolic strategies. This competition is classified as exploitative competition, as it involves indirect interactions involved in the consumption of a common resource (22). Exploitative competition is extremely important for colonization resistance as it results in competitive exclusion of the less-fit competitor, which is what we observe when endogenous Enterobacteriaceae successfully fend off colonization by invading *S.* Typhimurium. However, a prerequisite condition for exploitative competition is that the resource being competed for is limited (23). Clostridia are commonly found as a dominant class within human gut microbial communities, a privileged position in which they are able to consume large quantities of simple sugars, thereby driving scarcity of those resources (18, 24). This Clostridia-dependent carbohydrate scarcity that enables exploitative competition between Enterobacteriacae, and therefore mediates a proven mechanism of gastrointestinal colonization resistance.

Unknown Unknowns Become Known Unknowns

As is often the case with scientific pursuits, the generation of satisfactory answers leads to yet more questions. The work presented in Chapter 2 makes significant headway

in using the antibiotic-naïve mouse model of oral *S*. Typhimurium infection to uncover interactions of the pathogen with both the host and the microbiota but introduces more questions than it answers.

Further contextualization of the findings in Chapter 2 within the pre-existing field reveals the need for a detail-oriented revisiting of certain topics. The predominance of the streptomycin pre-treatment model of *S.* Typhimurium infection over the last two decades has led to many discoveries and conclusions about how *S.* Typhimurium harnesses the host inflammatory response for its own benefit, particularly in the context of inflammation-dependent carbon sources and electron acceptors. This accelerated model of infection causes acute enterocolitis in mice and bypasses any role that the microbiota would normally play in the story of *S.* Typhimurium pathogenesis (25).

Some findings made in the streptomycin pre-treatment model exhibit shared relevance with the antibiotic-naïve model. Loss of epithelial hypoxia due to a switch in epithelial cell metabolism grants *S.* Typhimurium access to aerobic respiration in both models (9). Another recent study using an antibiotic naïve mouse model found that tetrathionate respiration contributes to the expansion of *S.* Typhimurium at day 3 after infection, which was a virulence strategy first identified in the streptomycin pre-treatment model (26, 27). In contrast, nitrate respiration has been shown to contribute substantially to *S.* Typhimurium fitness in the streptomycin pre-treatment model, but our work and the work of others finds that nitrate respiration plays no role for *S.* Typhimurium during the first 7 or 10 days of an antibiotic-naïve infection (26). Additionally, it appears that *S.*

Typhimurium relies on different terminal oxidases for aerobic respiration at early and late stages of infection, a phenotype that was not apparent in the streptomycin pre-treatment model (9). This observation is mirrored by the pattern of utilization for 1,2-propanediol in the antibiotic naïve model, which only contributes significantly to *S.* Typhimurium fitness 7 days after infection (28). There are additional examples in the literature of *S.* Typhimurium phenotypes that deserve to be freshly assessed in the antibiotic-naïve model of infection, but these phenotypes are context-dependent and/or temporally nuanced. Previously unappreciated details like these represent potentially impactful biology, and only future studies will be able to reveal their secrets.

Chapter 2 identifies hypoglycemia and glucose malabsorption as a previously unreported effect of *S.* Typhimurium infection (**Fig. 2.2E-F**). While we were unable to link glucose malabsorption to an *S.* Typhimurium phenotype, it is possible that our attention to this detail was not as rigorous as it could be. For example, we did not attempt to determine if any other dietary nutrients are subject to this malabsorption, and it is possible that malabsorption of nutrients like amino acids could play a role in pathogen fitness. Although glucose malabsorption did not contribute to *S.* Typhimurium's access to cecal glucose, the fact that glucose was found to be present in high concentrations in the uninfected cecum came as a surprise (**Fig. 2.2H**). A recent pre-print also identified glucose as an abundant and preferred resource of *S.* Typhimurium in the gut, and this was true across multiple strains of mice and models of infection, suggesting that cecal glucose is a ubiquitous resource of the gut ecosystem (29). Dietary glucose is believed to be absorbed efficiently during transit through the small intestine, and the results of an

oral glucose tolerance test in uninfected mice support this idea (**Fig. 2.2E**) (30). Therefore, the source of cecal glucose remains an open question with potential implications for microbial ecology in the gut. Possible sources include liberation from dietary fiber by host- or microbiota-derived glycoside hydrolases or even delivery to the gut from the blood stream, passive or otherwise.

We did not predict that *S.* Typhimurium expansion would occur in the gut in the presence of an intact microbiota (**Fig. 2.4**), or that microbiota composition would be resilient to the presence of a host inflammatory response (**Fig. 2.3**). Microbiota composition did significantly diverge over the course of *S.* Typhimurium infection, but these effects were gradual out to day 10 (**Fig. 2.4**). This display of microbiota resilience in the face of acute inflammation implies that the obligate anaerobes of the gut microbiota can adapt and survive during short periods of abnormal habitat filtering characterized by the presence of oxygen, reactive oxygen species, and reactive nitrogen species. Increasing evidence exists that obligate anaerobes are likely to possess a variety of mechanisms for dealing with oxygen and other forms of redox stress, but in vivo studies of these mechanisms are rare (31). A recent study identified an adaptive response to periods of gastrointestinal inflammation by *Bacteroides thetaiotaomicron* that resulted in increased fitness during subsequent inflammatory events, but the response of gut commensals to adverse environmental conditions in the gastrointestinal tract remains a viable area of research (32).

Concluding Remarks

In conclusion, this dissertation showcases the power of *S.* Typhimurium as a tool for dissecting the mechanistic underpinnings of microbiota-mediated colonization resistance. We hope that antibiotic-naïve models of infection continue to gain in popularity as the limitations of antibiotic pre-treatment models are more commonly experienced by researchers. This may fail to occur as the golden age of antibiotics comes to an end and renewed importance is placed on antibiotic-centric models to help stem the tide of antibiotic-resistant infections, but there should always be a place for the microbiota in the study of infectious disease. After all, our microbes have always been with us and will always be a part of us.

References

1. Sender R, Fuchs S, Milo R. 2016. Revised Estimates for the Number of Human and Bacteria Cells in the Body. PLOS Biology 14:e1002533.

2. Aminov RI. 2010. A brief history of the antibiotic era: lessons learned and challenges for the future. Front Microbiol 1:134.

3. Keefer CS. 1951. Alterations in normal bacterial flora of man and secondary infections during antibiotic therapy. The American journal of medicine 11:665-666.

4. Meynell G. 1963. Antibacterial mechanisms of the mouse gut: II. The role of Eh and volatile fatty acids in the normal gut. British journal of experimental pathology 44:209.

5. Bohnhoff M, Miller CP, Martin WR. 1964. Resistance of the mouse's intestinal tract to experimental *Salmonella* infection: I. factors which interfere with the initiation of infection by oral inoculation. The Journal of experimental medicine 120:805-816.

6. Bohnhoff M, Miller CP, Martin WR. 1964. Resistance of the mouse's intestinal tract to experimental *Salmonella* infection: II. Factors Responsibie for its Loss Following Streptomycin Treatment. The Journal of experimental medicine 120:817-828.

7. Bohnhoff M, Drake BL, Miller CP. 1954. Effect of streptomycin on susceptibility of intestinal tract to experimental *Salmonella* infection. Proceedings of the Society for Experimental Biology and Medicine 86:132-137.

8. Velazquez EM, Nguyen H, Heasley KT, Saechao CH, Gil LM, Rogers AW, Miller BM, Rolston MR, Lopez CA, Litvak Y. 2019. Endogenous Enterobacteriaceae underlie variation in susceptibility to *Salmonella* infection. Nature microbiology 4:1057-1064.

9. Rivera-Chávez F, Zhang LF, Faber F, Lopez CA, Byndloss MX, Olsan EE, Xu G, Velazquez EM, Lebrilla CB, Winter SE. 2016. Depletion of butyrate-producing Clostridia from the gut microbiota drives an aerobic luminal expansion of *Salmonella*. Cell host & microbe 19:443-454.

10. Lee J-Y, Tsolis RM, Bäumler AJ. 2022. The microbiome and gut homeostasis. Science 377:eabp9960.

11. Jacobson A, Lam L, Rajendram M, Tamburini F, Honeycutt J, Pham T, Van Treuren W, Pruss K, Stabler SR, Lugo K. 2018. A gut commensal-produced metabolite mediates colonization resistance to *Salmonella* infection. Cell host & microbe 24:296-307. e7.

12. Byndloss MX, Olsan EE, Rivera-Chávez F, Tiffany CR, Cevallos SA, Lokken KL, Torres TP, Byndloss AJ, Faber F, Gao Y. 2017. Microbiota-activated PPAR-γ signaling inhibits dysbiotic Enterobacteriaceae expansion. Science 357:570-575.

13. Litvak Y, Byndloss MX, Bäumler AJ. 2018. Colonocyte metabolism shapes the gut microbiota. Science 362:eaat9076.

14. Wotzka SY, Kreuzer M, Maier L, Arnoldini M, Nguyen BD, Brachmann AO, Berthold DL, Zünd M, Hausmann A, Bakkeren E, Hoces D, Gül E, Beutler M, Dolowschiak T, Zimmermann M, Fuhrer T, Moor K, Sauer U, Typas A, Piel J, Diard M, Macpherson AJ, Stecher B, Sunagawa S, Slack E, Hardt W-D. 2019. *Escherichia coli* limits *Salmonella* Typhimurium infections after diet shifts and fat-mediated microbiota perturbation in mice. Nature Microbiology 4:2164-2174.

15. Sorbara MT, Dubin K, Littmann ER, Moody TU, Fontana E, Seok R, Leiner IM, Taur Y, Peled JU, van den Brink MRM, Litvak Y, Bäumler AJ, Chaubard J-L, Pickard AJ, Cross JR, Pamer EG. 2018. Inhibiting antibiotic-resistant Enterobacteriaceae by microbiota-mediated intracellular acidification. Journal of Experimental Medicine 216:84-98.

16. Rivera-Chávez F, Lopez CA, Bäumler AJ. 2017. Oxygen as a driver of gut dysbiosis. Free Radic Biol Med 105:93-101.

17. Savage HP, Bays DJ, Tiffany CR, Gonzalez MA, Bejarano EJ, Carvalho TP, Luo Z, Masson HL, Nguyen H, Santos RL. 2024. Epithelial hypoxia maintains colonization resistance against *Candida albicans*. Cell Host & Microbe.

18. Tiffany CR, Lee J-Y, Rogers AW, Olsan EE, Morales P, Faber F, Bäumler AJ. 2021. The metabolic footprint of Clostridia and Erysipelotrichia reveals their role in depleting sugar alcohols in the cecum. Microbiome 9:1-13.

19. Oliveira RA, Ng KM, Correia MB, Cabral V, Shi H, Sonnenburg JL, Huang KC, Xavier KB. 2020. *Klebsiella michiganensis* transmission enhances resistance to Enterobacteriaceae gut invasion by nutrition competition. Nature microbiology 5:630-641.

20. Spragge F, Bakkeren E, Jahn MT, B. N. Araujo E, Pearson CF, Wang X, Pankhurst L, Cunrath O, Foster KR. 2023. Microbiome diversity protects against pathogens by nutrient blocking. Science 382:eadj3502.

21. Eberl C, Weiss AS, Jochum LM, Durai Raj AC, Ring D, Hussain S, Herp S, Meng C, Kleigrewe K, Gigl M, Basic M, Stecher B. 2021. *E. coli* enhance colonization resistance against *Salmonella* Typhimurium by competing for galactitol, a context-dependent limiting carbon source. Cell Host Microbe 29:1680-1692.e7.

22. Lang JM, Benbow ME. 2013. Species interactions and competition. Nature Education Knowledge 4:8.

23. Moon DC, Moon J, Keagy A. 2010. Direct and indirect interactions. Nature Education Knowledge 3:50.

24. Huttenhower C, Gevers D, Knight R, Abubucker S, Badger JH, Chinwalla AT, Creasy HH, Earl AM, FitzGerald MG, Fulton RS, Giglio MG, Hallsworth-Pepin K, Lobos EA, Madupu R, Magrini V, Martin JC, Mitreva M, Muzny DM, Sodergren EJ, Versalovic J, Wollam AM, Worley KC, Wortman JR, Young SK, Zeng Q, Aagaard KM, Abolude OO, Allen-Vercoe E, Alm EJ, Alvarado L, Andersen GL, Anderson S, Appelbaum E, Arachchi HM, Armitage G, Arze CA, Ayyaz T, Baker CC, Begg L, Belachew T, Bhonagiri V, Bihan M, Blaser MJ, Bloom T, Bonazzi V, Paul Brooks J, Buck GA, Buhay CJ, Busam DA, Campbell JL, et al. 2012. Structure, function and diversity of the healthy human microbiome. Nature 486:207-214.

25. Hapfelmeier S, Hardt W-D. 2005. A mouse model for *S*. Typhimurium-induced enterocolitis. Trends in Microbiology 13:497-503.

26. Beutler M, Eberl C, Garzetti D, Herp S, Münch P, Ring D, Dolowschiak T, Brugiroux S, Schiller P, Hussain S, Basic M, Bleich A, Stecher B. 2024. Contribution of bacterial and host factors to pathogen “blooming” in a gnotobiotic mouse model for *Salmonella enterica* serovar Typhimurium-induced enterocolitis. Infection and Immunity 92:e00318-23.

27. Winter SE, Thiennimitr P, Winter MG, Butler BP, Huseby DL, Crawford RW, Russell JM, Bevins CL, Adams LG, Tsolis RM. 2010. Gut inflammation provides a respiratory electron acceptor for *Salmonella*. Nature 467:426-429.

28. Faber F, Thiennimitr P, Spiga L, Byndloss MX, Litvak Y, Lawhon S, Andrews-Polymenis HL, Winter SE, Bäumler AJ. 2017. Respiration of Microbiota-Derived 1,2-propanediol Drives *Salmonella* Expansion during Colitis. PLOS Pathogens 13:e1006129.

29. Schubert C, Nguyen BD, Sichert A, Näpflin N, Sintsova A, Feer L, Näf J, Daniel BBJ, Steiger Y, von Mering C, Sauer U, Hardt W-D. 2024. Monosaccharides Drive *Salmonella* Gut Colonization in a Context-Dependent Manner. bioRxiv doi:10.1101/2024.08.06.606610:2024.08.06.606610.

30. Palaniappan B, Sundaram S, Arthur S, Afroz S, Sundaram U. 2020. Inducible nitric oxide regulates na-glucose Co-transport in a spontaneous SAMP1/YitFc mouse model of chronic ileitis. Nutrients 12:3116.

31. Lu Z, Imlay JA. 2021. When anaerobes encounter oxygen: mechanisms of oxygen toxicity, tolerance and defence. Nature reviews microbiology 19:774-785.

32. Tawk C, Lim B, Bencivenga-Barry NA, Lees HJ, Ramos RJF, Cross J, Goodman AL. 2023. Infection leaves a genetic and functional mark on the gut population of a commensal bacterium. Cell Host Microbe 31:811-826.e6.